Leibniz Institut für Meereswissenschaften

IFM-GEOMAR

an der Christian-Albrechts Universität Kiel

Dissertation
zur Erlangung des Doktorgrades
der Mathematisch-Naturwissenschaftlichen Fakultät
der Christian-Albrechts-Universität zu Kiel

vorgelegt von

Christian Schlosser
Lutherstadt Wittenberg

Kiel, 2008

Hiermit erkläre ich, dass ich die vorliegende Doktorarbeit selbständig und ohne unerlaubte Hilfen erstellt habe. Ferner habe ich weder diese noch eine ähnliche Arbeit an einer anderen Abteilung oder Hochschule im Rahmen eines Prüfungsverfahrens vorgelegt, veröffentlicht oder zur Veröffentlichung vorgelegt.

Christian Schlosser

Referent: Prof. Dr. Douglas Wallace
Korreferent: Prof. Dr. Arne Körtzinger
Tag der mündlichen Prüfung: 04.07.2008
Zum Druck genehmigt: 25.06.2009

Kinetics and Thermodynamics of Iron Species in the Southern Ocean

This dissertation is based on the following research topics and prepared manuscripts

Schlosser C. S. and P. L. Croot, 2008. Application of cross-flow filtration for determining the solubility of iron species in open ocean seawater, $Limnology\ and\ Oceanography$: $Methods$, 6:630-642

Schlosser, C. S. and P. L. Croot, Controls on seawater Fe(III) solubility in the Mauritanian upwelling zone, 2008 (submitted to $Geophysical\ Research\ Letters$)

Schlosser, C. S., P.Streu, M. Ötztürk and P. L. Croot, Influence of iron binding ligands on Fe(III) solubility in a Southern Ocean iron enrichment experiment (EIFeX), 2008 (manuscript in prep. for $Marine\ Chemistry$)

Contribution of authors to the manuscripts

Application of ultrafiltration for determining the solubility of iron species in open ocean seawater, 2008

Christian Schlosser made the measurements and evaluated the results. Christian Schlosser and Peter L. Croot wrote the manuscript.

Controls on seawater Fe(III) solubility in the Mauritanian upwelling zone, 2008

Christian Schlosser collected the samples, made the measurements, evaluated the results and wrote the manuscript. Peter L. Croot gave advice and helped revise the manuscript.

Effect of Iron Binding Ligands on Fe(III) Solubility in a Southern Ocean Iron Enrichment Experiment (EIFeX), 2008

Christian Schlosser made the measurements, evaluated the results and wrote the manuscript. Peter L. Croot gave advice and helped revise the manuscript.

Zusammenfassung: Eisenlöslichkeits- und Ligandenmessungen, welche während dieser Doktorarbeit durchgeführt wurden, zeigten, dass stark bindende organische Liganden die Eisenlöslichkeit und die Verweildauer des Eisens im Meerwasser signifikant erhöhen. Ein mesoskaliges Eisendüngungsexperiment (EIFeX) im Südlichen Ozean zeigte, dass sich im Wasser gelöste organische Liganden aus einer kolloidalen und einer "wirklich" gelösten Phase zusammensetzen, welche beide thermodynamisch stabil sind. Die Zusammensetzung des Ligandenpools in der oberen Mixedlayer (20 – 80 m), welcher sich in einem Gleichgewicht zwischen kolloidal und "wirklich" gelöster Liganden befand, verschob sich zu einem prozentual größeren Anteil "wirklich" gelöster Liganden, nachdem die Biomasseproduktion ihren Höhepunkt erreicht hatte. Das neu eingestellte Gleichgewicht, welches sich nun in der oberen Wassersäule (20 – 300 m) ausgebildet hatte, zeigte eine Ligandenzusammensetzung, die vorher nur unterhalb von 80 m Wassertiefe beobachtet werden konnte. Ebenso konnte nachgewiesen werden, dass die im Meerwasser gelösten organischen Liganden hauptsächlich "absichtlich" von Bakterien in das Meerwasser abgegeben wurden. Ähnliche Messungen, welche in der Mauretanischen-Auftriebs-Zone durchgeführt wurden, zeigten, dass in diesem Meerwasser gelöste organische Liganden hauptsächlich durch den Abbau von organischer Biomasse erzeugt worden sind (lineare Korrelation von pH, Sauerstoff und Phosphat mit der Kapazität von Seewasser für "wirklich" gelöstes Eisen). Ultrafiltrationsversuche an verschieden Eisenligandenlösungen im Labor zeigten, dass diese Technik sehr gut geeignet ist, um die verschiedenen Größenklassen des Eisen voneinander zu trennen. Später durchgeführte Massenbilanzrechnungen ergaben, dass ein signifikanter Teil des dazugegebenen ^{55}Fe durch Adsorptionseffekte (Kunststoffwandung und Filtermembran) verloren ging. Diese Nebeneffekte müssen für folgende Ultrafiltrationsexperimente an Spurenmetallen in Betracht gezogen werden, da ansonst Massenbilanzrechnungen nicht erfolgreich durchgeführt werden können.

Abstract: Iron solubility and ligand measurements performed during this PhD work showed that strong organic ligands increase iron solubility and therefore the residence time of Fe in seawater. Measurements made during a mesoscale Fe fertilization experiment (EIFeX) in the Southern Ocean showed that both the soluble and colloidal fractions of dissolved organic ligands are thermodynamically stable in seawater. The composition of the ligand pool (in terms of the ratio of soluble to colloidal ligands) in the upper mixed layer ($20 - 80$ m) shifted towards a greater proportion of soluble ligands after the peak of biomass was reached in the Fe fertilization experiment. Prior to this, the soluble and colloidal ligand fractions were in some sort of equilibrium since dissolved ligand concentrations showed a linear correlation with iron solubility. After the peak of biomass was reached, the same ligand composition as observed below 80 m during the experiment was found in the whole upper mixed layer ($20 - 300$ m). Organic ligands appeared to have been directly released by bacteria. In contrast to the measurements from the Southern Ocean, measurements made in the Mauritanian upwelling zone showed a significant correlation between indicators of organic matter remineralization (pH, oxygen, and phosphate) and iron solubility in subsurface samples ($40 - 80$ m). The main increase in iron solubility could be attributed to the remineralization of organic matter. Lab based ultrafiltration experiments on ligand solutions made up in seawater showed that this technique is a powerful tool for separating the particulate and colloidal from the soluble iron fraction. Mass balance calculations showed that a significant portion of the added ^{55}Fe had disappeared from the feed solution before the ultrafiltration was started and yet more disappeared during each cycle of ultrafiltration. Iron was adsorbing onto bottle walls and onto surfaces within the ultrafiltration unit. Future work using trace-metal ultrafiltration needs to recognize that these effects (wall sorption and filter loading) occur and must be taken into account in mass balance calculations.

Contents

Chapter 1

Introduction

More than 71% of our planet's surface is covered by water and 97% of this water is located in the oceans. Unsurprisingly, the oceans play a major role for climate and life on Earth, acting, for example, as both a source and a sink for climatically relevant gases (e.g., CO_2, methane). Since the Industrial Revolution began in the 19th century, a considerable amount of fossil fuels has been burned, resulting in the production of a large quantity of CO_2. Not all of this CO_2 has not remained in the atmosphere, however where it would have contributed to greenhouse warming of the planet. Calculations suggest that instead more than 50% of the anthropogenically released CO_2 has been taken up by the oceans.

Containing more than 37,000 GtC to the atmosphere's approximately 750 GtC (Sundquist, 1993), the ocean is the largest rapidly reacting reservoir of carbon at the Earth's surface. The equilibrium which the surface ocean and atmosphere reach with respect to CO_2 controls atmospheric concentrations of the gas over centennial to millennial time scales. The balance between the upwelling of CO_2 rich deep waters and the drawdown of CO_2 in surface waters during photosynthesis by phytoplankton plays a key role in controlling atmospheric concentrations of CO_2. The upwelling brings with it high concentrations of nutrients, which

support the fixation of CO_2 into organic matter by phytoplankton. A portion of this organic matter then sinks into the deep before decomposing, concentrating CO_2 and nutrients in the deep ocean. The concentration of CO_2 in deeper waters, out of contact with the atmosphere, means that the atmosphere contains a lot less CO_2 for the total given amount of carbon in the oceans than it would in the absence of this biological pumping of carbon into the deep. The exact balance which is struck between the upwelling of CO_2 and its removal by phytoplankton is variable, and so, while the ocean as a whole is a net sink for CO_2, some regions serve as sources while other regions serve as sinks. In an ocean of unlimited nutrient availability, the CO_2 that mankind has added to the atmosphere would be utilized by phytoplankton and would result in the development of more biomass. But nutrient concentrations are limiting in the ocean and increases in atmospheric concentrations of CO_2 do not result in unlimited "greening" of the ocean. Phytoplankton require a considerable suite of different elements for growth. Nitrogen is, for example, a key component of proteins and phosphorus is critical for cellular energetics and the construction of DNA. Although metals such as Co, Zn, and Fe are important components of enzymes such as nitrogenase, superoxide dismutase, and carbonic anhydrase, classically it has been supposed that modern phytoplankton are limited in their ability to grow by the availability of the major nutrients, phosphate (PO_4^{3-}), nitrogen (NO_3^-, NO_2^-, NH_4^+), or silicate ($Si(OH)_4$).

The paradigm of major nutrients being the only routinely limiting nutrients for phytoplankton growth in the ocean has been challenged and overthrown in recent decades. For a long time it has been known that large parts of the ocean (e.g., the Southern Ocean and the north Pacific subarctic), the high nutrient, low chlorophyll (HNLC) regions, contain unusually low concentrations of chlorophyll despite having nutrient rich surface waters. In the 1980s, following some of the first truly "trace metal clean" work at sea, it was finally successfully shown that phytoplankton growth in HNLC regions of the ocean is limited by the availability of the micronutrient iron (Fe).

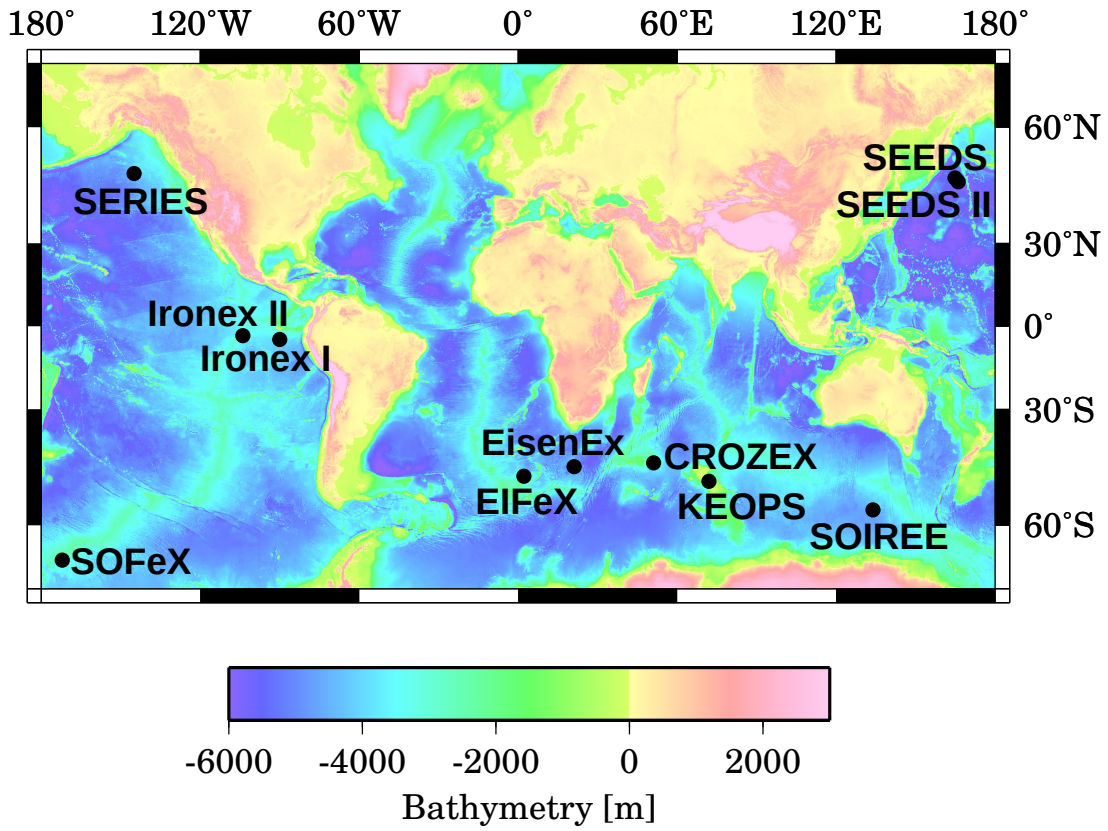

Figure 1.1: *Shown are the locations of the mesoscale Fe fertilization experiments of the last 15 years. Note that, unlike the others, the CROZEX experiment was naturally fertilized by dust and continental shelf sediments.*

Since the potential for Fe to be a limiting factor for phytoplankton growth in the ocean was first demonstrated in a set of shipboard bottle incubation experiments by Martin and Fitzwater (1988), several mesoscale Fe fertilization experiments have been carried out in various different HNLC regions (Fig. 1.1). Several of these experiments (including EisenEx, SOFeX, and EIFeX) have been carried out in the Southern Ocean to determine the biological response to the addition of Fe to this HNLC region that contains the greatest amount of unutilized macronutrients in the world ocean. In all of these experiments, Fe fertilization triggered a huge phytoplankton bloom, as shown by a factor of 10 increase in chlorophyll

concentrations (De Baar et al., 2005). At the same time, nitrate and phosphate concentrations decreased through utilization by phytoplankton.

One interesting result of the EIFeX experiment (Hoffmann et al., 2006) was that the added Fe was not used equally by the phytoplankton species present. Bigger species, usually large diatoms and flagellates, were the main beneficiaries of iron fertilization, and tended to show greater gains in biomass. Smaller species, such as the small diatom *Chaetoceros brevis*, showed almost no response to Fe fertilization, maintaining similar growth rates under several different Fe concentrations (Timmermans et al., 2001). This could suggest that this species is not Fe limited under natural conditions, although it may be that this species does not follow an ecological strategy of blooming in response to nutrient input (Assmy et al., 2007).

Ever since John Martin said "Give me a tanker full of iron and I will give you an ice age!", there has been interest in lowering atmospheric CO_2 concentrations by fertilizing HNLC regions with Fe and stimulating phytoplankton growth. To say the least, this is a controversial idea. Despite all of the mesoscale Fe fertilization experiments that have been carried out, it is not clear that carbon can be effectively exported to the deep sea simply by dumping iron sulfate into HNLC surface waters. There is much that remains to be understood about the behaviour of the Fe in the ocean (Fe solubility, Fe-ligand complexation, etc.), its availability to and utilization by phytoplankton, and the response of the entire food web following Fe addition.

On the following pages I give an introduction to the marine biogeochemical cycle of Fe. In particular, I focus on the deposition of Fe as dust on the sea surface and the chemical reactivity of different Fe species. I then show results of studies of Fe solubility and ligand concentrations which I conducted in the lab and on one seagoing expedition (Mauritanian Upwelling Zone). I will show in the next chapters how these results – the comparison of Fe solubility and ligand concentration – might change our understanding of Fe speciation

and cycling in seawater, how the cross-flow filtration can be used for the investigation of colloidal and truly dissolved trace metal species in oceanic seawater and what must be taken into account for such separation experiments.

1.1 Biogeochemical Fe cycle

1.1.1 Iron sources

Fe in seawater can be derived from the input of terrigenous materials via aeolian deposition (Jickells et al., 2005), rivers (Bergquist and Boyle, 2006; Buck et al., 2007), resuspension of material from continental shelf sediments (Eldridge et al., 2004; Johnson et al., 1999), and the melting of sea ice which contains dust (Fig. 1.2). Dust is an important external input of Fe to the ocean. The proportion of Fe dissolvable from dust varies greatly, ranging

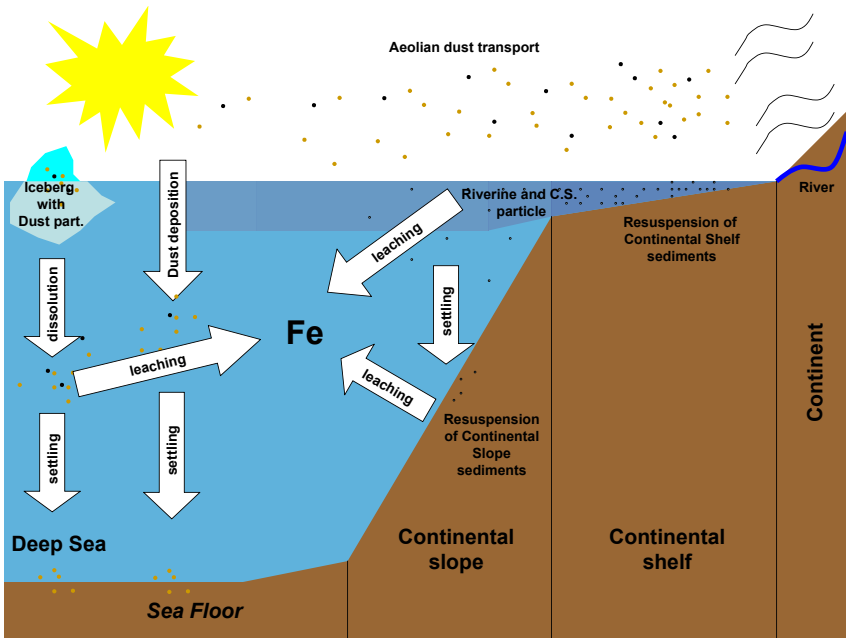

Figure 1.2: *Illustration of possible sources, which deliver Fe into seawater.*

anywhere from 2 to 20% (Baker and Jickells, 2006; Baker et al., 2006b), giving a global input of Fe to the ocean from dust of anywhere from $2 - 12$ x 10^9 mol Fe y^{-1} (Fung et al., 2000; Turner and Hunter, 2001a). Resuspension of material on continental shelves provides an additional source of Fe to surface waters; Elrod et al. (2004) and Lam et al. (2006) have proposed that, with a value of 8.9 x 10^{10} mol Fe y^{-1}, continental shelves provide almost eight times more Fe to the surface ocean per year than dust.

The huge range in the results of Baker and Jickells (2006) and other groups for the solubility of Fe in aeolian dust may be due to a combination of factors. The first is that dust from different sources contains different minerals, which in turn range in their content of Fe and in their "weatherability". A major part of the variability in the results, however, may be associated with the experimental setups used in the various experiments. The oversaturation of leached solutions, wall sorption effects, and the different pHs used in different experiments must all be taken into account for the comparison and evaluation of metal solubility measurements from mineral dust.

1.1.2 Iron species in seawater

The thermodynamically stable Fe species in seawater is Fe(III). Conceptually, Fe(III) has been traditionally divided into a dissolved ($Fe_D \leq 0.2$ μm) and a particulate phase ($Fe_P >$ 0.2 μm). Recent studies with ultrafiltration ($<$ 10 kDa) and syringe ($<$ 0.02 μm) filtration techniques have demonstrated the existence of soluble ($Fe_S < 0.02$ μm) and colloidal iron ($Fe_C = 0.2 - 0.02$ μm) phases within the dissolved size fraction (Wu et al., 2001; Nishioka et al., 2005; Cullen et al., 2006; Bergquist et al., 2007). All these different size fractionations are interconnected, with rapid transformations occurring between them.

Fe(III) ions in seawater at pH 8 have the strong tendency to hydrate ($Fe(OH)^{2+}$, $Fe(OH)_2^+$, $Fe(OH)_3$, $Fe(OH)_4^-$) and to form Fe oxides and $FeOOH$ (e.g., goethite). Organic ligands

(section 1.1.3), strong Fe chelators of low molecular weight produced by bacteria (Martinez et al., 2000; McCormack et al., 2003) under Fe limitation, form strong organic Fe complexes and are therefore in competition with the inorganic Fe pathway (Fig. 1.3). Fe-ligand complexes are more soluble and increase the residence time of Fe in seawater.

$$\tau_{Fe} = \frac{I_{Fe}}{F_{Fe}} \tag{1.1}$$

A larger inventory (I_{Fe}) of dissolved and soluble Fe in seawater with a constant Fe flux (F_{Fe}) leads to an increasing residence time of Fe (τ_{Fe}) in this seawater.

Due to its impact on the bioavailability, chemical reactivity, and residence time of Fe species

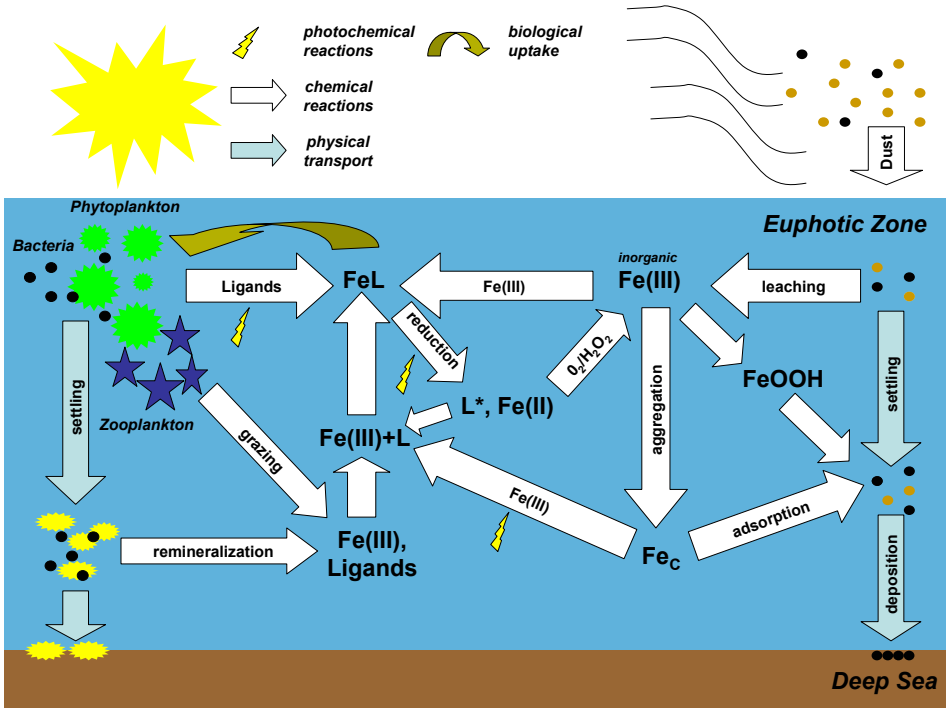

Figure 1.3: *Different pathways and exchange between Fe species (inorganic and organic) in the euphotic zone (first ≈ 200 m) of the seawater column.*

in the oceans, the redox cycling of iron in marine systems is of considerable interest. Fe(II),

which is the product of photochemical or other reduction mechanisms of Fe(III), is quickly oxidized by O_2 and peroxide (H_2O_2) (Millero et al., 1986; Millero and Sotolongo, 1989). H_2O_2 is photochemically produced by the reaction of Fe(II) and superoxide (O_2^-). The most common Fe redox reactions are (King et al., 1995):

$$Fe(II) + O_2 \rightarrow Fe(III) + O_2^- \tag{1.2}$$

$$Fe(II) + O_2^- \rightarrow Fe(III) + H_2O_2 \tag{1.3}$$

whereas Fe(III) is also in competition for superoxide,

$$Fe(III) + O_2^- \rightarrow Fe(II) + O_2 \tag{1.4}$$

$$Fe(II) + H_2O_2 \rightarrow Fe(III) + OH^* + OH^- \tag{1.5}$$

$$Fe(II) + OH^* \rightarrow Fe(III) + OH^- \tag{1.6}$$

Tropical waters have very low Fe(II) concentrations, on the order of pmol L^{-1} or less. However, during spring blooms in colder coastal waters (Kuma et al., 1992a), Fe(II) has been detected at relatively high concentrations ($\approx$ 1 nM), which suggest that Fe(II) is an important short-lived intermediate in the iron cycle (Johnson et al., 1994).

Several oxidation rate measurements of Fe(II) at the nM level have been performed (King et al., 1995; Santana-Casiano et al., 2006) and have shown that analytical measurements of Fe(II) in seawater are complicated by the low concentration and the possibility of artifacts. Fe(II) is significantly more soluble in seawater and thermodynamically less stable than Fe(III). In theory, kinetically labile species are more bioavailable than mineralized species. This would imply that Fe(II) and soluble Fe (monohydrolyzed and organically complexed Fe) are preferentially taken up by phytoplankton and bacteria. However, investigations of the consumption of soluble (organic complexed and monohydrolyzed Fe) and colloidal Fe by phytoplankton and bacteria have yielded conflicting results (Chen and Wang, 2001; Hutchins

et al., 1999b; Kuma et al., 2000). More work is needed to detail the biological uptake and redox cycling of Fe.

1.1.3 Origin and cycling of ligands

Organic ligands (e.g., siderophores) which complex with Fe in seawater (Fig. 1.4) can be produced by bacteria (Martinez et al., 2000; McCormack et al., 2003). Several bottle incubation experiments have shown that some bacteria species form and "intentionally" release organic ligands under Fe limitation. Production and release of ligands by phytoplankton and bacteria was also observed during several mesoscale Fe fertilization experiments. Wu et al. (2001) suggested that ligands were also produced during the degradation of organic matter by bacteria.

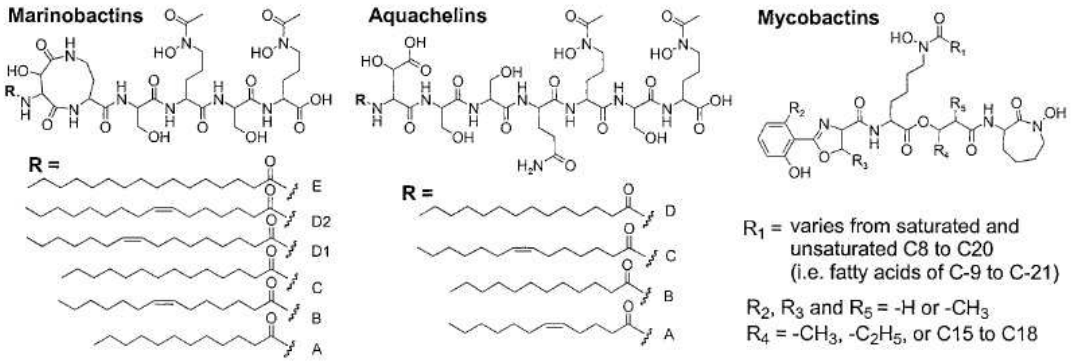

Figure 1.4: *The figure shows three different ligands produced by three different bacterial strains in the lab (Martinez et al., 2003). The number of functional groups (hydroxamate, catecholate and carboxylate) and their position in the molecule differ from ligand to ligand.*

From the middle of the 1990s up to the present, many studies have been performed to mea-

sure Fe ligand concentrations $[L]$ and conditional stability constants of Fe complexes ($K_{Fe'L}$) by competitive ligand exchange / adsorptive cathodic stripping voltammetry (CLE/ACSV) (Wu and Luther, 1995; Rue and Bruland, 1997). These studies have detected ligand concentrations and log $K_{Fe'L}$ ranging between 0.5 $-$ 2 nmol L^{-1} and 10 $-$ 13, respectively. The wide range of log $K_{Fe'L}$ (calculated with respect to Fe', which takes into account all inorganic hydrolyzed Fe species) was explained by the existence of two different ligands of different strengths (Barbeau, 2006; Cullen et al., 2006; Rue and Bruland, 1997, 1995).

It is more likely that the population of ligands present in ocean waters is considerably more diverse than that. Ligands are low molecular weight molecules with a large spread in composition and available functional groups. Analysis of structures has shown that some natural organic ligands ($ferrichrome$, $aquachelins$, $petrobactin$, etc.) in seawater have common functional groups of siderophores, like hydroxamate ($R-CNOOH$), catecholate ($R-(C(OH))_2$) and α-hydroxy carboxylate ($R-COOH$) (Macrellis et al., 2001). Normal intracellular ligand molecules, like porphyrins and simple sugar compounds, have also been found in seawater (Barbeau, 2006) and could potentially complex Fe.

The photochemical reactivity of these organic Fe complexes has been reviewed by Barbeau et al. (2003). Depending on the ligand, any outcome is possible, from outright destruction or deactivation of ligands in any form to no change in reactivity or integrity whatsoever. Barbeau et al's measurements showed that tris-hydroxamate siderophores, like desferrioxamine G, which are produced by $Vibrio$ bacteria (Martinez et al., 2000), are very stable and do not show any radiation-induced destruction of free or Fe-complexed ligands. Catecholates (common catecholate functional groups), on the other hand, appear to be susceptible to photooxidational processes in the uncomplexed form but are surprisingly stable when complexed with Fe. The aquachelin siderophore, when destroyed by UV-irradiation or natural sunlight, collapses into a hydrophilic peptide and a hydrophobic fatty acid tail fragment (Barbeau et al., 2003). The photoproduced peptide retains the possibility to complex Fe(III)

with its two hydroxamate groups.

These results confirmed the conclusions of Liu and Millero (1999) that UV-irradiation and the resulting H_2O_2 molecules do not destroy all organic Fe complexing compounds in seawater (section 1.1.5). At the same time, the existence of ligands that survive exposure to sunlight and those that do not helps to explain the CLE/ACSV data, which tends to group ligands into two general camps depending on their strength for complexing Fe.

Organic ligands produced by phytoplankton and bacteria directly influence the soluble Fe species and the whole Fe cycle in seawater. An accurate understanding of photochemical reactions of free, complexed, and photochemically degraded ligands is necessary for the description of the biological part of the Fe cycle in seawater. More work has to be done in this direction, especially on the structure, functional groups, and chemical reactivity of organic ligands and their impact on the capacity of seawater for soluble Fe.

1.1.4 Interconnection between soluble and colloidal iron species

Recent studies (Wu et al., 2001; Bergquist et al., 2007) demonstrated the existence of both soluble and colloidal Fe species and documented their distribution in the water column in the Pacific and Atlantic Oceans. Soluble Fe at all stations in these studies had nutrient-like profiles: low concentrations in surface waters (0.05 to 0.1 nmol L^{-1}) and higher concentrations in deeper waters (0.2 to 0.4 nmol L^{-1}). Colloidal Fe concentrations were just the opposite, with higher values occurring towards the surface (0.5 to 0.8 nmol L^{-1}) and lower ones in deeper waters (0.2 to 0.4 nmol L^{-1}).

Fe ligands also exist in both soluble and colloidal phases. The soluble ligand ($L_S < 0.02$ μm) measurements by Wu et al. (2001) using a syringe filtration (0.025 μm) setup showed concentrations of soluble ligands in surface waters that at 0.1 nmol L^{-1} were lower than expected. Previous measurements (which did not separate dissolved ligands into soluble and

colloidal fractions) had varied between 0.5 and 2 nmol L^{-1} for 0.2 μm filtered seawater (Rue and Bruland, 1997; Wu and Luther, 1995; van den Berg, 2006). Wu et al. (2001) concluded from this that soluble and colloidal ligands are in competition for the available Fe, with colloidal ligands making up a greater fraction of total dissolved ligands in surface waters than in deeper waters. Higher soluble ligand concentrations in deeper waters together with the release of Fe during the bacterial decomposition of organic matter would then lead to higher soluble Fe concentrations in deeper waters.

UV light can potentially impact the partitioning of Fe between soluble and colloidal phases. It has been shown that colloidal Fe is made soluble in seawater under UV-irradiation (Wells et al., 1991). In the reported study, the highest amount of redissolved Fe was produced from radiation between 300 and 400 nm in wavelength after 20 minutes of exposure. Given the levels of UV radiation seen in surface seawater, this process of solubilization of colloidal Fe should have a strong impact on the biogeochemical cycling of Fe in the euphotic zone (the upper $5 - 10$ m in coastal waters and the upper 100 m in open ocean waters).

1.1.5 Solubility of inorganic and organically complexed Fe

The first measurements of Fe solubility (cFe_S) in seawater were performed by Byrne and Kester (1976), Byrne et al. (2000), and by Kuma et al. (1996) (using the radioisotope, ^{55}Fe). Empirical models have also been developed (e.g., Liu and Millero (1999, 2002)) in an attempt to understand what factors control the capacity of seawater for soluble Fe (Equ. 1.7, 1.8, 1.9, 1.10 and 1.11).

$$logK^*_{Fe(OH)_3} = -13.486 - 0.1856I^{0.5} + 0.3070I + \frac{5254}{T} \ (\sigma = 0.08) \tag{1.7}$$

$$log\beta^*_1 = 2.517 - 0.8885I^{0.5} + 0.2139I - \frac{1320}{T} \ (\sigma = 0.03) \tag{1.8}$$

$$log\beta^*_2 = 0.4511 - 0.3305I^{0.5} - \frac{1996}{T} \ (\sigma = 0.1) \tag{1.9}$$

$$log\beta_3^* = -0.2965 - 0.7881I^{0.5} - \frac{4086}{T}\ (\sigma = 0.6) \tag{1.10}$$

$$log\beta_4^* = 4.4466 - 0.8505I^{0.5} - \frac{7980}{T}\ (\sigma = 0.2) \tag{1.11}$$

In these equations log $K^*_{Fe(OH)_3}$ is the stability coefficient of the hydrated Fe species, β^*_{1-4} are the different hydration coefficients, I is the ionic strength and T is the temperature, in Kelvin. Both the theoretical model and the measurements made in artificial seawater (0.7 M NaCl), and UV-irradiated and untreated seawater showed that the solubility of inorganic Fe ($cFe_{S,in}$) is indirectly proportional to pH, salinity, and temperature (Liu and Millero, 1999; Kuma et al., 1996). Between pH 7 and 9, pH appears to have little influence, on inorganic Fe solubility (Fig. 1.5). Temperature and salinity also influence cFe_S, with higher values occurring at lower temperatures and ionic strengths.

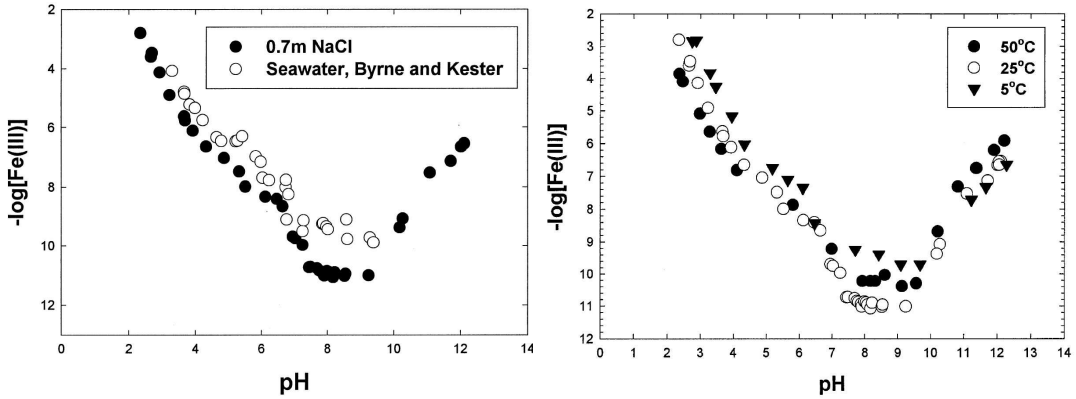

Figure 1.5: *Both panels show cFe_S versus pH. The left panel shows trends in both artificial and natural seawater. The right panels shows cFe_S versus pH at three different temperatures (5, 25 and 50° C) (Liu and Millero, 1999). Interesting is the overall higher solubility at 5° C.*

Differences in inorganic Fe solubility at pH 8 for UV irradiated (∼0.2 nmol L^{-1}, (Kuma et al., 1996)) and artificial seawater (∼10 pmol L^{-1}, (Liu and Millero, 1999)) suggested

that UV irradiation may not properly destroy all organic compounds dissolved in seawater. Barbeau et al. (2003) showed by investigating naturally occurring ligands, that photochemically degenerated ligands retain functional groups, which can still complex Fe(III) (section 1.1.3).

Natural organic ligands present in seawater increase Fe solubility (0.1 to 1 nmol L^{-1}) and have a direct and constant influence of Fe solubility between pH 7 to 9 (Kuma et al., 1996). At higher or lower pH, the influence of ligands on cFe_S is negligible (Fig. 1.5).

Fe solubility measurements in the northwest Pacific by Kuma and Isoda (2003) and Tani et al. (2003) showed very variable but generally higher cFe_S in the surface mixed layer and a solubility minimum between 80 and 100 m. cFe_S increased in intermediated waters along with nutrient concentrations, humic-acid fluorescence, and apparent oxygen utilization (AOU). There was also a slight and linear decrease of cFe_S at depths below 1000 m, which was also accompanied by a decrease in nutrient concentrations, humic-acid fluorescence, and AOU. The increase of cFe_S in intermediate waters was attributed to bacterial remineralization of organic matter below the chlorophyll maximum, suggesting that organic ligands are produced during the decomposition of settling organic matter and are available for the complexation of freely available Fe.

It is well known that nutrients are released during the remineralization of organic matter, leading to an overall increase of nutrient concentrations below the chlorophyll maximum. The structure and functional groups of released ligands are currently completely unknown and must be investigated if we are to understand how the production and release of ligands at depth differs from the intentional release of ligands in surface waters under conditions of Fe limitation.

1.2 Work performed

The measurements which are described in detail in the following sections were carried out as part of my PhD at the Leibniz-Institut für Meereswissenschaften (IFM-GEOMAR), Kiel. The goal of these studies was to advance our knowledge of the biogeochemical cycling of Fe in seawater. Fe ligand and Fe solubility measurements were made to investigate the kinetics of the formation and dissociation and the thermodynamics of Fe ligand complexes which are the most common Fe species in seawater. The ultrafiltration technique for the separation of colloidal and soluble trace metal species was also scrutinized in detail to determine possible artifacts and problems that can occur during ultrafiltration. The following subsections provides a brief overview of the studies and study sites which the next few chapters of this dissertation are devoted to detailing.

1.2.1 Instrumental setup

Separation of colloidal and soluble Fe phases by ultrafiltration

For many years, filters have been used to separate particulate, colloidal, and soluble Fe phases from each other. Many different techniques are available, such as flow injection analysis (FIA) (de Jong et al., 2000; Obata et al., 1993), graphite furnace atomic absorption spectrometry (GFAAS), and inductively coupled plasma based methods (ICP-MS, ICP-OES), for analysis of the dissolved or soluble Fe concentration in the resulting filtrate. The obvious problem with these techniques is that the Fe which is in the upper size fraction and therefore collected by the filter is not easily available for measurement.

Ultrafiltration is a technique that allows more than one phase to be measured from the same water sample. In the ultrafiltration measurements reported here (Fig. 1.6 and Chapter 2), a 10kDa membrane filter was used to separate the colloidal and particulate phases from

the soluble phase. The membrane filter in the ultrafiltration device allowed the passage of seawater and Fe in the soluble phase through to the permeate reservoir. The colloidal and particulate phases, however, did not pass through the membrane filter but were instead sent back to the initial feed solution. This caused the concentration of colloidal/particulate Fe in the feed solution to increase over time. From the final concentrations of Fe in the permeate and retentate it was possible to calculate the soluble and colloidal/particulate Fe concentrations.

This technique was used, as described in section 2.3, to determine the effect of different ligands (DFO, protoporphyrin IX, etc.) on the capacity of seawater for soluble Fe. As a part of this work, it was necessary to improve the way ultrafiltration data are handled in order to accurately account for the adsorption of Fe onto surfaces in the ultrafiltration system.

Separation of colloidal and soluble Fe phases by syringe filtration

The main objective of one of the studies presented here was to track changes in Fe solubility during a mesoscale Fe fertilization experiment in the Southern Ocean (EIFeX) (Chapter 4). Because we only needed to quantify Fe in one phase, it was possible to use a relatively simple syringe filtration technique in this work.

During another experiment in the Mauritanian Upwelling Zone, the same technique was used to investigate how parameters such as temperature and pH influence Fe solubility (Chapter 3).

The radionuclide ^{55}Fe

For both the syringe filtration and ultrafiltration techniques, the radionuclide ^{55}Fe was used. The method for investigating Fe solubility in seawater using a radioactive Fe nuclide was developed by Kuma et al. (1996). The ^{55}Fe nuclide (half-live = 2.7 y) decays by low energy

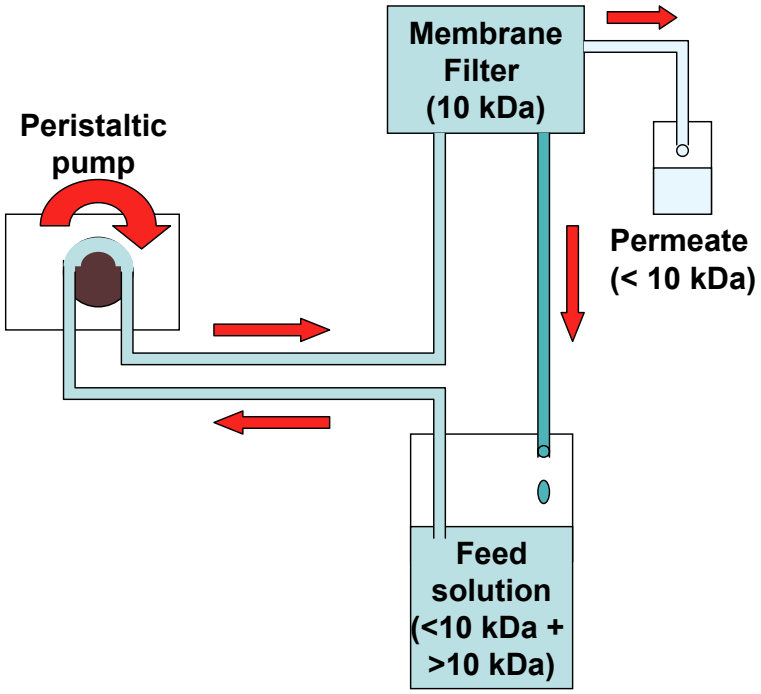

Figure 1.6: *Illustration of the cross-flow ultrafiltration system. The sample is pumped through a 10 kDa membrane filter using a peristaltic pump. A portion of the size fraction smaller than 10 kDa passes through the membrane filter into the permeate. Material larger than 10 kDa is pumped back into the feed solution.*

β^+ emission to a stable isotope of manganese (^{55}Mn). The β^+ decay of ^{55}Fe is easy to detect via a liquid scintillation method. The emitted radiation reacts with a scintillation liquid and produces a photon, which is photometrically measured in a liquid scintillation counter.

To quantify Fe solubility, a known amount of ^{55}Fe was added to seawater samples and given time to equilibrate with the *in situ* Fe. Then the samples were filtered and the amount of ^{55}Fe that went into different phases could be measured by liquid scintillation counting.

Ligand measurements

Ligand concentration measurements were made on EIFeX samples so that a comparison with Fe solubility could be made. The ligand measurements were carried out by the established competitive ligand equilibration / adsorptive cathodic stripping voltammetry (CLE/ACSV) method (Croot and Johansson, 2000) with 2-(2-thiazolylazo)-p-cresol (TAC) as competitive ligand (described in detail in section 4.3.4).

1.2.2 Description of study sites

The Southern Ocean

The Southern Ocean is the biggest HNLC region of the planet. As mentioned in an earlier section, the nutrient limiting phytoplankton growth in this oceanic region is Fe (Boyd et al., 2000; Coale et al., 2004; De Baar et al., 2005; Gervais et al., 2002; Takeda and Tsuda, 2005; Wells, 2003). Dissolved Fe in surface waters in the present day Southern Ocean (Fig. 1.7) is mostly delivered in the form of dust from Patagonia, the Kerguelen Islands, South Africa, and Australia. Other sources of Fe are melting ice bergs which contain dust and other airborne particles and the resuspension of sediments from the continental shelf. These non-airborne sources can be important on local scales.

In addition to being the world's largest HNLC region, the Southern Ocean is also the only ocean of the planet without any meridional boundaries that would support the formation of western boundary currents and wind driven gyres. Instead, the biggest and strongest current in the Southern Ocean, the Antarctic Circumpolar Current (ACC), flows uninterruptedly eastwards and encircles Antarctica. South of the ACC, close to the Antarctic continent, two major embayments can be found, the Weddell Sea and the Ross Sea. These seas have western boundaries which support regional wind-driven gyres with western boundary

currents.

The ACC is divided by four major fronts which separate it into four zones in which isopleths are more widely spaced (Orsi et al., 1995). The mixing between the different zones is mostly controlled by eddies. Fronts of the ACC are the Subantarctic Front (SAF), the Polar Front (PF), the Southern ACC Front ($SACCF$), and the Southern Boundary (SB) and they demarcate the Subantarctic Zone (north of the SAF), the Polar Frontal Zone (between the SAF and the PF), the Antarctic Zone (between the PF and $SACCF$), and the Continental Zone (south of the $SACCF$ and including the SB) (Fig. 1.7).

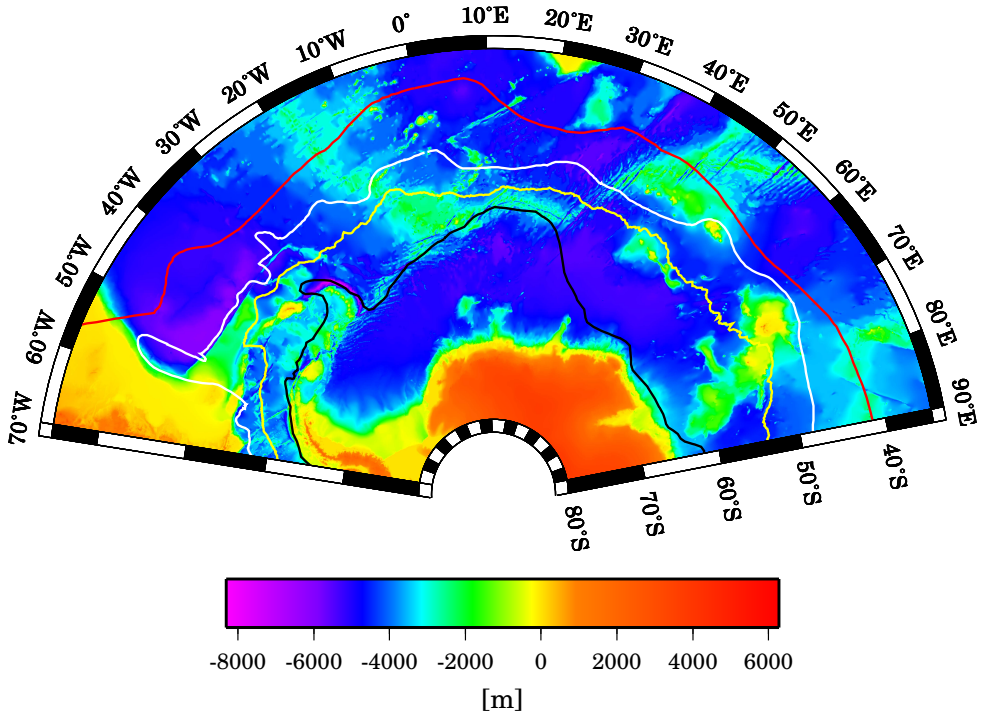

Figure 1.7: *The illustration shows the Atlantic sector of the Southern Ocean. The different frontal boarders are given by different colors, such as red – SAF, white – PF, yellow – SACCF and black – SB.*

Mass and heat transport between the different zones, which have different salinities and temperatures, are mostly carried out by the aforementioned eddies. Eddies are large scale objects, several kilometers to several hundred kilometers in diameter, with an elliptical shape in the horizontal direction. Eddies may persist for several months to more than a year and transport heat, nutrients, and other properties of a particular water mass (salinity, etc.) over great distances. One such eddy that had crossed the Polar Front from south to north was used in 2004 for a mesoscale Fe fertilization experiment (EIFeX) in the Southern Ocean.

The Mauritanian upwelling zone

Upwelling regions are easy to detect by sea surface temperature (SST) anomalies (upwelled waters are colder than normal surface seawaters) and by measurements of CO_2 concentrations. The CO_2 concentration of upwelled waters is 2 to 3 times higher (Steinhoff, T., personal communication) than it is in surface waters, which have had time to come closer to equilibrium with the atmosphere.

Upwelling occurs along many coasts of the world. One upwelling area is the Mauritanian upwelling zone (Fig. 1.8) on the northwest African coast ($16 - 31$ °N and $16 - 20$ °W). Here the most intense upwelling occurs during the spring. During this season, strong trade winds from the northeast push coastal waters offshore, driving the upwelling of nutrient-rich deep waters to replace them.

In a strong upwelling season (early spring), north Atlantic central water ($NACW$) and south Atlantic central water ($SACW$) supply the Mauritanian upwelling with oxygen depleted and nutrient enriched deep waters. Another source of upwelled deep water at this location can be the more shallow north equatorial countercurrent ($NECC$) and the upwelling undercurrent (UUC) which is supplied by the $NECC$. $NACW$ and $SACW$ are at the same depth between 100 to 400 m and show differences in their ages, since the formation of $NACW$

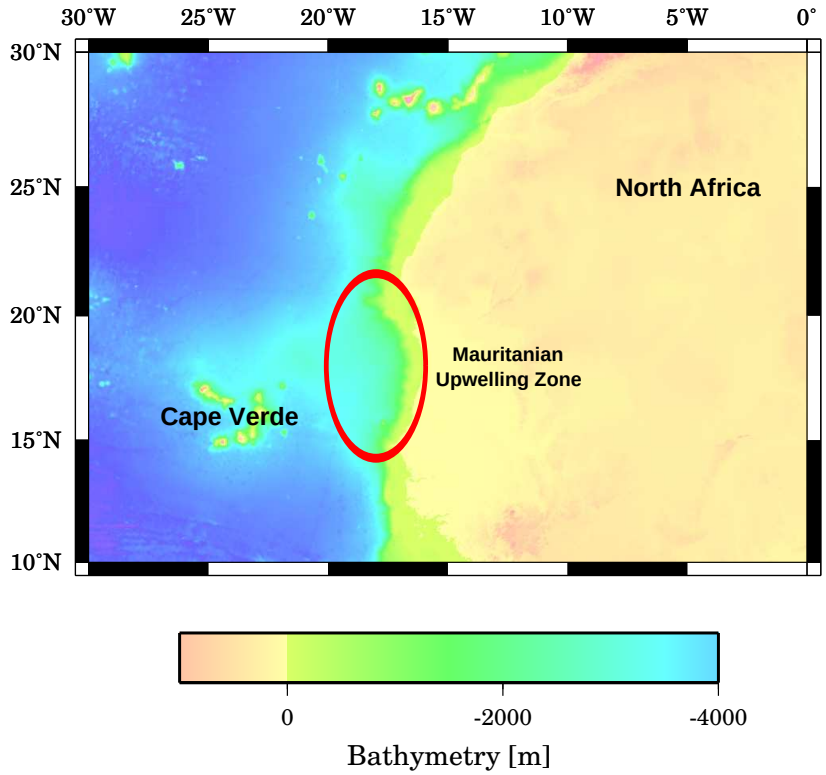

Figure 1.8: *Picture shows the western North African coast with the Mauritanian upwelling zone (red ellipse).*

water is 5 to 10 degree north and therefore much closer to the upwelling area than the $SACW$ (Stramma et al., 2005).

Recent studies showed that the UUC water, which follows the African continent from south to north in a direct way to the upwelling area, plays a major role for the supply of deep water masses during an upwelling season (Schafstall, J., personal communication). During weaker upwelling times (summer, autumn), when the wind comes from a direction other than NE, the warmer surface layer (first 30 m) of the coastal ocean is stable enough to prevent the break-through of huge deep water masses to the surface. During the Meteor cruise M68/3 in summer 2006, the upwelling that occurred was very weak and just a few upwelling filaments were found.

The overall higher nutrient concentration in deeper waters of the Mauritanian upwelling zone during the upwelling season are due to the transport of nutrient rich deep water to the upper water column and/or to the remineralization of organic matter below the euphotic zone.
Measurements of chemical parameters (such as nitrate, phosphate, oxygen, iron, etc.) during M68/3 suggested that during weak upwelling seasons the increasing nutrient concentrations with depth are mostly due to the bacterial remineralization of sinking particulate organic matter and not so much to the upwelling of nutrient-rich waters. Events which can be observed at any point during the whole season are big dust storms, which come from the Sahara. Very fine dust particles can be delivered this way all the way to the Caribbean. Bigger dust particles are harder to transport and fall out earlier (i.e. in the Mauritanian upwelling zone).
After dust deposition, the soluble Fe fraction ($2 - 20\%$; section 1) of dust particles can be used by phytoplankton and bacteria to support growth and the development of biomass.
An interesting aspect of the Mauritanian upwelling is the establishing of the Oxygen Minimum Zone (OMZ) in shallow depths (below 30 m). The oxygen (O_2) concentration rapidly decreases to much smaller values than found in the surface. This strong decrease of O_2 concentrations during weak upwelling seasons can be explained by oxygen consumption by zooplankton and bacteria during the remineralization of particulate organic matter and a strong thermal stratification, which prevents the formation of a deep mixed layer.

Chapter 2

Ultrafiltration for determining the solubility of iron species in open ocean seawater

2.1 Introduction

It is now widely accepted that in large parts of the ocean, principally the high nutrient, low chlorophyll (HNLC) regions, phytoplankton growth is limited by the low availability of iron (Boyd et al., 2007; Martin et al., 1994). The main controlling factor on iron (Fe) concentrations in the ocean is its solubility, as in ambient oxygenated seawater the thermodynamically favoured redox state, Fe(III) is poorly soluble ($20 - 500$ pmol L^{-1}) (Liu and Millero, 1999). Measurements of the physical speciation of Fe in seawater are traditionally operationally defined by the filtration system used by the researchers: dissolved (< 0.2 or 0.4 μm) and particulate (> 0.2 or 0.4 μm) phases, depending on the filters used by the researchers. More recent work has further divided the dissolved phases into soluble (< 10 kDa or < 200 kDa) and colloidal ($10 - 200$ kDa to 0.2 μm) components (Bergquist et al., 2007; Cullen et al., 2006; Nishioka et al., 2005; Wu et al., 2001).

The colloidal phase in the productive zones of the open ocean is dominated by organic colloidal aggregates ($5 - 200$ nm), which may provide numerous binding sites for trace metals such as Fe (Wells and Goldberg, 1993, 1994). It is also likely that considerable differences exist in the bioavailability of soluble versus colloidal Fe (Wang and Dei, 2003), and so to truly understand Fe as a limiting nutrient in the ocean, the relationship between dissolved Fe and Fe solubility needs to be better understood.

Both soluble and colloidal Fe in the oceans are derived from the input of terrigenous materials to the global ocean via aeolian deposition (Jickells et al., 2005), riverine input (Bergquist and Boyle, 2006; Buck et al., 2007; Gaiero et al., 2003), or resuspension of material from continental shelf sediments (Eldridge et al., 2004; Johnson et al., 1999). The amount of dissolvable Fe in aeolian transported materials varies greatly, ranging anywhere from 2 to 20% (Baker and Jickells, 2006; Baker et al., 2006b) whereas indirect estimates for the Pacific are higher at $\sim 40\%$ (Boyle et al., 2005). The amount of dissolved Fe (Allard et al., 2004;

Turner and Hunter, 2001b) carried by rivers varies strongly and is influenced by pH and the lithology of the river catchment and its vegetation cover. Much of the river transported soluble Fe in estuaries, however, is quickly converted, at higher salinity values, into the biologically unavailable colloidal and particulate phases (Boyle et al., 1977; Guieu et al., 1996). As shown in numerous works more than 99% of the dissolved Fe (< 0.2 μm) is bound by organic ligands throughout the world oceans (Croot and Johansson, 2000; Rue and Bruland, 1997; van den Berg, 1995; Witter and Luther, 1998; Wu and Luther, 1995). Hutchins et al. (1999b) concluded that the organic complexation of Fe increases the amount of dissolved Fe species and consequently the biological availability of Fe. However, the difference in the bioavailability of organically complexed versus colloidal Fe is not well understood (Chen and Wang, 2001; Hutchins et al., 1999a; Kuma et al., 2000). The presence of siderophores and other Fe complexing ligands produced, or released via grazing or viral lysis, from phytoplankton, and bacteria may stabilize soluble Fe, increasing both the residence time and total pool size of bioavailable Fe in the surface ocean (Barbeau et al., 2001, 2003).

Recent studies have shown that a significant fraction of the dissolved Fe pool exists as colloidal Fe species (Bergquist et al., 2007; Nishioka et al., 2001; Wu et al., 2001), with dissolved Fe concentrations in the euphotic zone being dominated by the variability of the colloidal Fe fraction. The colloidal Fe variability in the NW Atlantic was suggested to be seasonally dependent, with higher concentrations occurring in winter (Bergquist et al., 2007).

Some fundamental issues that remain to be answered in the marine biogeochemistry of Fe are the extent to which organic binding agents increase Fe solubility and how those ligands prevent the formation of colloidal Fe in seawater. Until now, only studies from Fe enrichment experiments have examined Fe ligand complexation and the formation of colloidal Fe (Boye et al., 2005; Wells, 2003) with little attention paid to the overall solubility of Fe. Here we present a study that, through the careful use of cross-flow filtration technique and theory, outlines the impact of different ligands on Fe speciation and solubility.

2.2 Materials and procedures

2.2.1 Reagents

The impact of various different organic ligands on the speciation of Fe in seawater was measured via cross-flow filtration using the radioisotope, ^{55}Fe (Hartmann Analytics, Braunschweig, Germany). The iron isotope had a specific activity of 157.6 MBq/mg Fe, a total activity of 75MBq and was dissolved in 0.51 mL of 0.1 M HCl. ^{55}Fe dilutions were produced with 18 MΩ deionized, ultrapure water and were acidified with quartz-distilled HCl (Q−HCl) to a pH below 2. The 7 ligands tested (desferrioxamine B (DFB), ethylenediaminetetraacetic acid ($EDTA$), 2-(2-thiazolylazo)-p-cresol (TAC), phytic acid ($IP6$), protoporphyrin IX ($PPIX$), phytagel and 2-keto-D-gluconic acid ($2kDG$) were obtained from Sigma-Aldrich. Ligand solutions were made up in 0.2 μm pre-filtered Antarctic seawater (sampled during Eifex 2004 under trace metal clean conditions; total dissolved Fe concentration (Fe_d = 0.2 nmol L^{-1})). Prior to use, this seawater was irradiated with UV light (UV-Digester 705 from Metrohm) for 75 minutes to destroy any organic compounds present. All labware used was soaked in 10 M HCl for at least 7 days and then rinsed with ultrapure water prior to use.

2.2.2 Ultrafiltration setup and cleaning procedure

The ultrafiltration of Fe and ligand containing solutions was carried out using a Masterflex L/S system with a Vivaflow 50 membrane (10kDa) constructed of PES (*polyethersulfone*) with an active membrane area of 50 cm^2. The recirculation rate was set to approximately 300 mL/min, which typically gave a permeate flow rate of 5 mL/min. All ultrafiltration work was carried out using an acid-cleaned polycarbonate (PC) container and polyethylene (PE) tubing. The Vivaflow 50 was pre-cleaned by sequential rinsing with 100 mL ultrapure

water, 100 mL of a 1% solution of 6 M Q-HCl, a 100 mL EDTA wash solution (10 mmol L^{-1}) and then finally a last rinse with ultrapure water to remove trace metal contamination. The ultrafilter could be reused several times following this procedure.

2.2.3 ^{55}Fe measurements

^{55}Fe in the various ultrafiltration fractions was quantified using a liquid scintillation counter (Tri-Carb 2900TR) from Packard and the cocktail, Lumagel Plus (Lumac LSC). The efficiency (55 − 60%) of the instrument was determined by several quench curve calibration measurements. The lowest measurable Fe concentration (detection limit) was at 8.1 ± 1.5 pmol L^{-1}, equivalent to 1 count per minute (CPM). The ultrafiltration setup (PC container, PE tubing and 10 kDa membrane filter) was cleaned prior to each experiment with a sequence of two short washes (0.1 mol L^{-1} Q-HCl followed by 10 mmol L^{-1} EDTA) and a rinse with ultrapure water.

2.2.4 Theory ultrafiltration

The theory for the ultrafiltration of solutes has been described in detail previously by other researchers in this field: Reitmeyer et al. (1996), Guo et al. (2001), and Hasselloev et al. (2007). In general, the separation of Fe species by ultrafiltration can be represented as a simple mass balance in a closed system with a fixed total solution volume:

$$c_i V_i = c_R V_R + c_P V_P \tag{2.1}$$

where c is the concentration of total Fe in the initial sample (i), the permeate (P) and the retentate (R), and V is the associated liquid volume. Since the colloidal fraction of Fe is too large to pass through the 10 kDa membrane filter, the difference between the concentration

of Fe in the retentate and permeate is the concentration of Fe that is colloidal:

$$c_{Col}V_i = c_R V_R - c_P V_P \tag{2.2}$$

The extent to which the feed solution has passed across the membrane filter may be described in terms of a concentration factor (*CF*), the volume ratio between the initial and retentate solution (Logan and Qing, 1990; Reitmeyer et al., 1996):

$$CF = \frac{V_i}{V_i - V_P} = \frac{V_i}{V_R} \tag{2.3}$$

The colloid Fe concentration (c_{Col}), is then determined from the concentration of Fe in the permeate (c_P) and in the retentate (c_R) and *CF*:

$$c_{Col} = \frac{c_R - c_P}{CF} \tag{2.4}$$

At any given time of filtration, the relationship between the concentration of a given chemical species in the instantaneous permeate (ic_P) outflow and the *CF* can be described by the following equation (Guo et al., 2001; Logan and Qing, 1990):

$$lnic_P = ln(P_C * c_i) + (1 - P_C) * lnCF \tag{2.5}$$

where P_C is the permeation coefficient, defined as the ratio of ic_P to c_R at any given time during the filtration, where c_i is the initial concentration of the permeable species in solution. Under constant permeation behaviour, a plot of ln ic_P versus ln CF will be linear with slope (1 - P_C). When $P_C = 1$, the solute is not retained by the ultrafiltration membrane and $ic_P = c_R$ for all values of CF. Lower values of P_C indicate discrimination by the membrane of the ultrafilter either by size exclusion or by polarization effects. Note that this equation

holds only for the instantaneous permeate concentration (ic_P) flowing out of the ultra filter and not the concentration (c_P) in the bottle collecting the permeate (see also App. A).

2.2.5 Colloidal fouling of cross-flow filtration membranes

Iron colloids are well known to cause fouling of ultrafiltration membranes (Soffer et al., 2004, 2002; Waite et al., 1999) leading to a reduction of permeate flow. In studies of Fe solubility this also presents a problem as colloidal Fe will be adsorbed on the filter membrane instead of pooling in the retentate, resulting in an apparent loss of Fe from the system. Thus it is crucial that a mass balance consider all aspects of the ultrafiltration procedure.

Fouling occurs initially by the advection and deposition of colloids onto the membrane, causing pore blockage, and is dependent on the permeate flux, colloid size and zeta potential (Soffer et al., 2004). The rate at which the colloid is deposited on the membrane can be written as (adapted from Soffer et al. (2004)):

$$\frac{\partial n_{uf}}{\partial t} = A(J - J_{cr})c_{Col} \tag{2.6}$$

where n_{uf} is the number of moles of Fe deposited on the membrane, A is the area of the membrane, J is the permeate flux (L m^{-2} h^{-1}) and J_{cr} is the critical permeate flux (L m^{-2} h^{-1}) below which no deposition can occur and is dependent on surface interactions. Integration over time of Equ. 2.6 and assuming J is constant leads to a relationship between Fe accumulation on the filter and the permeate volume:

$$n_{uf} = \beta V_P c_{Col} + n^0_{uf} \tag{2.7}$$

where $\beta = (1 - J_{cr}/J)$ is a unitless constant term (valid only for $J > J_{cr}$ relating the fraction of colloidal Fe lost to the filter, n^0_{uf}, is the amount of Fe deposited on the membrane prior

to $t = 0$. The value of n_{uf} is experimentally determined from the mass balance between permeate and retentate ($n_{uf} = c_i V_i - c_R V_R - c_P V_P$). While it would be beneficial to keep the Fe adsorption on the filter to a minimum, in practice this may not be possible as the value of J_{cr} will vary between samples, depending on the colloid content and composition, and the required permeate flow may be too low for adequate sample throughput. Thus for our experimental work we focused on evaluating this loss term and its impact on the mass balance for Fe in the system and not on the permeate flux rate that minimised this loss term. Based on the theory outlined above, we constructed a simple two species model, including fouling of the membrane, to analyze our results. The first Fe complex was allowed to pass through the ultrafiltration membrane while the second component was purely colloidal and retained. A full description of the model can be found in App. A.

2.2.6 Conditional stability constants of iron-organic species estimated by solubility

For the experiments with well-characterized chelators, conditional stability constants for the complexation with Fe, in seawater, can be calculated using the following assumptions:

$$Fe + L \Leftrightarrow FeL \tag{2.8}$$

$$[L]_T = [L] + [FeL] \tag{2.9}$$

$$K'_{Fe'L} = \frac{[FeL]}{[Fe'] + [L]} \tag{2.10}$$

where [*Fe'*] is the sum of the inorganic Fe(III) (Fe not complexed with L), and [*L*] is the concentration of the ligand not complexed with Fe in seawater (this may include ligands

bound to Ca^{2+} and Mg^{2+}). The solubility of Fe(III) in seawater is given by the following equation:

$$[Fe(III)]_{SW} = [Fe'] + [FeL] \tag{2.11}$$

The concentration of FeL in seawater can be calculated from the measured value by correcting for the contribution from inorganic Fe(III) species:

$$[FeL] = [Fe(III]_{SW} - [Fe(III)]_{NaCl} \tag{2.12}$$

Thus in the absence of organic chelators we have the following relationship:

$$[Fe'] = [Fe(III)]_{NaCl} \tag{2.13}$$

For our experiment solutions where colloidal Fe dominates, we can assume that the solution is saturated for Fe', and it is in turn controlled by the solubility of inorganic Fe formed under these conditions. Under the experimental conditions employed during the present work we find $[Fe'] = [Fe(III)]_{NaCl} \sim$ 150 pmol L^{-1} (Liu and Millero, 1999).
Under saturated conditions, combining L and the permeate concentration ($[Fe(III)]_{SW}$), we can estimate K'_{FeL} for each ligand tested (adapted from Liu and Millero (2002)).

$$K'_{Fe'L} = \frac{[Fe(III)]_{SW} - [Fe(III)]_{NaCl}}{[Fe(III)_{NaCl}][L]} \tag{2.14}$$

which rearranges to the following equation derived from measured quantities:

$$K'_{Fe'L} = \frac{[Fe(III)]_{SW} - [Fe(III)]_{NaCl}}{[Fe(III)]_{NaCl}([L]_T[Fe(III)]_{SW})} \tag{2.15}$$

In the case of an excess of strong Fe binding ligands, the system will be undersaturated with respect to the formation of colloidal Fe, and Fe' will be less than the inorganic solubility term, $[Fe(III)]_{NaCl}$. In this situation only a lower boundary for $K'_{Fe'L}$ can be estimated. In the case of saturated natural seawater samples where the concentration of L is not known, it is not possible to calculate $K'_{Fe'L}$. However we can compare ultrafiltration data with published Fe speciation data for $K'_{Fe'L}$ and L via the maximum permitted soluble Fe (derived from rearranging Eq. 2.15):

$$[Fe(III)]_{SW} = \frac{[Fe(III)]_{NaCl}(1 + K'_{FeL}[L]_T)}{1 + K'_{FeL}[Fe(III)]_{NaCl}}. \tag{2.16}$$

Using this approach, the maximum soluble Fe can be determined by inputting the observed values of K'_{FeL} and L, along with the value of $[Fe(III)]_{NaCl}$ for a saturated Fe solution under the appropriate experimental conditions.

2.2.7 Side reaction coefficient ($\alpha_{Fe'}$) for Fe' in seawater

The value of the side reaction coefficient for Fe' relative to Fe(III) is critical for calculating conditional stability constants for Fe organic complexes and for determining the solubility of iron in seawater under different environmental conditions. Recently, there has been a consensus towards using $\alpha_{Fe'} = 10^{10.0}$ (pH = 8.02, salinity 35), based on the earlier work by Kuma et al. (1996) and Millero (1998), complementing reactivity measurements by Hudson et al. (1992). More recently, an extremely good data sets for a range of environmental conditions that have been recently made using EDTA (Sunda and Huntsman, 2003) and solubility measurements made via filtration (Liu and Millero, 1999, 2002). What differences there are between experiments appear to be related to the age of the Fe colloids employed (Kuma et al., 1996; Sunda and Huntsman, 2003).

2.2.8 Experimental procedure

Experiments were performed (App. B) using 7 different Fe binding ligands in UV-treated, 0.2 μm filtered, Antarctic seawater (collected during EIFeX). A further set of experiments was performed using 0.2 μm filtered non-UV irradiated Antarctic seawater and coastal seawater (fjord seawater; Bergen, Norway). Initial volumes of 200 mL seawater were used throughout. In the ligand experiments, ligand concentrations in the solution were $\sim$ 100 nmol L^{-1}. Ligand solutions were allowed to equilibrate with seawater for 4 hours before addition of ^{55}Fe (c_{tot} = 60 nmol L^{-1} in all, except for PP IX c_{tot} = 40 nmol L^{-1}). The Fe concentration was checked immediately after Fe addition ($t = 0$) and then again after the equilibration period of 24 h. Ultrafiltration of the sample was commenced at 24 h after the Fe addition.

Ultrafiltration of the samples was performed under constant pressure and flow rate conditions. Samples were always collected from both the permeate and the retentate at each sampling period. Samples were taken based on the collected permeate volume, starting at 5 mL, 20 mL and then every further 20 mL until 180 mL (corresponding to the *CF* range 1.03 – 10). For each of the permeate samples, the last 2 mL passing through the membrane filter were collected into a 60 mL PTFE bottles and 20 μL of HCl was added to prevent the sorption of Fe onto the bottle walls. Triplicate 400 μL subsamples of the retentate and of the permeate were transferred into 6 mL scintillation counting vials. The vials were then filled with 4.5 mL of cocktail and the ^{55}Fe activity was measured by liquid scintillation counting. At the end of each ultrafiltration experiment, 40 mL of ultrapure water acidified with a 1% solution of 6 M Q-HCl were flushed through the ultrafiltration system to desorb any Fe from the walls of the PC container, the PE tubing, and the membrane filter. The Fe concentrations in the permeate and in the retentate samples taken at 5 and 20 mL were then used for mass balance calculations.

A SenTix 81 combination pH electrode and WTW model 720 pH meter were used to de-

termine the pH. The electrode was calibrated on the free hydrogen scale (pH_F) using TRIS seawater buffers (Millero, 1986). All pH data reported here is based on the free hydrogen ion concentration scale and data from other pH scales was converted using the appropriate algorithms (Dickson and Goyet, 1994).

2.3 Assessment

2.3.1 Iron loss to the walls of the sample container

Initial measurements of the ^{55}Fe activity ion solution prior to the start of the ultrafiltration are shown in Fig. 2.1. It can be clearly seen that in most cases there was a considerable loss of ^{55}Fe to the walls on the polycarbonate sample container 24 hours after addition of the ^{55}Fe and the organic complexing agent.

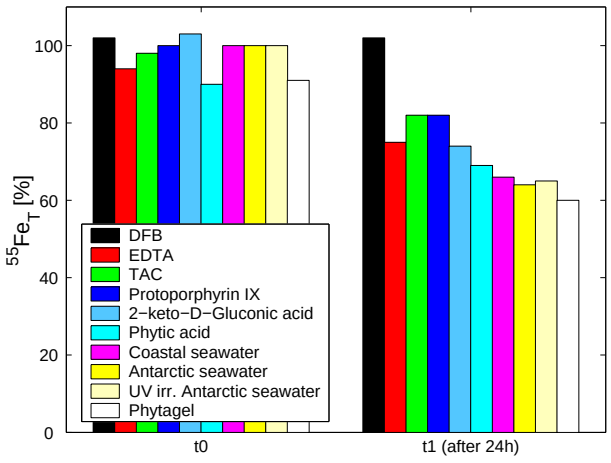

Figure 2.1: *Measured Fe concentrations in the feed solution at hour 0 and 24. For saturated solutions, approximately 20 − 40% of the Fe was lost to the walls of the sample container. Only for the undersaturated solution containing DFB there was no apparent wall adsorption effect.*

The equivalent loss to wall (c_W) sorption (App. A and B) was similar to that recently observed by Fischer et al. (2007) and in earlier work by Robertson (1968). Only with the strong complexing agent DFB was no wall sorption effect observed.

All other Fe ligands tested and natural seawater solutions showed a strong decrease ($20 - 40\%$) of ^{55}Fe in solution. Mass balance considerations (see below) indicate that the wall adsorbed ^{55}Fe was not remobilized during the ultrafiltration procedure. Indeed only a strong acid solution (e.g. HCl) was able to return the wall adsorbed ^{55}Fe to the solution phase. Thus wall sorption appears to be unavoidable with solutions saturated for Fe' and needs to be considered carefully in the experimental procedure. For undersaturated solutions, such as with DFB in the present work and in the case of some natural seawater, this adsorption to the walls may be not significant. This result also has implications for voltammetric studies in which high concentrations of added ligands (e.g. 10 μmol L^{-1} TAC (Croot and Johansson, 2000)) should minimize wall adsorption for iron speciation studies.

2.3.2 Permeation coefficients for soluble Fe species

The permeation behavior of selected soluble Fe species are shown in Fig. 2.2. A frequent observation was that initially the permeation varied at low *CF* values (Fig. 2.2). However at $CF > 1.2$ (ln $CF > 0.2$), constant permeation behavior was observed in all experiments. The initial variation in permeation behaviour differed between natural seawater samples (slightly higher initial permeation) and ligand-amended UV seawater (reduced initial permeation) and was possibly related to adsorption of the permeable Fe species and/or permeable ligands to the outlet tubing.

Calculated values of P_C for the different Fe species, excepting phytagel (App. A and B), ranged from 0.58 for UV-irradiated Antarctic seawater to 1 for Fe-EDTA, with most in the range $0.88 - 1.0$ indicating that soluble organic Fe species were only weakly retained by

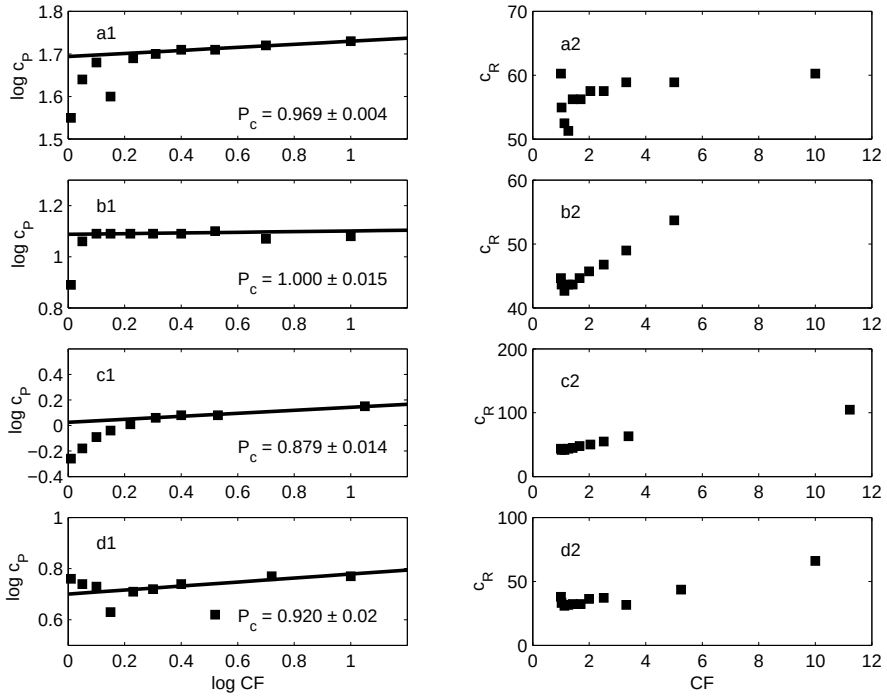

Figure 2.2: *Shows the log-log diagram of CF vs. c_P (1) and the diagram CF vs. c_R (2), of a: DFB; b: EDTA; c: 2kDG and d: Antarctic seawater. Furthermore, the regression lines and the calculated P_C value are inserted in the CF vs. c_P diagrams. Outliers and filter loading effects were not respected for the calculation of the regression line and P_C value.*

the 10 kDa filter used in this study. In contrast, soluble inorganic Fe species were strongly retained by the 10 kDa filter ($P_C = 0.58$), possibly by interaction with weak binding sites on the filter itself. Data for phytagel (not shown) indicated a decrease in permeation of the soluble Fe species with increasing *CF*, leading to an estimated $P_C > 1$. This was probably due to blocking of the ultrafiltration membrane by the high molecular weight of phytagel as evidenced by an increase in the observed pressure across the membrane.

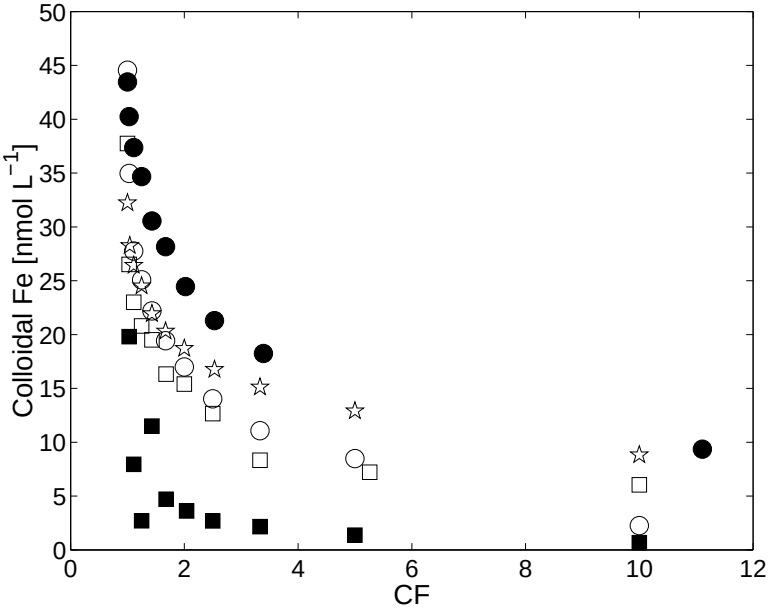

Figure 2.3: *Estimated colloidal Fe concentrations (See equation 4 in the text) of Antarctic seawater (squares), DFB (filled squares), EDTA (circles), 2kDG (filled circles), PP IX (stars) as a function of CF.*

2.3.3 Colloidal iron loss on the membrane

Colloidal Fe concentrations (Fig. 2.3) calculated using Equ. 2.4 exhibited significant decreases with increasing *CF*. This result indicates that there is an appreciable loss of colloidal Fe during the process of ultrafiltration as has been observed for other ultrafiltration systems (Wells, 2003). Consideration of the mass balance for the ultrafiltration procedure indicated that this loss of colloidal Fe was due to adsorption to the filter membrane (Fig. 2.4), which was also confirmed by later recovery of ^{55}Fe in the permeate after acidification (see below). For samples that were saturated with respect to Fe' formation, at CF of 10, approximately 50% (equivalent to 6 nmol) of the total Fe was adsorbed on the filter. The overall loss of colloidal Fe (n_{Fil} [mol]) adsorbed to the membrane filter was linearly dependent on the volume of permeate (Fig. 2.4) that passed through the filter as expected for both saturated

and unsaturated solutions (Equ. 2.7 above). Comparison of the Fe adsorbed to the filter (V_P = 180 mL) and the initial colloidal Fe concentration (Fig. 2.5) were highly correlated (n = 10, R = 0.91) as expected from Equ. 2.7. Calculated values for β ranged from 0.49 - 0.88 (mean: 0.70 $\pm$ 0.13), this in turn implies that under our constant permeate flow (60 L m^{-2} h^{-1}), we can calculate a critical permeate flux for iron colloids in our system; J_{cr} = 18.1 $\pm$ 7.8 L m^{-2} h^{-1}. This result implies that with a slower permeate flux value than used in the present work, we would expect less retention of colloidal iron on the filter. However, this finding ignores the link between recirculation rate and the permeate flux, and in our preliminary work, we found that slowing the recirculation rate to reduce the permeate flux did not enhance recovery. We had also anticipated that the linear relationship predicted from Equ. 2.7 should break down at higher CF as c_R increases due to the retention of colloidal Fe, but for the range of CF surveyed here, we did not observe this phenomenon.

2.3.4 Overall mass balance and recovery of adsorbed iron

To complete mass balance calculations and to ensure complete recovery of the ^{55}Fe tracer, the ultrafiltration system was rinsed with a dilute QD-HCl rinse with subsequent analysis of the permeate and retentate. Typically, we observed that after addition of the acid solution, initial measurements showed $ic_P > c_R$, indicating there had been some Fe adsorbed to materials downstream of the filter membrane, presumably on the tubing walls. This may be partly the reason for the lower ic_P values encountered at low CF with unacidified seawater solutions.

However, for all later measurements $ic_P = c_R$ indicating that all the Fe was solubilized at this low pH. Calculated overall mass balances, incorporating a 40 mL dilute QD-HCl rinse, (Fig. 2.6) showed complete recovery ($98 \pm 4\%$, n = 3) of the added ^{55}Fe indicating that both the wall-adsorbed and filter-adsorbed ^{55}Fe was recovered. Using only 20 mL of the

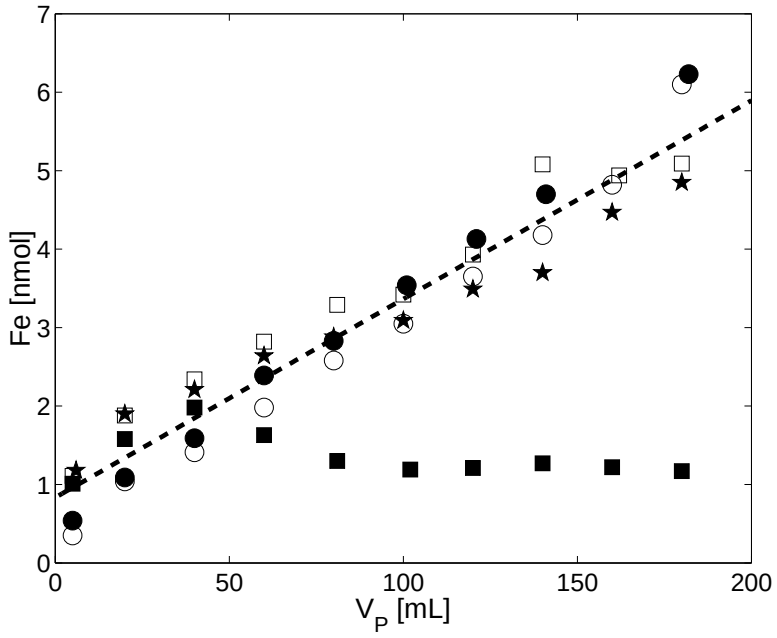

Figure 2.4: *Filter-loading Fe capacity with increasing V_P of Antarctic seawater (squares), DFB (filled squares), EDTA (circles), 2kDG (filled circles) and coastal seawater (stars).*

dilute QD-HCl rinse, we observed, in general, only the recovery of the filter-adsorbed ^{55}Fe, indicating this volume was insufficient to completely remove Fe adsorbed on the walls of the polycarbonate container to the solution phase. In all cases, a further cleaning rinse with either dilute QD-HCl or the EDTA rinse solution used for pre-cleaning resulted in the remaining ^{55}Fe being recovered and subsequent filter blanks returning to below detection limits ($<$ 7 pmol L^{-1}).

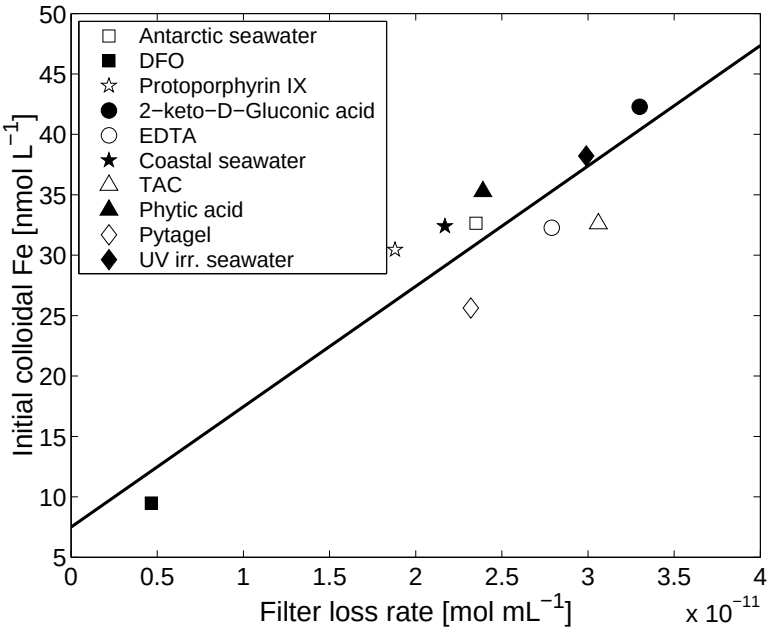

Figure 2.5: *Loss of ^{55}Fe (moles per milliliter of permeate) to the filter (estimated from mass balance considerations) versus initial colloidal Fe concentrations during cross-flow filtration of natural seawater or seawater amended with different Fe chelators.*

2.4 Discussion

2.4.1 Calculation of "true" colloidal iron concentrations

Implicit in the calculation of c_{Col} (Equ. 2.4) are the following assumptions:

i: that there is no retention of the permeable species ($P_C = 1$) and

ii: that no Fe is lost from the solution phase within the ultrafiltration system.

As detailed above, both of these assumptions are not always valid for the ultrafiltration of soluble Fe species. However, the "true" colloidal Fe concentration (c'_{Col}) can be calculated by completing the mass balance throughout the sampling procedure:

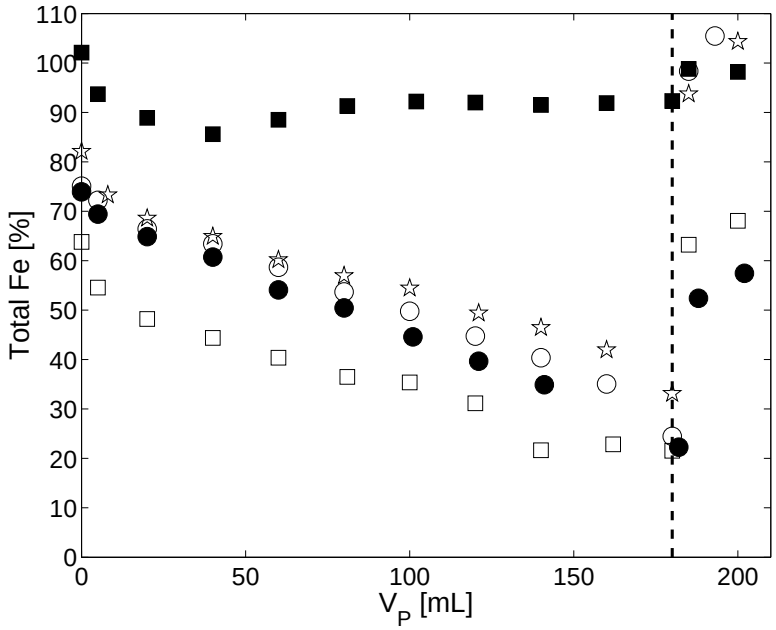

Figure 2.6: *Mass balance data for ^{55}Fe in the permeate and retentate for selected experiments. 20 ml QD-HCl rinse: Antarctic seawater (squares), 2kDG (filled circles), EDTA (circles). 40 ml QD-HCl rinse: DFB (filled squares) and PP IX (stars). The dashed line indicates the initial point of flushing the system with MQ and QD-HCl (6 M, 10 L per mL MQ water).*

$$c`_{Col}V_i = c_R V_R - \frac{c_P}{P_C} V_R + n_{uf} \tag{2.17}$$

or alternatively in terms of CF

$$c`_{Col} = \frac{c_R \frac{c_P}{P_C}}{CF} + \frac{n_{uf}}{V_i} \tag{2.18}$$

As the n_{uf} is derived from mass balance considerations, Equ. 2.18 can be converted into a form which is dependent only on directly measured quantities.

$$c`_{Col} = c_i - \frac{c_P}{V_i}\left(\frac{V_R}{P_C} + V_P\right) \tag{2.19}$$

Values of $c`_{col}$ calculated using Equ. 2.19 (App. A, App. B, and Fig. 2.7) show that after $CF = 2$ a constant value for almost all samples. 2kDG and UV-irradiated Antarctic seawater presented the highest amount of colloidal Fe ($c`_{col}$ = 59 nmol L^{-1}) at $CF = 10$. DFB formed the highest amount of organically complexed Fe (c_P = 53 nmol L^{-1}) and, in a similar manner, a very low colloidal Fe concentration ($c`_{col}$ = 5 nmol $L^{-1}$). All other samples, except for DFB, EDTA ($c`_{col}$ = 48 nmol L^{-1}) and TAC ($c`_{col}$ = 44 nmol $L^{-1}$), showed similar values for $c`_{col}$ (51 − 54 nmol L^{-1}).

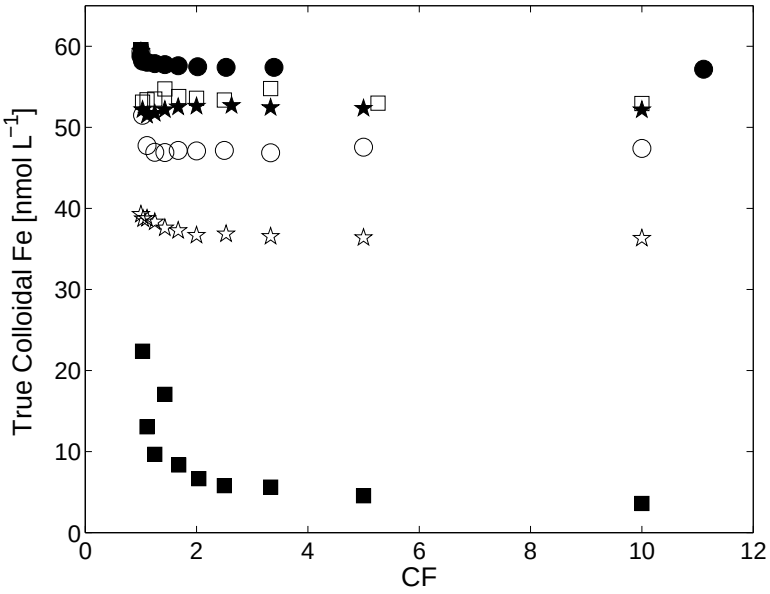

Figure 2.7: *Ambient "true" colloidal Fe concentration (Equ. 2.19) with increasing CF, of Antarctic seawater (squares), DFB (filled squares), EDTA (circles), 2kDG (filled circles), PP IX (stars) and coastal seawater (filled stars).*

2.4.2 Solubility of iron-complexes in seawater

Iron was poorly soluble in UV-irradiated Antarctic seawater ($ic_P \approx$ 0.15 nmol L^{-1}) (App. B), which is in good agreement with other recent solubility studies performed with conventional filtration systems in UV-irradiated seawater (Kuma et al., 1998a, 1992b, 1996; Liu and Millero, 2002) and in NaCl solutions (Liu and Millero, 1999). Interestingly, ic_P increased with increasing CF (P_C = 0.58), which may indicate that one or more of the inorganic hydrolyzed Fe species is discriminated against by interaction with the filtration membrane, possibly via polarization/charge effects.

Natural seawater (Antarctic and coastal seawater) had significantly more soluble Fe ($ic_P \approx$ 6 nmol L^{-1}) than UV-irradiated seawater and in both samples ic_P increased with increasing CF (P_C = 0.92 and 0.96 respectively) indicating small but significant retention effects on the soluble Fe species in these samples. This is an important finding as it indicates that accurate determination of the soluble Fe concentration in a sample is dependent on making multiple measurements of ic_P as a function of CF as a single measurement does not provide any information on P_C. The natural seawater Fe solubility values measured here are comparable to earlier studies (Kuma et al., 1998a,b, 1996) in which nM levels were found in coastal and open ocean seawaters. Additionally, the apparent ligand concentrations measured in the Antarctic seawater (5.4 nmol L^{-1}) were higher than the maximal solubility (Equ. 2.16) values ($1 - 3$ nmol L^{-1}) calculated from published speciation parameters in the same region measured using voltammetric methods (Boye et al., 2005, 2001; Croot et al., 2004a; Croot and Johansson, 2000). This difference between the actual solubility and the predicted values is probably in part related to the detection window used for voltammetric analysis, which would preclude weaker Fe-binding ligands (Croot and Johansson, 2000). It is clear that more detailed work using both chemical and physical methods on the same samples is still required.

DFB is a hydroxamate siderophore, which forms strong complexes with Fe(III) (Schwarzenbach and Schwarzenbach, 1963) even under ambient seawater conditions (Hudson et al., 1992). Due to its high-binding strength, DFB is frequently used to limit the bioavailability of Fe to phytoplankton in experimental studies (Hutchins et al., 1999a; Wells, 1999). In the present work, DFB strongly enhanced the Fe solubility (c_P = 53 nmol L^{-1}) and limited the formation of colloidal Fe (c'_{col} = 5 nmol L^{-1}). For DFB, P_C = 0.97, indicating that there was some small discrimination by the filter membrane for this soluble species. In an earlier study it was found that only 50% of the $FeHDFB^+$ (MW = 803) species was found to pass through a 1 kDa membrane at pH 4.8 (Batinic-Haberle et al., 1994). Furthermore, the authors found that $FeHDFB^+$ could form higher MW complexes with micelles at concentrations above the critical micelle concentration. While the colloidal concentration would have been expected to be near zero with DFB, as the solution was undersaturated with respect to Fe', it does appear that some of the ^{55}Fe was retained in the colloidal phase, though this colloidal Fe may still have been associated with DFB. As the DFB solution was undersaturated it was only possible to estimate a lower bound for log K for this complex in seawater (App. A and B).

The speciation of Fe-EDTA complexes in seawater is well described (Gerringa et al., 2000; Hudson et al., 1992; Sunda and Huntsman, 2003). EDTA forms three relatively weak Fe ligand complexes in seawater at pH 8.10, ~68 % $Fe(OH)(EDTA)^{2-}$ (log $K'_{Fe'L}$ = 7.7), ~24% $Fe(EDTA)^-$ (log $K'_{Fe'L}$ = 7.3) and ~7% $Fe(OH)_2(EDTA)^{3-}$ (log $K'_{Fe'L}$ = 6.7), due to strong side reactions with Ca^{2+} and Mg^{2+} (App. A and B). In the present work, we found that 100 nmol L^{-1} EDTA maintained ~ 12 nmol L^{-1} in the soluble phase and that there was effectively no retention effect on these soluble complexes (P_C = 1.00). Estimates of the conditional stability constant (App. A and B) for the soluble $Fe-EDTA$ complexes (log $K'_{Fe'L}$ = 9.0) were significantly higher than predicted values (overall log $K'_{Fe'L}$ = 7.9). An earlier study by Sunda and Huntsman (2003), using a solid phase extraction technique

(SPE) to determine soluble Fe-EDTA species, found good agreement with values predicted by Hudson et al. (1992). As equilibration times were the same in both studies, the reasons for the apparent discrepancy between our results and those of Sunda and Huntsman (2003) may be due to the experimental setup. This could indicate that the presence of EDTA in solution has some effect on the size range of the Fe colloids formed (see also phytic acid below) by adsorbing to the surface and preventing further aggregation (Nowack and Sigg, 1996). Such colloids may have been retained by the SPE technique employed by Sunda and Huntsman (2003) but passed through our ultrafiltration system. The photolysis of Fe-EDTA complexes to form Fe(II) (Kari et al., 1995; Sunda and Huntsman, 2003) may also have played role here in maintaining a fresh source of small Fe colloids that passed through the ultrafilter. Further studies on the solubility of Fe-EDTA complexes are currently being pursued.

TAC is from the family of thiazolylazo compounds (Hovind, 1975) that are known to form relatively strong Fe complexes. TAC is used as a reagent in voltammetric analysis for Fe speciation in seawater (Croot and Johansson, 2000). In the solubility experiments that we conducted with 100 nmol L^{-1} TAC, we found $\sim$ 16 nM in the soluble phase ($P_C = 0.99$). This result is slightly higher than we had anticipated given the published estimated conditional stability constant for seawater of log $\beta_{Fe'(TAC)_2} = 12.4$ (Croot and Johansson, 2000). However, this high solubility may indicate the presence of a strong 1 : 1 Fe-TAC species that was not anticipated in Croot and Johansson (2000).

PP IX has previously been found to be a strong Fe chelator by voltammetric studies (Rue and Bruland, 1995; Witter and Luther, 1998) though more recently this has been brought into question by photochemical (Rijkenberg et al., 2006) and bioavailability studies (Sato et al., 2007). In the present work, we find little evidence supporting PP IX as a strong Fe chelator in seawater as 100 nmol L^{-1} of this ligand were only able to maintain $\sim$ 2.5 nmol L^{-1} Fe in solution. The apparent discrepancy between the earlier voltammetric measurements and

later measurements may be due to either an insufficient equilibration time (Rue and Bruland, 1995), as suggested by Town and van Leeuwen (2005), or the lower pH (6.9) used in the Witter et al. (2000) study.

Phytic acid ($myo-$insitol hexakisphosphate) is a major component of eukaryotic cells (Turner et al., 2002) and has been suggested to be capable of forming strong Fe complexes in seawater (Witter et al., 2000). In the present study, phytic acid was found to be a relatively weak Fe ligand, complexing only $\sim$ 6 nmol L^{-1} Fe under the conditions employed here. Recently published thermodynamic data (Torres et al., 2005) for phytic acid complexes with Ca^{2+}, Mg^{2+}, H^{+} and Fe^{+++} indicate that under the seawater conditions employed here, there should be no appreciable Fe^{+++} complexes formed. However, a recent study using Field Flow Fractionation (FFF) showed that solutions of Fe and phytic acid at pH 7 formed complexes and/or colloids in the size range $1 - 500$ kDa (Purawatt et al., 2007). Higher concentration ratios of phytic acid to Fe shifted the mean colloid size to lower molecular weights (Purawatt et al., 2007). This behavior is probably related to the ability of the phosphate groups present in phytic acid to act as bridging groups between Fe colloids (Mali et al., 2006). The case of phytic acid then adds a new twist to the Fe solubility story as it apparently has an important role to play in stabilizing colloidal Fe but does not directly form soluble Fe.

The ligand 2kDG is a natural product of glucose oxidation and has been suggested as an important component of trace metal binding in soils (Nelson and Essington, 2005). Related compounds to 2kDG have been implicated in the production of Fe(II) in seawater through photochemical reduction of the Fe-carboxylic complex (Kuma and Matsunaga, 1995; Kuma et al., 1992a; Oeztuerk et al., 2004). In this study, we found only a small enhancement in soluble Fe with 2kDG ($c_P \approx 2$ nmol L^{-1}). Analysis of recent complexation data for 2kDG (Essington et al., 2005) indicates that it would not be expected to retain Fe in solution under seawater conditions due to the strong interactions with Ca^{2+}.

Phytagel ("Gellan Gum"; (Miyoshi et al., 1996; Nishinari, 1999)) is a sugar-like macromolecule with a mean molecular weight of 490 kDa (Milas et al., 1990) and has been previously found to bind Th(IV) (Quigley et al., 2002) in seawater. Thus we anticipated only a trace amount of ^{55}Fe would pass through the membrane, due to the high molar mass of the ligand, however we surprisingly measured a high concentration ($c_P = 9.54$ nmol L^{-1}). This apparent discrepancy may be due to the ability of some of the long chained molecules to pass through the membrane as coils (Nakajima et al., 1996) and transport Fe with it. However, clogging of the membrane filter by the large phytagel molecules was also an issue here, and this greatly reduced the permeate flow rate and concentration with time.

2.4.3 Implications for ultrafiltration of natural seawater solutions

The results found here have strong implications for the ultrafiltration of natural seawater solutions for the determination of soluble and colloidal Fe without the use of radio-isotopes. The analysis of the retentate and permeate fluxes can be achieved with other methods for stable Fe; such as chemiluminescence (Croot and Laan, 2002; Obata et al., 1993) or ICP-MS techniques (Saito and Schneider, 2006; Wu, 2007). It is clear that in seawater samples with considerable colloidal concentrations there will be retention of these species on the filter membrane and walls. These species are recoverable with a later acid or combined dilute acid/DFB rinse and can be corrected for in the overall mass balance. A potential problem here is the contribution of Fe from the filter apparatus itself, from our preliminary studies on this we have found that an EDTA, DTPA or DFB solution in ultra-pure water passed through the system prior to the sample reduced the blank to very low levels (< 30 pmol L^{-1} - our detection limit with FIA-chemiluminescence (Obata et al., 1993)). The use of strong acids should be avoided as much as possible as in our experience this leaches Fe out of the plastic walls.

If the solution is undersaturated, as most natural samples from the open ocean would be, the problems of wall adsorption should be minimized greatly simplifying the analytical procedures. However, it is critical that measurements (for mass balance purposes) be made as a function of the CF in both the retentate and permeate and that a recovery rinse be employed. We have recently employed a combined Vivaflow-50 and FIA-chemiluminescence system on several cruises in the Atlantic with reasonably good success (Croot et al. in preparation). The only major problem we have encountered so far has been from insufficient cleaning of ultrafilters overloaded with colloidal material (e.g. Saharan dust, colloidal Fe from iron enrichment experiments).

2.4.4 Overall performance of cross-flow filtration system

The overall performance of this cross-flow filtration system for Fe measurements was particularly good as sample processing times were relatively short compared to other cross-flow filtration systems currently available, and the system was easily manageable for a single operator. The problem of colloidal Fe loss on the filter and walls of the system is common to all such ultrafiltration methods but good mass balances can be obtained by employing a recovery rinse as used in this study and by monitoring both the retentate and permeate flow over time. Our results strongly suggest that ultrafilters should not be used in a single pass mode, but instead should only be used in the normal recirculation mode, as critical information would otherwise be lost. While this does significantly increase the processing time compared to conventional filtration systems, it does also provide valuable checks and balances on the behavior of the system being investigated. We also suggest that these filters can be extensively reused, provided attention is paid to the use of recovery and cleaning solutions.

2.5 Conclusions and Recommendations

Our work has shown that good mass balances for Fe can be obtained using an cross-flow filtration system when employing a final rinse to recover Fe adsorbed to the filter membrane. It is also very important to monitor both the retentate and permeate fluxes as a function of CF to determine P_C for the solution as soluble Fe may also be partially retained by the ultrafilter. We conclude that cross-flow filtration systems such as the one employed in our study can provide valuable information on colloidal and soluble Fe in the ocean. Furthermore, we recommend future studies should concentrate on examining the relationship between solubility and iron speciation in the colloidal and soluble phases through the careful use of ultrafiltration techniques such as we described here.

2.6 Acknowledgement

We thank Uwe Rabsch and Petra Krischker for technical support with the radio-isotope work performed in the radio chemistry suite at IFM−GEOMAR. Thanks also to Peter Streu (IFM−GEOMAR) for help in this work. Christina De La Rocha (AWI) is thanked for her comments on earlier versions of this manuscript. The helpful comments of two anonymous reviewers and the associate editor Steven Wilhelm greatly improved this manuscript. This study was supported by Deutsche Forschungsgemeinschaft (DFG) grants CR 145/5 and CR145/9 (to PLC).

Chapter 3

Controls on seawater Fe(III) solubility in the Mauritanian upwelling zone

3.1 Introduction

Iron (Fe) is a micronutrient whose low availability in seawater restricts the growth of phytoplankton over broad swaths of the surface ocean (Boyd et al., 2000; Coale et al., 2004; De Baar et al., 2005; Gervais et al., 2002; Martin et al., 1994; Takeda and Tsuda, 2005; Wells, 2003; De Baar et al., 1990; Sato et al., 2007). Fe in seawater occurs in both dissolved ($Fe_d < 0.2$ μm) and particulate ($Fe_P > 0.2$ μm) phases, and it is believed that 99$\%$ of the dissolved Fe is organically complexed (Rue and Bruland, 1997; Wu and Luther, 1995). The recent advent of microfiltration and ultrafiltration techniques has shown that the dissolved phase consists of both soluble ($Fe_S < 0.02$ μm) and colloidal (0.02 μm $< Fe_C < 0.2$ μm) fractions (Bergquist et al., 2007; Cullen et al., 2006; Nishioka et al., 2005; Wu et al., 2001). Currently it is however not yet fully understood, what are the key controls on the fraction of the dissolved phase which occurs as soluble rather than colloidal Fe.

Measurements of Fe solubility (cFe_S) are performed by adding a saturating amount of Fe to seawater and then determining the concentration of the filtrate that has passed through a 0.02 μm, or smaller, filter. The pioneering works of Kuma et al. (1996, 1992b, 1998a), Liu and Millero (1999, 2002), and Byrne et al. (2005); Byrne and Kester (1976); Byrne et al. (2000), suggest that cFe_S largely depends on temperature, pH, and ligand concentration, with higher concentrations of inorganic soluble Fe possible at lower pHs and temperatures. Fe solubility in both UV irradiated and artificial seawater (i.e. seawater containing no dissolved organic matter (DOM)) at 0.01 nmol L^{-1} between pH 7.5 and 9 has been shown to be lower than in untreated seawater ($cFe_S = 0.5$ nmol L^{-1}; (Liu and Millero, 2002)). This difference can be explained by the existence of natural organic ligands (Kuma et al., 1996; Liu and Millero, 2002; Rue and Bruland, 1995; van den Berg, 1995), which enhance the Fe solubility in seawater by organic complexation of the trace metal.

Concentrations of Fe binding ligands in surface seawater vary from region to region. Coastal

seawater, related to its overall higher biological activity, has significantly higher ligand concentrations (7 to 70 nmol L^{-1}; (Powell and Wilson-Finelli, 2003a; Croot and Johansson, 2000)) than open ocean seawater (0.5 to 6 nmol L^{-1}; (Powell and Donat, 2001; Croot et al., 2004a)). A slight increase in Fe binding ligand concentrations with depth has also been seen in the Atlantic (Powell and Donat, 2001) and ascribed to the release of Fe binding organic ligands during the remineralization of settling organic matter. These results suggest that a significant amount of uncomplexed ligands exists in seawater.

At times, cFe_S appears to be correlated to concentrations of nutrients (e.g., nitrate, phosphate) (Nakabayashi et al., 2002; Tani et al., 2003), possibly due to the release of organic ligands to seawater during the decomposition of sinking particulate organic matter (POM). Fe binding ligands could be released to seawater directly from phytoplankton when the cells are lysed (Gobler et al., 1997; Hutchins and Bruland, 1994; Hutchins et al., 1999b), or indirectly by grazing (Sato et al., 2007). In addition, Fe binding ligands are produced by bacteria (Haygood et al., 1993; Martinez et al., 2000; McCormack et al., 2003) in response to iron limitation and their increase could be associated with the growth of the population of heterotrophic bacteria decomposing the organic matter. Fe-binding ligands may also be directly released to seawater by growing phytoplankton, which may often excrete dissolved organic matter (DOM, as waste product or intentional released), some of which may be able to bind Fe (Fuse et al., 1993).

It is clear that we are a long way off from fully understanding the extent to which organic ligands and other parameters influence the capacity of seawater to hold soluble Fe. In an attempt to shed light on this question, which has implications for the bioavailability and transport of Fe in the surface ocean, we measured the solubility of Fe of seawater in a tropical upwelling zone to understand what processes were important in this region.

3.2 Methodology

3.2.1 Overview of the study site in the Mauritanian upwelling zone

During springtime, when the trade winds blow from the northeast, the Mauritanian upwelling zone is marked by strong upwelling. In summer, however, the winds come more predominantly from the north and upwelling is confined closer to the coast. Our work was performed during Meteor cruise M68/3 in July 2006, when upwelling only occurred close to the coast.

3.2.2 Sampling of subsurface seawater

Samples of seawater between 20 and 200 m were collected using trace metal clean GO-FLO bottles (General Oceanics, Miami, USA) deployed on a Kevlar line. The GO-FLO bottles were transferred into a class 100 clean container where all sample handling was performed. The collected seawater was filtered through a 0.2 μm membrane filter (Sartorius) under nitrogen overpressure (0.2 $-$ 0.3 bar) into 125 mL acid cleaned HDPE bottles (Nalgene).

3.2.3 Sample treatment

Fe solubility measurements were performed immediately using the radioisotope, ^{55}Fe (Hartmann Analytics, Braunschweig, Germany). The experimental setup (described below) was adapted from Kuma et al. (1996). The ^{55}Fe isotope had a specific activity of 157.6 MBq/mg Fe, a total activity of 75 MBq, and was dissolved in 0.1 mol L^{-1} HCl. ^{55}Fe dilution standards were produced with Milli-Q (MQ) water and acidified with quartz distilled (Q) HCl to a pH below 2.

After the addition of ^{55}Fe ($t_0 = 0$ h; total Fe $Fe_T = 20$ nmol L^{-1}; pH 7.9) to each sample, a small subsample was filtered through a 0.02 μm Anotop syringe filter (Whatman) and acidified with (QD) HCl, to keep the Fe from adsorbing to the bottle walls (Fischer et al.,

2007; Schlosser and Croot, 2008). Duplicates of unfiltered and 0.02 μm filtered samples (400 μL) were transferred into 6 mL counting vials to which 4.5 mL of scintillation fluid (Lumagel Plus®) were then added. This procedure was repeated for subsamples taken at 3, 6, 24, 48 and 72 h. Sample storage, treatment and measurement were performed at room temperature (20°C). Counts per minute of ^{55}Fe were made in a scintillation counter (Packard, Tri-Carb 2900TR) and then converted to soluble Fe concentrations, taking into account the activity of the added isotope solution and the dissolved Fe concentration of each sample. The ^{55}Fe technique was chosen to investigate the true capacity of seawater for soluble Fe.

The dissolved Fe concentration (Fe_d)was measured onboard with the luminol chemiluminescence method (de Jong et al., 2000; Obata et al., 1993) in an online flow injection analysis (FIA) system. Macronutrient concentrations (nitrate, nitrite, phosphate and silicate) for each sample were measured on board with an auto-analyzer following the methods outlined in Grasshoff et al. (1999). Dissolved oxygen was also measured on board via classic Winkler titration. Chlorophyll a concentrations were measured via high performance liquid chromatography (HPLC) (Hoffmann et al., 2006). The free pH of the samples was calculated using the CO2SYS software (Lewis and Wallace, 1998) from measured alkalinity, temperature, salinity, and TCO_2 (Steinhoff, T., personal communication).

3.3 Results

3.3.1 Iron solubility in seawater

The solubility of Fe was lowest at the sites located furthest offshore (Station 258 and 261; Figs. 3.1, 3.2 and App. C). At these stations cFe_S generally increased with depth from minimum values at around 40 m. In all cases, cFe_S was higher at deeper depths. The more

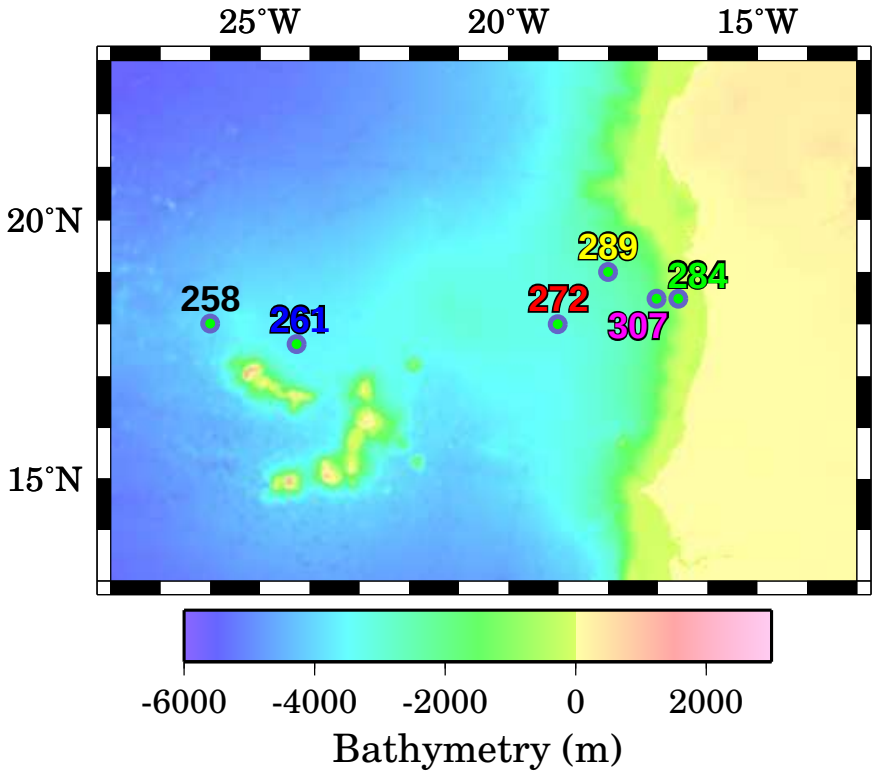

Figure 3.1: *Shown are the sampling positions in the Mauritanian upwelling zone, combined with bathymetric data.*

shoreward casts (261, 284, 289 and 307) showed a Fe solubility minimum at 20 m (Figs. 3.1 and 3.2). As with the offshore sites, Fe solubility at shoreward sites was highest at deeper depths below the pycnocline.

When the data are plotted together, they fall into two distinct groups (Fig. 3.3). In the first group, that of samples taken from depths $\geq$ 40 m, values of cFe_S are greater than 0.3 nmol L^{-1} and show strong linear relationships with *in situ* pH ($R^2 = 0.91$), phosphate concentrations ($R^2 = 0.77$), and apparent oxygen utilization (AOU) ($R^2 = 0.80$) (see also App. C). The shallower samples make up the second group, with values of cFe_S that fall between 0.1 and 0.4 nmol L^{-1} and do not sit on the trend lines. These low concentrations

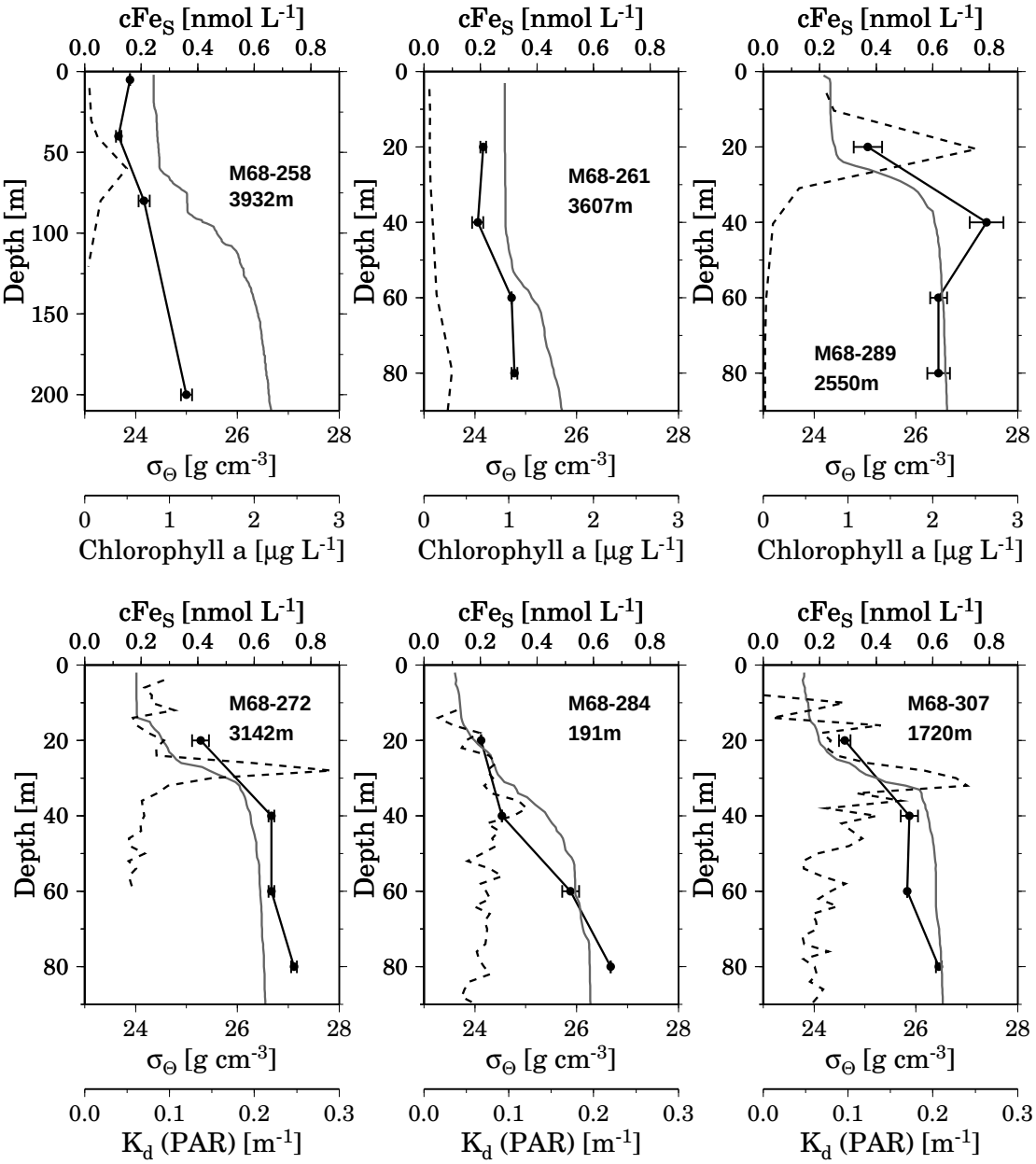

Figure 3.2: *Shown are the results of cFe_S (black squares), density (σ_θ, solid grey line) and chlorophyll a (dashed black line, upper diagrams), and irradiance attenuation coefficient (PAR), K_d (dashed black line, lower diagrams) versus water depth. Note that the upper left picture uses a different depth scale.*

of Fe solubility occur at high values of dissolved oxygen and pH and low values of phosphate of near surface waters.

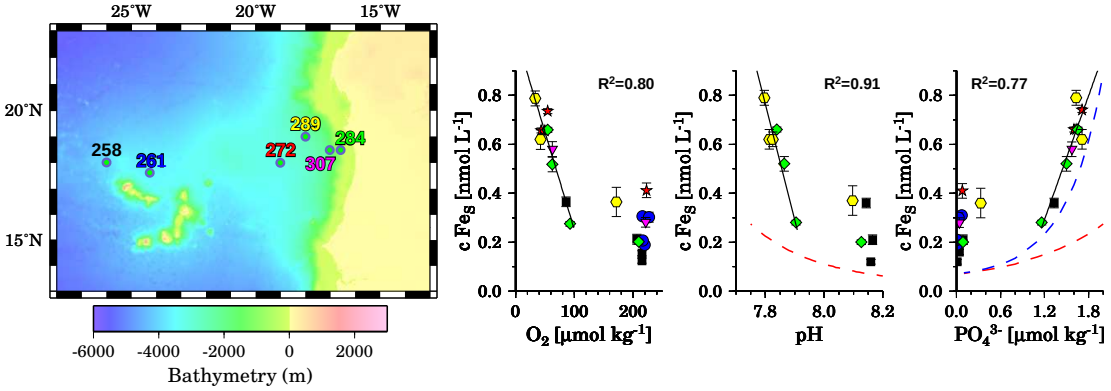

Figure 3.3: *Shown are the sampling positions in the Mauritanian upwelling zone, combined with bathymetric data. Each sampling locations has a different color on the diagrams. All subsurface samples ($\geq$ 40 m) from the onshore casts show a linear correlation of cFe_S with O_2, pH and PO_4^{3-}. The dashed red lines illustrate the capacity of seawater for the inorganic soluble Fe species. The dashed blue line indicates the capacity of seawater for the inorganic and phosphate complexed Fe species.*

3.3.2 Irradiance attenuation coefficient and seawater density

Light irradiance data (irradiance attenuation coefficient (PAR), K_d) are available for three locations (272, 284, and 307) (Fig. 3.2). These data indicate the location of particle maxima in seawater and can be used as an indicator for the potential loss of organic ligands by adsorption onto particle surfaces (Campbell et al., 1997; Mayer, 1999). If adsorption onto particles is the reason for the lower Fe solubility in surface waters, increases in particle abundances as shown by K_d should be associated with decreases in cFe_S. However, this was not observed at all three stations, suggesting that removal of ligands by particle scavenging

is not the main parameter controlling cFe_S and it is likely that photooxidation of organic ligands (Barbeau et al., 2003; Powell and Wilson-Finelli, 2003b) is responsible for the lower cFe_S values in these surface waters.

A distinct minimum in Fe solubility at 40 m at the Open Ocean stations 258 and 261 (Fig. 3.2) was not apparently related to any other measured parameter (chlorophyll a, density (σ_θ), etc.). It appears that this minima represents a region where processes that remove Fe ligands dominates over production terms and it is intriguing that it is immediately above the deep chlorophyll maximums that are found in this oligotrophic waters.

Seawater density (σ_θ) shows a strong positive correlation with cFe_S (Fig. 3.2). This suggests that the pycnocline acts as a strict barrier at these sampling locations, between primary production, above, and remineralisation of biomass, below.

3.3.3 Nutrient regeneration and relationship to cFe_S

The simplest possible explanation for the increasing Fe solubility at greater depths and lower pHs is that the solubility of inorganic Fe is higher at lower pHs. It should also be remembered here that our experiments were all conducted at 20°C and thus the solubility is not dependent on the $in\ situ$ temperature that the samples were collected from. The expected solubility of inorganic Fe ($Fe' = Fe(OH)^{2+} + Fe(OH)_2^+ + Fe(OH)_3 + Fe(OH)^{4-}$) can be calculated using the equations of Liu and Millero (1999) and is shown by the dashed red line in Fig. 3.3. It is clear in Fig. 3.3 that inorganic solubility is insufficient to account for the higher Fe solubility at deeper depths, nor the lower levels of Fe solubility of the near surface, and thus organic complexation is required.

Fe complexing ligands are known to be produced by bacteria or phytoplankton, and released to the environment as metabolites or in the strategy for obtained trace elements necessary for growth. The production/release of organic ligands (e.g. siderophores) by bacteria, however,

is inhibited if cells are Fe-sufficient (Martinez et al., 2003). All the stations in the Mauritanian upwelling zone higher dissolved Fe concentrations at depth ($0.5 - 1.25$ nmol L^{-1}) than in the surface ($0.3 - 0.4$ nmol L^{-1}) were observed. These dissolved Fe concentrations could be considered for many oceanic bacteria and phytoplankton Fe sufficient and suppressive of siderophore production particularly in light of the high aerosol Fe deposition rates and fast Fe turnover time in this region (Croot et al., 2004b).

Alternatively, the changes in Fe solubility may be associated with organic matter remineralization (Nakabayashi et al., 2002; Sato et al., 2007; Kuma and Isoda, 2003; Tani et al., 2003), through the release of ligands into the water. DOM (including Fe-binding ligands) will be released directly into seawater from bacteria and phytoplankton cells following breakage of those cells via zooplankton grazing (Hutchins and Bruland, 1994), viral lysis (Gobler et al., 1997), or bacterial attack with ectoenzymes (Nagata et al., 1998). Similarly, a rise in soluble ligand concentrations (and therefore Fe solubility) could be the result of production by heterotrophic bacteria obtaining their carbon via the oxidation of DOM but coming into Fe limitation. Thus the degradation of organic matter could see the production of siderophores in an effort to obtain Fe to fuel their growth. Finally, binding sites on ligands in the colloidal (Boye et al., 2005) or particulate phases could be converted to the truly soluble phase. This is an important point as though there are few data for iron binding ligands in the soluble and colloidal portions of the dissolved phase, results suggest that the soluble fraction is significantly smaller than the colloidal (Boye et al., 2005; Schlosser and Croot, 2008). Thus comparison between measurements of dissolved ligand concentrations and cFe_S are only indicative as most of the ligand is in the colloidal phase and not in the soluble phase which determines cFe_S.

That it is some process related to remineralization controlling Fe solubility in the samples $\geq$ 40 m depth is strongly supported by the significant correlations between cFe_S and pH, phosphate, and AOU (Fig. 3.3 and App. C). Both the solubilization, via microbial ectoen-

zymes, of Fe-binding materials present in phytoplankton cells and the release of Fe-ligands by bacteria as they grow remain plausible explanations for the observed patterns in Fe solubility (Fig. 3.3 and 3.2).

The high correlation with phosphate also suggests a simple alternative hypothesis for Fe solubility that has been seemingly overlooked – simple inorganic complexation by phosphate. Currently the methods (Rue and Bruland, 1995; van den Berg, 1995) used to measure organic complexation do not consider phosphate complexation and strong phosphate complexation would be interpreted as being organic with present methods. Phosphate could be important when present in higher concentrations than hydroxide. Interestingly data from Khoe and Robins (1988) for Fe-phosphate complexes indicate that these complexes could be significant: $Fe(PO)_4$ (log K = 19.50) and $Fe(HPO)_4^+$ (log K = 9.30). However a closer look at the Khoe and Robins (1988) study shows it was carried out at pH 2 (3 M $NaNO_3$) and there is no available data at seawater pH that would help to explain our correlation between phosphate and cFe_S.

For the sake of examination, the stability coefficients of the Fe-phosphate complexes from Khoe and Robins (1988) were used to calculate the Fe solubility at our sampling sites with respect to phosphate species, pH, and temperature. The dashed blue line in Fig. 3.3 shows the solubility of Fe for phosphate-complexed and inorganic Fe species together. The closeness of the theoretical curve to the data suggests that the higher Fe solubility in the deeper samples could be caused by complexation with phosphate or the formation of a meta-stable ferric phosphate phase. However correlation is not causation and solubility experiments in our lab with UV irradiated high phosphate Southern Ocean waters indicates much lower solubilities in agreement with only hydroxide complexation, seemingly ruling out phosphate as an important complexing agent. Though, the match is striking enough to warrant further study of phosphate-Fe species complexes with a view to assessing their contribution to Fe solubility in deeper waters.

Table 3.1: *The table shows cFe_S/PO_4^{3-} ratios of this and reference studies.*

Location	Filter [μm]	cFe_S/PO_4^{3-} [$*10^3$]	Reference
Mauritanian upwelling zone	0.02	0.68±0.09	This study
Western North Pacific Ocean	0.025	0.14±0.03	[Kuma, et al.,1996]
Eastern Indian Ocean	0.025	0.08±0.01	
Subarctic WN Pacific Ocean	0.025	0.23±0.04	[Kuma and Isoda, 2003]
Subtropical WN Pacific Ocean	0.025	0.18±0.01	
Boundary Zone	0.025	0.23±0.03	
Okhatsk Sea	0.025	0.35±0.04	[Tani, et al., 2003]
Okhatsk Sea	0.025	0.29±0.03	
NWN Pacific Ocean	0.025	0.38±0.04	
NWN Pacific Ocean	0.025	0.34±0.02	

3.3.4 Ratio of cFe_S/PO_4^{3-}

The cFe_S/PO_4^{3-} ratio in the Mauritanian upwelling zone, calculated from the linear part of the cFe_S and phosphate diagram (i.e. essentially the nutricline) is $2-9$ times higher than in studies carried out in the Pacific and Indian Ocean (Kuma and Isoda, 2003; Kuma et al., 1996; Tani et al., 2003) (Table 3.1). However, in these previous studies cFe_S/PO_4^{3-} ratios were estimated for deep water masses (i.e. between 80 and 800 m) whereas the Mauritanian samples come from the upper 80 m of the water column. The higher Fe solubility with respect to phosphate concentrations in our shallower samples are more likely from the presence of fresher, more labile dissolved organic matter released in the more productive Mauritanian upwelling zone, than in deeper waters, below 100 m.

3.4 Conclusion

In the Mauritanian upwelling zone, Fe solubility was lower in the upper mixed layer (20 m) than directly below the mixed layer (40 – 80 m). The lower Fe solubility in the surface appears to be tied to the photooxidation of organic ligands. A significant correlation of pH, oxygen, and phosphate with cFe_S of subsurface samples strongly suggests the conversion of POM to soluble organic Fe binding ligands. The exact mechanism of this process, be it via grazing or bacterial degradation is unclear at present and the further investigation of this pathway and elucidation of the mechanism and fluxes is clearly required if we are to truly understand what controls iron solubility in the ocean.

3.5 Acknowledgements

The authors would like to appreciation to the crew of the R.V. Meteor (M68/3). Special thanks to Peter Streu, Frank Malien, and the Chief Scientist Arne Körtzinger. Many thanks to Christina De La Rocha for her useful comments. This work was supported by a DFG grant awarded to PLC (CR145/5−1).This work is a contribution to SOPRAN (German SOLAS).

Chapter 4

Influence of iron binding ligands on Fe(III) solubility in a mesoscale iron fertilization experiment (EIFeX) in the Southern Ocean

4.1 Introduction

It is now widely accepted that in large parts of the ocean, i.e. high nutrient, low chlorophyll (HNLC) regions, primary production is limited by the availability of iron (Fe). Since this was demonstrated back in the late 1980's in bottle incubations (De Baar et al., 1990; Martin and Fitzwater, 1988) and in subsequent mesoscale $in\ situ$ Fe fertilization experiments (Boyd et al., 2000; Coale et al., 2004; De Baar et al., 2005; Gervais et al., 2002; Takeda and Tsuda, 2005; Wells, 2003), the operational definition has been that Fe exists in only two phases in seawater, dissolved and particulate (as defined by what passes through an 0.2 μm filter and what does not). Recent studies have shown the existence of soluble (Fe_S) and colloidal Fe phases (Fe_C) within the dissolved fraction (Bergquist et al., 2007; Cullen et al., 2006; Nishioka et al., 2005; Wu et al., 2001). The vast majority of the dissolved Fe (Fe_d) is organically complexed (Rue and Bruland, 1997; Wu and Luther, 1995) further complicating the picture.

Both the dissolved and particulate size fractions of Fe in seawater are derived from terrigenous materials via aeolian deposition (Jickells et al., 2005; Baker et al., 2006a), river inputs (Buck et al., 2007; Allard et al., 2004), the resuspension of material from continental shelf sediments (Elrod et al., 2004; Johnson et al., 1999), and the melting of ice bergs loaded with sediments and dust (Raiswell et al., 2008a,b). Upwelling of Fe containing waters is also an important source of Fe to surface waters (Chase et al., 2005; Bruland et al., 2005; Fitzwater et al., 2003).

The major external input of Fe to the Southern Ocean is dust (Wagener et al., 2008) blown off of southern hemisphere land masses (Patagonia, the Kerguelen Islands, and Australia) and the input of dissolved Fe by wet deposition (Halstead et al., 2000). The solubility of Fe from deposited dust is greatly variable, ranging between 2 and 20% (Baker and Jickells, 2006; Baker et al., 2006b), depending on the origin of the dust and the capacity of the

seawater to hold dissolved Fe (Baker and Croot, 2009). The full extent of this natural Fe fertilization and its exact impact on primary production and nutrient cycling in the Southern Ocean are not yet fully understood (Pollard et al., 2009; Blain et al., 2007; Planquette et al., 2007).

Organic Fe-complexing ligands have been found to be produced by bacteria under Fe limitation (Martinez et al., 2000), and to be released to seawater directly from phytoplankton, either when the cells are lysed (Gobler et al., 1997; Hutchins and Bruland, 1994), or indirectly by grazing (Sato et al., 2007). Fe-binding ligands may also be directly released to seawater by growing phytoplankton, which may often excrete dissolved organic matter (DOM, as waste product or intentionally released), some of which may be able to bind Fe (Fuse et al., 1993). These organic compounds are low molecular weight (LMW) molecules that form six-fold coordinated complexes with freely available Fe.

The concentration of these dissolved ligands in open ocean seawater ($1 - 4$ nmol L^{-1}) (Boye et al., 2005) exceeds that of dissolved Fe ($0.02 - 0.5$ nmol L^{-1}), perhaps providing excess binding capacity useful for coping with episodic inputs of Fe such as from dust events (Wagener et al., 2008; Erickson III et al., 2003; Cassar et al., 2007).

In oxygenated seawater, the thermodynamically favoured redox state of inorganic Fe (Fe(III), hydrolyzed Fe) is poorly soluble ($20 - 500$ pmol L^{-1}) (Liu and Millero, 1999). Organic Fe complexes are more soluble than inorganic Fe species and therefore increase both the residence time and overall concentration of soluble and of dissolved Fe in seawater. Hutchins et al. (1999b) further suggested that because the organic complexation of Fe increases the total amount of dissolved Fe species, it increases the total amount of Fe that is biologically available. This may be true, but at the present time there are no data to say whether ligand-bound dissolved Fe is more, equally, or less bioavailable than dissolved Fe that is not ligand-bound (Chen and Wang, 2001; Hutchins et al., 1999a; Kuma et al., 2000).

Measurements of the capacity of seawater to hold soluble Fe (cFe_S, Fe solubility) suggest

that cFe_S depends on temperature, pH, and ligand concentrations (Byrne et al., 2005; Kuma et al., 1996; Liu and Millero, 1999, 2002). Inorganic Fe solubility increases with decreasing temperature and pH tied to the associated drop in the concentration of hydroxyl ions, which promote the formation of the particulate Fe hydroxides. That ligands enhance Fe solubility is shown by the 50-fold lower solubility of Fe (0.01 nmol L^{-1}) in UV-irradiated and artificial seawater lacking dissolved organic matter than in untreated seawater (0.5 nmol L^{-1}) (Liu and Millero, 2002).

The Fe redox cycle in the euphotic zone is also effected by photochemical reactions (Barbeau et al., 2001, 2003; Wells et al., 1991). Sunlight of wavelengths between 300 and 400 nm (UVA and UVB) can penetrate a reasonable distance into the water column, destroying organic ligands, reducing Fe(III) complexed to organic ligands (Barbeau et al., 2003), and reducing colloidal, inorganic Fe(III) to Fe(II) (Wells et al., 1991). This Fe(II), although more soluble and bioavailable than Fe(III), is thermodynamically unstable and is quickly reoxidized by O_2 and H_2O_2 or complexed by organic ligands. Organic ligands which are only partly destroyed by UV-irradiation may still complex freely available Fe by forming organic Fe complexes that are weaker than the ones made by unaltered ligands (Barbeau et al., 2003).

We present here ligand concentrations and Fe solubility measured during a mesoscale Fe fertilization experiment in the Southern Ocean (EIFeX) in an attempt to investigate the impact of artificial Fe fertilization on ligand cycling and Fe solubility.

4.2 EIFeX settings

The EIFeX study was performed in the Southern Ocean in a mesoscale cyclonic eddy embedded in a meander of the Antarctic Polar Front. For more details on the Fe fertilization in EIFeX (Fig. 4.1) see Croot et al. (2007, 2008), and Hoffmann et al. (2006). The ten sampling sites reported in this chapter were located within the patch of fertilized water which

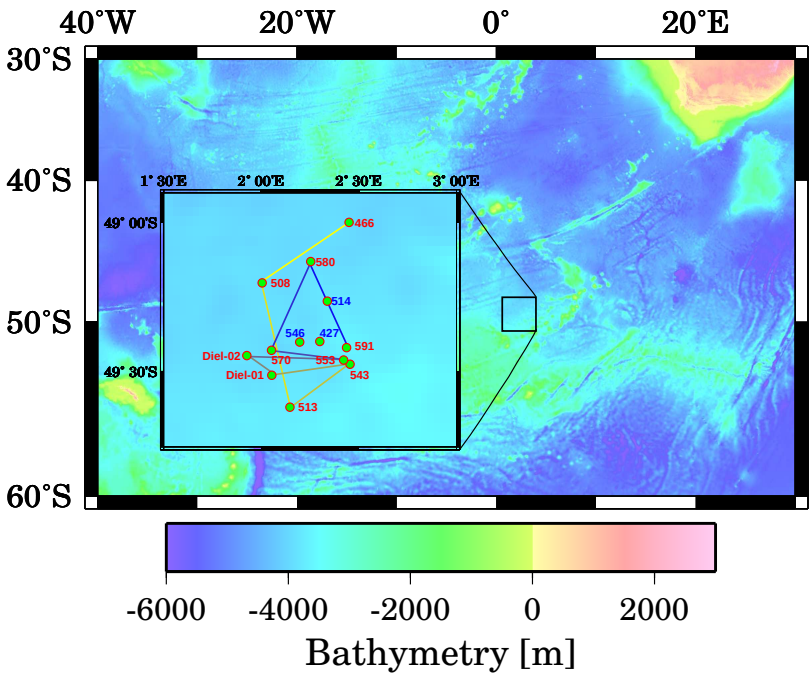

Figure 4.1: *The picture shows the cruise track (equivalent to the eddy motion and water mass transport, respectively) and sampling locations during EIFeX. The red-labeled numbers are marking stations located inside the patch (blue - outside the Fe patch).*

was identified using several criteria: elevated Fe concentrations, elevated quantum yield of photosynthesis (Fv/Fm), diminished concentrations of pCO_2 and elevated chlorophyll a concentrations (Smetacek and participants, 2005). Two stations conducted before the Fe fertilization and two stations located outside of the fertilized patch served as controls.

4.3 Methodology

4.3.1 Water sampling

Teflon-coated 8 liter PVC GO-FLO bottles (General Oceanics, Miami, FL, USA) deployed on a Kevlar line were used for the sampling of subsurface seawater. Immediately upon

recovery the bottles were transferred to a Class 5 clean container (Clean Modules, UK). There the seawater was filtered through 0.2 μm in-line filter cartridges (Sartorious Sartobran filter capsule 5231307H5) by N_2 overpressure into acid-cleaned 100 mL HDPE bottles for Fe solubility measurements and into 1 L LDPE bottles for Fe-ligand measurements. All Fe solubility and Fe ligand samples were frozen onboard at -20°C, shipped frozen, and then analyzed in laboratories at IFM-GEOMAR, Kiel.

4.3.2 Instruments and reagents

The Fe solubility measurements were performed with the radioactive Fe isotope ^{55}Fe (received from Hartmann Analytics, Braunschweig, Germany), using a method introduced by Kuma et al. (1996). The ^{55}Fe isotope used in this study had a specific activity of 157.6 MBq/mg Fe, a total activity of 75 MBq and was dissolved in 0.1 M HCl. ^{55}Fe dilutions were produced with 18 MΩ water and were acidified with quartz distilled HCl (Q-HCl) to a pH lower than 2. The radioactive decay of ^{55}Fe was measured using a liquid scintillation counter (Packard, Tri-Carb 2900TR).

For the determination of natural, organic ligand concentrations, competitive ligand equilibration / adsorptive cathodic stripping voltammetry (CLE/ACSV), was used. The voltammetric apparatus consisted of a voltammeter with a static mercury drop electrode (Metrohm 757 VA Computrace), a double-junction Ag/saturated AgCl reference electrode with a salt-bridge filled with 3 M KCl and a glass rod as a counter electrode. Fe standards were prepared with Q-HCl and 18 MΩ water. In our experiment, 2-(2-thiazolylazo)-p-cresol (TAC) was used as competitive ligand and N-(2-hydroxyethyl) piperazine-N';-2-propanesulfonic acid (EPPS) as a buffer to hold seawater at pH 8. Both substances were acquired from Sigma-Aldrich. The TAC solution, as described in Croot and Johansson (2000), was prepared in HPLC grade methanol and EPPS with 1 M NH_4OH.

4.3.3 Fe solubility measurements

After the addition of ^{55}Fe ($t_0 = 0$ h) to a defined concentration of $^{55}Fe_T = 20$ nM, a small subsample of the treated seawater sample was taken in a Teflon syringe and filtered through a 0.02 μm Anotop syringe filter that had been flushed and filled with 18 MΩ ultrapure water. The first $6 - 7$ mL of the filtrate were discarded to avoid dead volume artifacts. The next $1 - 2$ mL were filtered, immediately placed in a 60 mL acid-cleaned Teflon bottle, and acidified with Q-HCl to avoid losses to wall sorption. Duplicates of filtered and unfiltered samples were transferred into counting vials to which 4.5 mL of counting cocktail (Lumagel Plus®) were added. The same procedure was repeated for subsamples taken after 3, 6, 24, 48 and 72 h. After filtration and cocktail addition, the vials were placed in a liquid scintillation counter and counted for at least 30 minutes. Recorded decays were converted to Fe concentrations and corrected for the $in\ situ$ dissolved Fe concentration. All work was performed at 20°C. Some samples were also measured at 4°C ($in\ situ$ seawater temperature) to investigate the kinetics of Fe solubility at different temperatures.

4.3.4 Fe-ligand measurements

Subsamples (20 mL) of each seawater sample were pipeted to a series of 10 Teflon bottles (Croot and Johansson, 2000). 100 μL of 1 M EPPS solution and the Fe standard solution were added, to yield concentrations from 0 to 7.16 nmol L^{-1} Fe. The added Fe was allowed to equilibrate with the natural organic ligands for one hour at room temperature (20°C). 20 μL of 10 mmol L^{-1} TAC, as competitive ligand, were added and the sample was left to equilibrate for 4 hours at 4°C. The samples were then transferred to the voltammeter and put into a temperature-controlled, quartz glass cell cup held at 4°C for the voltammetric measurement. The measurements began with a gas purge for 4 minutes with dry nitrogen gas to remove dissolved oxygen from the sample. In the second step, $Fe(TAC)_2$ complexes

that had formed were adsorbed onto a fresh Hg drop by applying a potential of -0.4 V for 4 minutes and stirring the sample. After the electrolysis, stirring was stopped and the potential was scanned by the cyclic voltammetry mode from -0.4 to -0.9 V at 2 V/s. After each measurement the cell cup was rinsed with 18 MΩ water and the samples were run in duplicate in order of increasing iron concentration.

Kinetic approach

Kinetic Fe-TAC measurements of EIFeX samples were performed to determine the formation (k_f) and dissociation constant (k_d) of the FeL complex. Therefore, 200 mL of sample were transferred in a Teflon bottle and pH stabilized with EPPS. At the beginning of the experiment (t_0) Fe was added to a defined concentration of 17.9 nM. Subsequently, a small subsample (20 mL) was pipeted in a separate Teflon bottle and treated with 20 μL of a 10 mM TAC solution. This subsample was than transferred in the quartz glass cell cup held at 4°C for the voltammetric measurement. The voltammetric measurements were performed as described above for normal organic Fe ligand titration. After the measurement was done, the subsample was passed back in the Teflon bottle and a new subsample was taken out of the feed solution and processed as described above for subsample number one. After subsample two was measured, the first subsample was remeasured. After every completed cycle, a new subsample was transferred in a new teflon bottle, treated with TAC, and voltammetrically measured several times.

4.3.5 Theory of Fe-ligand complexation

The CLE−CSV method has been described previously by Rue and Bruland (1995), and Croot and Johansson (2000). A short introduction is given below. The mass balance for Fe in

seawater is shown in Eq. 4.1.

$$[Fe_T] = [Fe'] + [FeL] \tag{4.1}$$

$[Fe_T]$ represents the total amount of Fe, $[Fe']$ all the inorganic Fe species (e.g. hydrolyzed species) and $[FeL]$ the amount of complexed Fe by natural organic ligands. Eq. 4.2 shows the formation and dissociation reaction of organically complexed Fe.

$$Fe' + L \leftrightarrow FeL \tag{4.2}$$

The conditional stability constant of the organic Fe complex, with respect to Fe', can be expressed with the equilibrium constant equation of the formation reaction (shown above).

$$K_{Fe'L} = \frac{[FeL]}{[Fe'][L]} \tag{4.3}$$

To convert $K_{Fe'L}$ to $K_{Fe^{3+}L}$ (conditional stability constant of FeL with respect to dissolved Fe^{3+}), the inorganic side reaction coefficient $\alpha_{Fe'}$ (10^{10}, (Hudson et al., 1992)), can be used. After the addition of TAC the new mass balance of iron can be expressed as:

$$[Fe_T] = [Fe'] + [FeL] + [Fe(TAC)_2] \tag{4.4}$$

where the TAC complexation of Fe' can be formulated as:

$$\beta'_{Fe(TAC)_2} = \frac{[Fe(TAC)_2]}{[Fe'][TAC]^2} \tag{4.5}$$

The sensitivity, S, which is the relationship between the voltammetrically measured peak current and the concentration of $Fe(TAC)_2$, in the linear part of the titration curve. The sensitivity varies strongly between seawater samples from coastal and open ocean environments. In our study, S was calculated for all measured samples, by the following equation:

$$S = \frac{i_P}{[Fe(TAC)_2]} \tag{4.6}$$

$\alpha_{Fe(TAC)_2}$ is the side reaction coefficient for $Fe(TAC)_2$ with respect to Fe' and can be formulated as:

$$\alpha_{Fe(TAC)_2} = \frac{[Fe(TAC)_2]}{[Fe']} = \beta'_{Fe(TAC)_2} * [TAC]^2 \tag{4.7}$$

$[Fe']$ can then easily calculated by the relationship:

$$[Fe'] = \frac{i_P}{S\alpha_{Fe(TAC)_2}} \tag{4.8}$$

The side reaction coefficient of Fe for all naturally occurring ligands is related to the concentration of $[Fe']$ by the relationship:

$$\frac{[Fe']}{[Fe_T] - [Fe(TAC)_2]} = \frac{1}{1 + \sum K_i L_i'} \tag{4.9}$$

The measured data were analyzed with a single ligand model, which was a nonlinear fit to a Langmuir adsorption isotherm. This model was first detailed described in detail by Gerringa et al. (1995). The single ligand model is derived from Eq. 4.3, where $[L_T] = [L'] + [FeL]$. The rearrangement of Eq. 4.3, 4.4 and 4.9 yields to a reciprocal Langmuir isotherm:

$$\frac{[FeL]}{[Fe']} = \frac{K[L_T]}{1 + K[Fe']} \tag{4.10}$$

For this study, calculations were performed by an executable LabView© fitting program (Version: Ligfitv2.4; programmed by Peter L. Croot, IFM-GEOMAR). The calibration of the side reaction of TAC at pH 8 in seawater was previously described by Croot and Johansson (2000) and is not shown here.

4.3.6 Reaction kinetics

The kinetic approach of voltammetric FeL measurements was first described for the artificial ligand 1N2N by Wu and Luther (1995) and Witter et al. (2000). For this experiment, TAC was used to measure the dissociation rate (k_d) and the formation rate constant (k_f) of the FeL complex. With both rate constants the conditional stability constant ($K_{Fe'L}$) can be easily calculated.

The formation rate constant (k_f)

The formation rate constant (k_f) of the FeL complex can be calculated by the decreasing amount of free inorganic Fe'. Prior works used the well established initial rate theory (Eq. 4.11) (Wu and Luther, 1995; Witter and Luther, 1998). The "rate" was calculated by the initial (within the first couple of minutes) decrease in Fe concentration detected as $Fe(TAC)_2$.

$$k_f[Fe][L] = rate[Ms^{-1}] \tag{4.11}$$

where $[Fe]$ is the added Fe and $[L]$ the measured ligand concentration. Following just this theory implies that any other slower formation rate information are not be recognized. Please find more about this in the result and discussion section.

The dissociation rate constant (k_d)

The dissociation rate constant (k_d) was determined using the steady state approximation from the substitutional reaction:

$$FeL + 2(TAC) \rightarrow Fe(TAC)_2 + L \tag{4.12}$$

Eq. 4.12 can be divided in two separate equations: the dissociation and formation of the FeL complex and the formation of the Fe(TAC)$_2$ complex:

$$FeL \underset{k_f}{\overset{k_d}{\rightleftharpoons}} Fe' + L \tag{4.13}$$

$$Fe' + 2TAC \overset{k_2}{\rightarrow} Fe(TAC)_2 \tag{4.14}$$

Since Fe' is very reactive in the presence of TAC, any generated Fe' by the dissociation of the FeL complex, will react very quickly with TAC. Accepting that Fe' will be very small and applying the steady state approximation:

$$0 \approx \frac{\delta[Fe']}{\delta t} = k_d[FeL] - k_f[Fe'][L] - k_2[Fe'][TAC'] \tag{4.15}$$

leads to:

$$[Fe'] = \frac{k_d[FeL]}{k_f[L] + k_2[TAC']} \tag{4.16}$$

Eq. 4.17 is the rate law of the formation of $Fe(TAC)_2$ from Fe' (Eq. 4.12):

$$-\frac{\delta[FeL]}{\delta t} = \frac{\delta[Fe(TAC)_2]}{\delta t} = k_2[Fe'][TAC'] \tag{4.17}$$

Substituting Eq. 4.17 into Eq. 4.16 gives:

$$\frac{-\delta[FeL]}{\delta t} = \frac{\delta[Fe(TAC)_2}{\delta t} = \frac{k_2[TAC']k_d[FeL]}{k_f[L] + k_2[TAC']} \tag{4.18}$$

Assuming, that k_f and k_2 are similar, that the rate limiting step is the dissociation of FeL (TAC independent), and that $[TAC']$ (1 x 10^{-5} M) is much larger than $[L]$ (2 x 10^{-9} M), then $k_f[L] \ll k_2[TAC']$ and Eq. 4.18 reduces to:

$$\frac{-\delta[FeL]}{\delta t} = k_d[FeL] \tag{4.19}$$

The integration of Eq. 4.19 gives:

$$ln[FeL] = k_d t \tag{4.20}$$

A plot of ln[FeL] versus time allows than for the calculation of k_d. With both rate constants it is now possible to calculate the conditional stability constant ($K_{Fe'L}$) for the FeL complex.

$$K_{Fe'L} = \frac{k_f}{k_d} = \frac{[FeL]}{[Fe'][L]} \tag{4.21}$$

Using $\alpha_{Fe'}$ (10^{10}, (Hudson et al., 1992)), the conditional stability constant with respect to dissolved Fe^{3+} can be calculated.

$$K_{Fe^{3+}L} = \alpha_{Fe'} * K_{Fe'L} \tag{4.22}$$

4.4 Results

4.4.1 Dissolved Fe

On two different occasions during the EIFeX experiment, $Fe(SO)_4$ was injected into the seawater. The first addition increased the dissolved Fe concentration at 35 m from 0.2 nmol L^{-1} to 0.69 nmol L^{-1} (as measured at station 466; App. D). Elevated concentrations of dissolved Fe at station 466 persisted for several days in this upper mixed layer. Between 35 and 120 m (the deepest depth sampled), no significant change was observed in [Fe_d], and the concentrations remained similar to concentrations present in waters outside of the fertilized patch (station 427).

On day 9, in between the first and second Fe infusion, there was a storm which drove convective mixing down to nearly 100 m (as shown from the chlorophyll fluorescence at day 10 on Fig. 4.2). Rather than homogenizing Fe_d concentrations throughout the mixed layer, however, this mixing event produced Fe concentrations that alternated from slightly higher to slightly lower values with depth (App. D). A similar zig-zag pattern was seen for other parameters, e.g., DOM (I. Peeken, pers. comm.), suggesting this is not just analytical noise. However, this obvious structure cannot be explained so far.

One day after the second Fe infusion, performed at day 14 of the experiment, an elevated concentration of dissolved Fe of 0.5 nmol L^{-1} was found at 55 m depth (station 513). Above and below that depth, however, [Fe_d] were essentially at background levels (0.2 - 0.3 nmol L^{-1}) (App. D).

In the following days of the experiment (days 21 and 28), concentrations of Fe_d in the upper mixed layer decreased slowly, but remained higher than before the infusion or outside the patch. The last three stations (St. 570, 580, and 591) at days 31, 33 and 36, which were sampled down to 300 m, had two obvious maxima in Fe_d, one in the upper mixed layer and the other below 150 m. All three stations showed a slightly different maximum at 300 m.

4.4.2 Fe solubility

Although Fe fertilization had a clear biological impact (e.g., chlorophyll fluorescence notably increased; Fig. 4.2, App. D), Fe fertilization did not initially have a strong impact on Fe solubility (Fig. 4.2). Samples collected during the experiment, but located outside the patch (station 514), showed slightly higher Fe solubility in the upper mixed layer than at 120 m (0.35 vs. 0.10 nmol L^{-1}). Inside the patch, 5 days after the first infusion, Fe solubility was also highest in the upper mixed layer (0.41 vs. 0.20 nmol L^{-1} at depth).

This pattern was disrupted, at least inside the patch (there is no data for outside the patch), by a storm on day 9. The high shear force generated by this storm ($>$ 9 on the Beaufort scale) induced mixing and resulted in an almost constant Fe solubility in the first 120 m of the water column (0.26 nmol L^{-1}). The were two other storms (days 20 and 35), both of which broke down the upper to lower mixed layer differences in cFe_S.

The second Fe infusion took place on day 14 at the same part of the eddy where the first infusion was carried out. Samples taken one day later showed a minimum in Fe solubility inside the patch of 0.18 nmol L^{-1} in the upper mixed layer and higher Fe solubility at depths between 50 and 120 m (average of 0.34 $\pm$ 0.03 nmol L^{-1}). The chlorophyll fluorescence also increased rapidly at this time (Fig. 4.2).

On day 20, 6 days after the second infusion, a third storm came through. Sampling on day 21, showed that the storm homogenized Fe solubility values throughout the mixed layer again (average values of 0.30 $\pm$ 0.05 nmol L^{-1}). Samples taken inside the patch (day 36, station 591) after a weaker storm on day 35 also showed fairly uniform cFe_S values throughout the mixed layer. The average mixed layer cFe_S was 0.36 $\pm$ 0.03 nmol L^{-1} at this time, giving the entire mixed layer a higher total capacity for soluble Fe than at any other time during the experiment.

Figure 4.2: *Shows Fe solubility (cFe_S), ligand concentration [L] and chlorophyll fluorescence versus depth of one station outside the patch (station 546), one station (427) in the selected eddy, before the Fe infusion, and 8 stations performed after Fe injection, located inside the patch.*

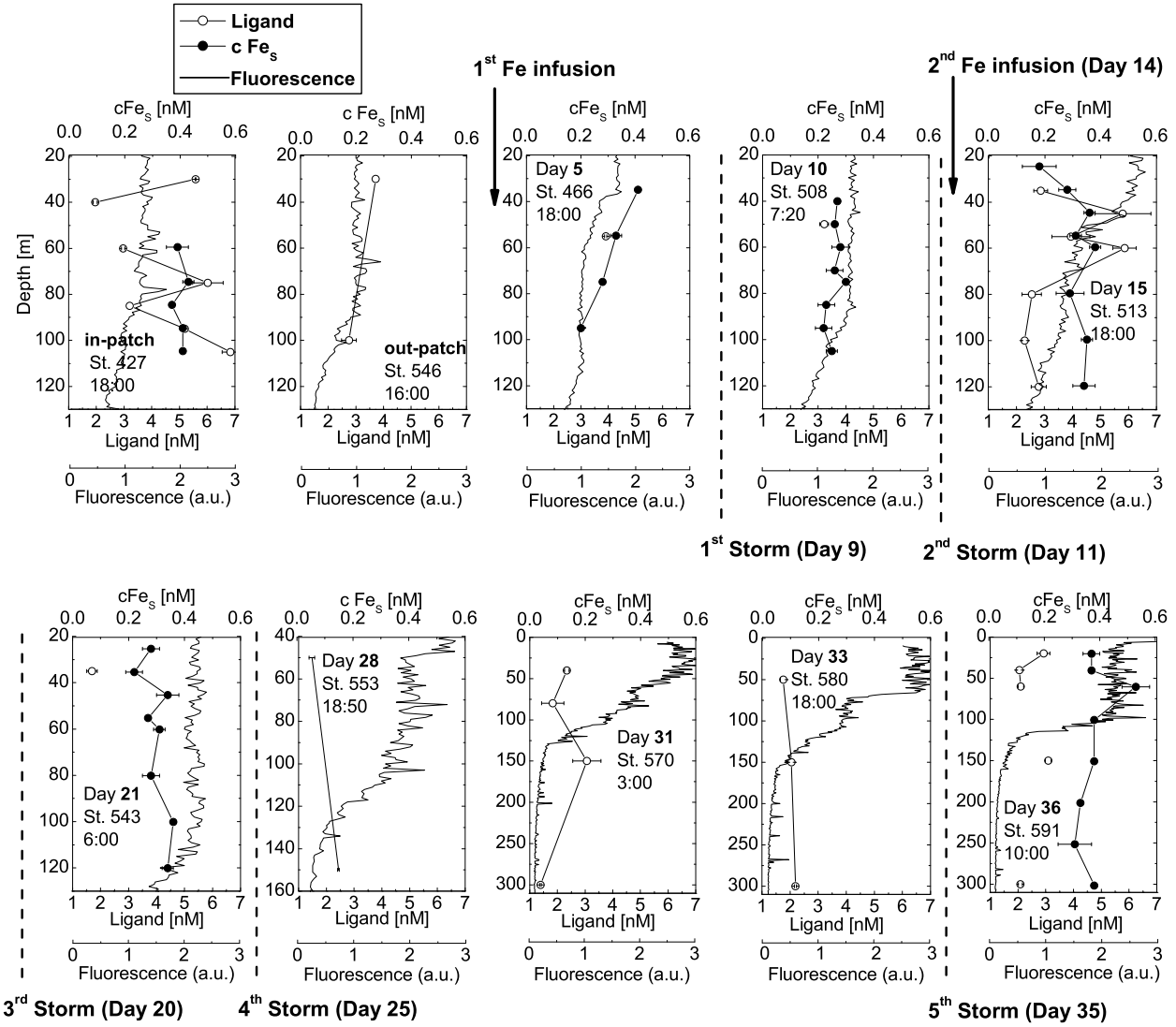

4.4.3 Organic ligands

Outside the Fe fertilized patch, at station 546, concentrations of natural, organic ligands, which have a strong influence on Fe solubility, were higher in near surface waters (3.72 nmol L^{-1} at 30 m), than in deeper waters (2.75 nmol L^{-1} at 100 m). Ligand concentrations inside the patch slightly increased to 3.9 nmol L^{-1}) after the first Fe infusion.

One day after the second Fe infusion, organic ligand concentrations in the patch showed dramatic changes between 40 and 70 m at station 513. At these depths, ligand concentrations alternated between 4 nmol L^{-1} and 6 nmol L^{-1}, an oscillation comparable with the alternation of Fe solubility values in the same part of the water column (Fig. 4.2). Above 35 m and below 70 m, nearly constant ligand concentrations (1.63 $\pm$ 0.26 nmol L^{-1}) were found.

After a third and a fourth storm (days 20 and 25), ligand concentrations dropped down to much lower values in the surface (1.69 $\pm$ 0.16 nmol L^{-1}) and displayed slightly higher values at depth (between 2 and 3 nmol L^{-1}). These rather low concentrations relative to the high ligand values found at station 513 persisted until the end of the experiment. However, station 591, sampled one day after the last storm event, showed a slightly increased ligand concentration (3 nmol L^{-1}) at 20 m depth and nearly constant values of 2 nmol L^{-1} at deeper depths.

4.4.4 Diel cycle of Fe solubility

Diel cycle stations, inside the fertilized patch, were performed during EIFeX to investigate possible diurnal cycles of Fe solubility, something which has not been studied previously. Fe solubility results (Fig. 4.3) show changes in Fe solubility at 20 and 60 m water depth. At both stations, which were performed on 2 consecutive days, there was a slight decrease in Fe solubility at both depths during the day. A decrease was also seen at 40 m but it was

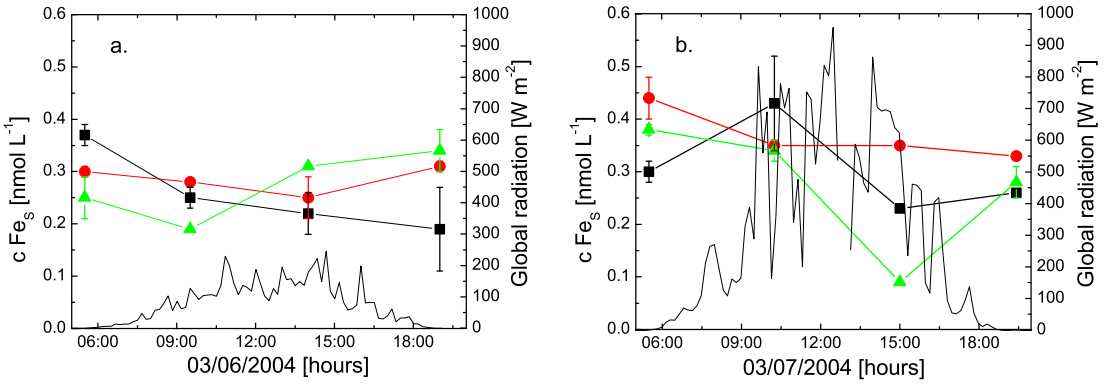

Figure 4.3: *The illustration shows the diel cycle results of Fe solubility measurements on 2 consecutive days during EIFeX in the water column (black squares – 20 m, red circles – 40 m, green triangles – 60 m). Fe solubility is plotted versus time. Additionally, is shown the measured global radiation strength during the day.*

not as strong. After sunset a slight increase in Fe solubility was seen for both diel cycle stations. However, seawater from 20 and 60 m showed again a bigger amplitude of cFe_S, than seawater samples from 40 m.

These data are shown in Fig. 4.3 alongside data for local sunlight which had been measured onboard of the research vessel R.V. Polarstern. The first diel cycle station was carried out on a day that had an approximately 3 – 4 times lower global radiation flux (≈200 W m^{-2} at 12 p.m.) than the day of the second diel cycle station (≈700 W m^{-2} at 12 p.m.). The effect of global radiation on Fe solubility was of special interest since certain wavelengths of UV radiation are thought to destroy organic ligands (Barbeau et al., 2003) and reduce Fe(III) to the more bioavailable Fe(II) species (Croot et al., 2008).

4.4.5 Kinetic approach

Fe solubility measurements

For the Fe solubility experiment, small subsamples were taken over 3 days (72 h) and filtered through 0.02 μm syringe filters in an attempt to study the equilibrium between colloidal and soluble Fe in a kinetic approach to the study of Fe solubility and the exchange of radiolabeled with non-radiolabeled Fe in FeL complexes. Fe solubility results from Kuma et al. (1996) have shown a decrease of the radiolabeled Fe in the soluble Fe fraction,suggesting the transformation of the well soluble $Fe(OH)_3$ species to the amorphous and insoluble FeOOH fraction over the duration of the experiment. However, our solubility experiments showed an exponential increase of the Fe solubility (dashed black line in Fig. 4.4 a.). The obtained data could be described by the following equation:

$$cFe_S = cFe_{S,t0} + (cFe_{S,max} - cFe_{S,t0}) * \left(1 - e^{-k_{obs,2} * t}\right) \tag{4.23}$$

where $cFe_{S,t0}$ is cFe_S at the time where the first measurement was performed, $cFe_{S,max}$ the maximum Fe solubility , t the time and $k_{obs,2}$ the rate constant of the reaction. The theoretical approach shows that two different reactions appear at the same time. One reaction is the complexation of radiolabeled Fe with available organic ligands.

$$^{55}Fe + L \rightleftharpoons ^{55}FeL \tag{4.24}$$

If that this reaction is very fast and takes place just in the first minutes of the experiment, it can not be measured by our technique because each sample takes 15 minutes to be counted in the scintillation counter. The other reaction is the exchange of ^{55}Fe with non-radiolabeled Fe in existing organic complexes.

$$^{55}Fe + FeL \overset{k_{obs,2}}{\rightleftharpoons} Fe + ^{55}FeL \tag{4.25}$$

There is clear evidence for the occurrence of this exchange reaction between dissolved ^{55}Fe and organically complexed Fe. Assuming, the formation of non-radiolabeled FeL complexes can be neglected, since the ^{55}Fe concentration is much higher than the natural Fe concentration and the dissociation of FeL complexes is the rate-limiting step for ^{55}Fe complexation, the observed rate constant is equivalent to the dissociation constant (k_d) of FeL complexes. The calculated $k_{obs,2}$ values (4.45 $\pm$ 1.16 x 10^{-5} s^{-1}) are in good agreement with literature values of k_d (3.06 x 10^{-5} s^{-1} (Wu and Luther, 1995); 3.92 x 10^{-5} s^{-1} (Witter and Luther, 1998)).

The experiment was performed for some samples (n = 7) at both 4 and 20°C to also examine the influence of temperature on Fe solubility kinetics. The lower temperature, here 4°C, did not cause significantly higher cFe_S ((n = 7) 4°C: cFe_S = 0.514 $\pm$ 0.074 nmol L^{-1}; 20°C: cFe_S = 0.523 $\pm$ 0.089 nmol L^{-1}). This is not in accord with the model of Liu and Millero (1999), which projected a higher inorganic Fe solubility at lower temperatures ($\approx$ 0.5 nmol L^{-1}), caused by a higher pK_W. Similarly to cFe_S, the values of the rate constants $k_{obs,2}$ did not significantly vary with temperature ((n = 5) 4°C: $k_{obs,2}$ = 9.60 $\pm$ 4.28 x 10^{-5} s^{-1}; (n = 20) 20°C: $k_{obs,2}$ = 4.45 $\pm$ 1.16 x 10^{-5} s^{-1}).

During this experiment, the total amount of radiolabeled Fe in the feed solution was also measured (^{55}FeF). The feed solution showed decrease in concentration of radiolabeled Fe over the duration of the experiment down to 40 - 60% of the initial concentration. This loss can be explained by an increasing amount of adsorption of Fe onto the walls of the sample bottles over the duration of the experiment (Fig. 4.4 b.). The sorption of uncharged molecules, like $Fe(OH)_3$ (the most common inorganic Fe species in seawater at pH 8), on container walls has been observed by Fischer et al. (2007), Schlosser and Croot (2008), and in earlier work by Robertson (1968).

The data points can be described by two intersecting linear functions (the solid black lines in Fig. 4.4 b.) that, unfortunately do not contain kinetic information (e.g. the rate constant

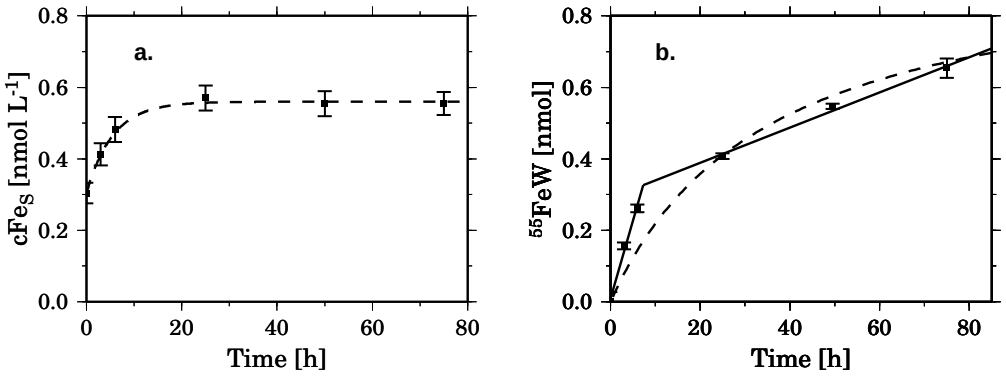

Figure 4.4: *Shown are the increasing concentrations of cFe_S (a.) and wall adsorbed Fe (b.) over the duration of one Fe solubility experiment (sample 102425, station 420, 40 m water depth). The increase of Fe solubility and wall adsorbed Fe were described by an exponential function and a nonlinear regression fit, respectively (dashed black lines). Two distinct linear regression fits conducted for the wall adsorbed Fe data set are shown by the black line in Fig. b.*

for wall adsorbed Fe, $k_{f,^{55}FeW}$). Alternatively, a non-linear curve may be fit through the data points (the dashed black line in Fig. 4.4 b.):

$$^{55}FeW = \frac{^{55}FeW_{max} * t}{K_d + t} \tag{4.26}$$

where ^{55}FeW is the amount of wall adsorbed ^{55}Fe at time (t), $^{55}FeW_{max}$ is the maximum amount of wall adsorbed ^{55}Fe, and K_d is the dissociation equilibrium constant. K_d can be derived from the following equation:

$$^{55}Fe + W \rightleftharpoons ^{55}FeW \tag{4.27}$$

where W is the wall surface capacity of Fe and ^{55}FeW is the concentration of Fe that is bound to the wall surface. K_d can than be expressed as:

$$K_d = \frac{[^{55}Fe][W]}{[^{55}FeW]} \tag{4.28}$$

The conditional stability constant of wall adsorbed Fe (K_{FeW}) can then be calculated by the inverse formulation of the dissociation equilibrium constant ($K_{FeW} = K_d^{-1}$). However, both terms, K_d and $^{55}FeW_{max}$, were estimated by the slope and x-intercept of the Rosenthal (Scatchard) linearization plot.

Our results suggest that about 93 $\%$ of the added ^{55}Fe can be adsorbed onto the bottle surface at pH 8. This amount corresponds to a surface capacity of 0.157 $\pm$ 0.093 x 10^{-6} mol Fe per m^2 (moistened bottle surface area: 59.61 x 10^{-4} m^2) and a surface coverage of approximately 0.3 $\%$, by atomic Fe of radii 10^{-10} m. The average value of the stability constant, $K_{^{55}FeW}$, for adsorption onto the walls, calculated from the slope by the Scatchard linearization, was low (2.59 x 10^9) compared to values of stability coefficients for FeL complexes (10^{12}-10^{14} for this study).

By comparison, Fischer et al. (2007) showed for polymethylmethacrylate (PMMA) bottles a ten times smaller surface capacity (4.2 x 10^{-8} mol m^{-2}), a three times smaller surface coverage (0.1$\%$), and a $K_{^{55}FeW}$ value that is two orders of magnitude higher (1 x 10^{11}) than the values we measured. Fischer et al. (2007) also showed that this wall adsorption effect occurrs, in order of increasing strength, on surfaces of polyethylene or polycarbonate; PMMA, high-density polyethylene (HDPE) or polytetrafluoroethylene; and glass or quartz bottles. This is in disagreement with our results for $K_{^{55}FeW}$ and the total surface capacity for added ^{55}Fe that showed that HDPE bottles have a weaker Fe binding strengths but a higher Fe capacity and surface coverage than PMMA bottles.

It should be noted that despite our findings of the weaker binding, the Fe wall adsorption effect of HDPE sample bottles cannot be neglected and should be taken into account during investigations of Fe speciation in seawater, since the HDPE binding strengths and capacity are almost the same order of magnitude as the binding strengths of organic ligands investigated in natural seawater.

Frozen versus unfrozen

The time course of Fe solubility measured from EIFeX samples (which were frozen at -20^{circ}C and shipped back to IFM-GEOMAR for analysis) was different to that of samples measured directly after sampling. Fe solubility samples from the Mauritanian upwelling zone (Tropical Atlantic) that were measured directly after sampling (M68/3 on the R.V. Meteor, Schlosser and Croot, chapter 3) had higher cFe_S values at the beginning of the experiment than at the end (after 72 h). The same pattern was observed with unfrozen samples taken on another Southern Ocean cruise in 2007 (ANTXXIII/9 at R.V. Polarstern, Schlosser et al., in prep. to $Marine\ Chemistry$). During the ANTXXIII/9 cruise some of the samples were also frozen and store for a few days prior to analysis. Other samples were measured straight after sampling. Fig. 4.5 shows the different time course of cFe_S for frozen and unfrozen samples taken on ANTXXIII/9.

The overall higher concentration of cFe_S of samples measured straight after sampling could be explained by the rapid formation of soluble $Fe(OH)_3$ at pH 8 (Kuma et al., 1996). Over the course of the 72 hours of the experiment, a portion of this uncharged Fe species would have been transformed into colloidal Fe species too large to pass through the syringe filter. The lower concentrations of soluble $Fe(OH)_3$ at the end of the experiment, although in part controlled by temperature and pH, would have reflected an approach to equilibrium with colloidal Fe species. The organic complexation of Fe with freely available ligands would have takes place in the first few minutes of the experiment, as it is a very fast reaction, and should not have affected the amount of cFe_S very much.

The difference between the non-frozen and frozen samples suggests that freezing promoted the formation of colloidal ligands that were slowly solubilized over the 72 hours of the experiment. Alternatively, freezing may have pushed up the pH of the samples due to the exclusion of gases (such as CO_2) from the ice. As the concentrations of dissolved CO_2 in

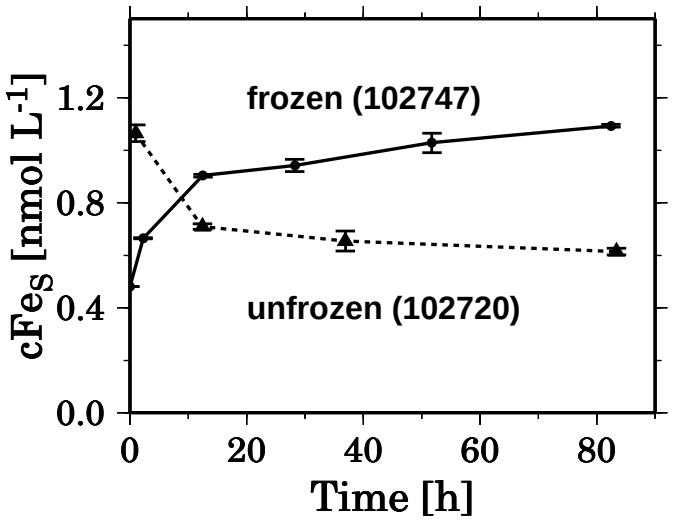

Figure 4.5: *Shown are two differentially treated solubility samples from the Southern Ocean (ANTXXIII/9, R.V. Polarstern, 2007),measured like EIFeX samples. Sample number one was stored in a freezer at -20° C before the measurement (solid black circles and line), sample two was immediately measured after sampling (solid black triangles and dashed black line).*

the thawed samples came back into equilibrium with the atmosphere, the pH of the samples could have decreased (causing a slow increase in inorganic Fe solubility) during the duration of the experiment.

Unfortunately, the data collected are not enough to distinguish between these two possibilities. The difference in behavior of the frozen and non-frozen samples is troubling, especially considering the frequency with which trace metal samples are frozen prior to analysis, and suggest that this is a topic which needs to be investigated in more detail.

FeL measurements

Kinetic FeL - $Fe(TAC)_2$ measurements on some samples were performed to investigate the rates of dissociation (k_d) and formation (k_f) of FeL complexes. Each TAC-treated subsample

showed with increasing time an increasing $Fe(TAC)_2$ concentration. This increase was used to calculate k_d from Eq. 4.20. Subsequently, each TAC-treated subsample started with a lower $Fe(TAC)_2$ concentration than the subsample treated before it (Fig. 4.6). This decrease was than used to calculate k_f from Eq. 4.11. The dissociation rate constants

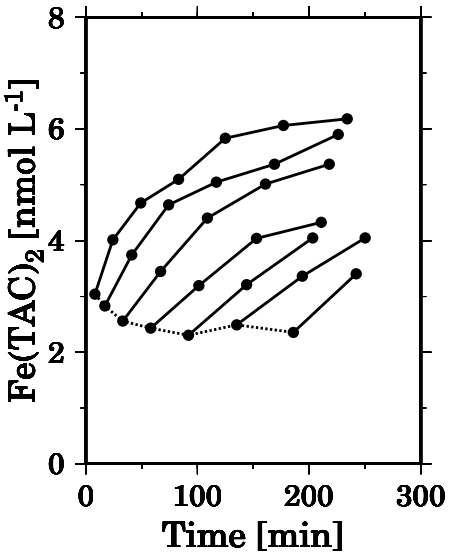

Figure 4.6: *Shows the increasing $Fe(TAC)_2$ concentration of the 7 taken subsamples (black lines) versus time. The dashed black line point out the decreasing amount of Fe' available for TAC complexation over the duration of the experiment. Proportional to the increasing amount of organically complexed or wall adsorbed Fe.*

calculated from Eq. 4.20 (7.7 $\pm$ 0.84 x 10^{-5} s^{-1}) are similar to the $k_{obs,2}$ determined in the Fe solubility experiment and to the previously mentioned values from the literature (Witter and Luther, 1998; Wu and Luther, 1995).

The formation rate calculated from the slope of the dashed black line in Fig. 4.6 are in the range of 3.10 $\pm$ 1.52 x 10^3 $M^{-1}s^{-1}$. This is two orders of magnitude lower than expected and compared to values from previous publications (5.08 until 0.42 x 10^5 $M^{-1}s^{-1}$ (Witter and Luther, 1998)). It may be that the 8 minutes that elapsed prior to the first measurement

after TAC addition was too long for an accurate estimation of the rate since most of the formation of FeL complexes would have take place during the first minutes after Fe addition. If the concentration of added Fe is used as the starting concentration and the first measured $Fe(TAC)_2$ concentration of the first subsample as the end concentration, than the calculated formation rates (8.86 $\pm$ 4.20 x 10^5 $M^{-1}s^{-1}$) are in much better agreement with the values from the literature.

This would further suggest that the formation of FeL complexes in seawater is too fast to be precisely quantified with voltammetric methods. Faster measuring techniques are required.

There is a possibility that the observed decrease of Fe available for TAC complexation in the feed solution might not have been caused by the complexation with organic ligands but by the aforementioned adsorption of Fe onto the bottle walls (Fischer et al., 2007; Schlosser and Croot, 2008). The conditional stability constant of inorganically complexed Fe by functional groups of the container wall has an average value of 2.59 x 10^9 (see previous section). The dissociation rate constant of wall-adsorbed Fe, $k_{d,FeW}$, can be calculated from the conditional stability constant of 2.59 x 10^9 for Fe inorganically complexed by functional groups on the container wall and the low values for the formation rate constant (expected to be the formation rate constant of FeW ($k_{f,FeW}$). The results obtained (1.04 $\pm$ 0.71 x 10^{-6} s^{-1}) are one order of magnitude lower than dissociation rates found for FeL complexes. This implies that the surface adsorbed ^{55}Fe is strongly bound, and as shown by Schlosser and Croot (2008), only removable with a HCl solution of at least 0.1 M.

4.5 Discussion

4.5.1 Fe and ligand cycling

The major conclusion of Boye et al. (2005) and Kondo et al. (2008) concerning the EisenEx and SEEDS II mesoscale Fe fertilization experiments, respectively, was that the observed decrease in dissolved Fe and organic ligand concentrations during the experiments were due to dilution caused by wind-induced mixing. Strong storm events can lead to considerable horizontal and vertical mixing, for example, if there is no strong temperature gradient in surface waters. In the Southern Ocean, where deep mixed layer depths (100 m and more) are not unusual, the induced wind stress in the surface layer can affect the water column down to 100 m or more.

Although there were several storm events during the mesoscale Fe fertilization experiment discussed here, it is difficult to pinpoint the exact impact mixing had on Fe and organic ligand concentrations. Dissolved Fe concentrations in near-surface waters ($0 - 60$ m) only slightly decreased following storm events. These slight decreases in $[Fe_d]$ could be explained by wind induced dilution with surrounding waters, such as described by Boye et al. (2005), or they could be explained by the biological uptake of Fe by phytoplankton and bacteria. At least some of the slight decrease was certainly due to biological consumption, as suggested by the increase in chlorophyll fluorescence, an indicator of phytoplankton biomass, that is contemporaneous with the drop in $[Fe_d]$ (App. D and Fig. 4.2).

Concentrations of organic ligands were somewhat more impacted by storm events than $[Fe_d]$. A drop in ligand concentrations was, for instance, seen at station 508 after the first storm event.

Organic ligands were in excess relative to Fe_d over the duration of the experiment which means that there were enough organic ligands dissolved in seawater to complex all of the naturally existing and artificially added Fe. Measured ligand concentrations inside the patch

at the beginning of the experiment ($2 - 7$ nmol L^{-1}) and outside the Fe patch ($1 - 4$ nmol L^{-1}) were slightly higher than found for unfertilized open ocean seawaters (Rue and Bruland, 1995, 1997; Witter and Luther, 1998) and during other fertilization experiments in the Southern Ocean ($3 - 4$ nmol L^{-1}, (Boye et al., 2005; Boyd et al., 2000)).

The ligand concentrations in the beginning of the experiment were not strongly affected by the weak increase in biological activity that followed the first Fe infusion (Fig. 4.2). After the second infusion of Fe, a considerable quantity of organic ligands were formed in the upper mixed layer below the chlorophyll fluorescence maximum ($40 - 70$ m), something which might be attributed to the production of organic ligands in association with the decomposition of organic matter below the mixed layer (Croot et al., 2007).

After the third storm, ligand concentrations remained stable and low through to the end of the experiment. The overall low concentration of ligands during this fertilization experiment might reflect diminished release of Fe binding ligands by phytoplankton and bacteria. For example, Haygood et al. (1993) pointed out that some marine bacteria produce Fe-binding ligands under Fe stress but stop ligand production if Fe is not limiting. The availability of Fe could be seen as a chemical cue controlling the production and release of ligands by biota. If so, the enhancement of Fe concentrations in surface waters brought about by Fe fertilization during EIFeX could have triggered some species to discontinue the energy-intensive production of Fe binding ligands after 20 days of the experiment.

4.5.2 Changes in Fe solubility after Fe fertilization

As explained in the results section, the first Fe infusion had a lesser impact on ligand concentration and Fe solubility than the second Fe infusion. The pattern of higher Fe solubility in the surface was broken down during storm events. The resulting homogenization of Fe solubility values in the upper 120 m indicates that the properties of the water that

control Fe solubility (pH, organic ligands, etc.) became evenly dispersed throughout the water column because of the mixing.

Interestingly, the capacity of seawater for soluble Fe averaged over the upper 120 m of the water column changed significantly during storm events. This is clear between days 5 and 10 (stations 466 and 508), when integrated cFe_S values between 40 and 90 m decreased by approximately 16%. This decrease occurred alongside a decrease in ligand concentrations of 18% in 55 m implicating organic ligands as one of the major controlling factors for Fe solubility.

4.5.3 Interconnection of Fe solubility and ligand concentration

During the first part of the experiment, ligand concentrations and Fe solubility are significantly related ($cFe_S = 0.04 * L + 0.16; R^2 = 0.88$) between 25 and 80 m both outside of and inside of the patch (Fig. 4.7). The situation is different in deeper waters. Below 100 m at stations 427 and 513, Fe solubility is high, ligand concentrations are low, and there is no correlation between them. This is also the case for all depths (20 to 300 m) at station 591.

Inorganic Fe solubility

The regression line in Fig. 4.7 gives an Fe solubility of 0.16 nmol L^{-1} at an Fe ligand concentration of zero. This can be interpreted as the solubility of inorganic Fe ($cFe_{S,in}$). This value closely matches the 0.15 nmol L^{-1} measured by ultrafiltration for Antarctic seawater that had been irradiated with UV radiation for a period of time (75 min) long enough to destroy dissolved organic matter therein (Schlosser and Croot, 2008). This conclusion is also supported by measurements of Fe solubility of $0.2 - 0.3$ nmol L^{-1} made by Kuma et al. (1996) and Liu and Millero (2002) on UV-irradiated seawater.

However, results obtained by Liu and Millero (1999, 2002) for inorganic Fe solubility in

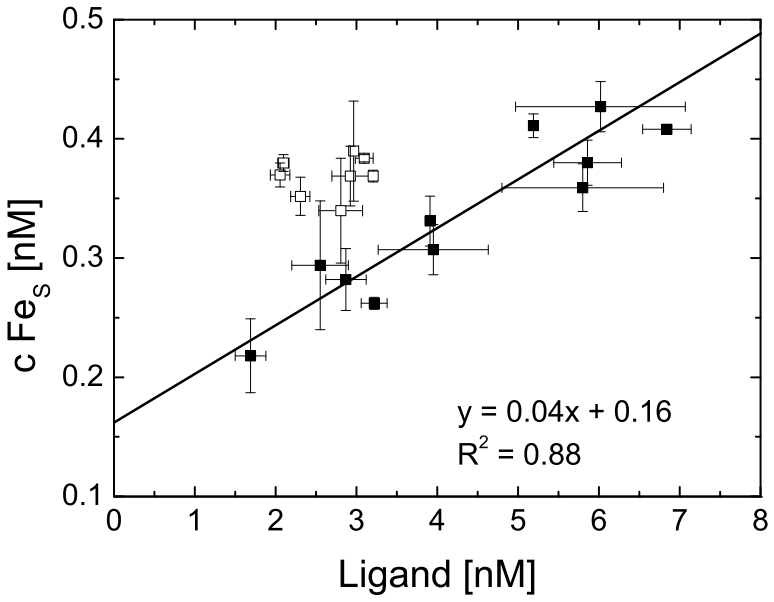

Figure 4.7: *Shown is the diagram of ligand concentration vs. Fe solubility. Filled squares are the results from samples taken inside and outside the fertilized patch above 80 m depth. Open squares are samples taken below 80 m depth at station 427, 513 and at station 591 between sea surface and 300 m water depth.*

artificial seawater is one order of magnitude smaller ($cFe_{S,in}$ = 0.01 $\pm$ 0.002 nmol L^{-1}). Liu and Millero (2002) concluded, with respect to the measurements made by Kuma et al. (1996) and to their own measurements of UV-irradiated Florida Bay seawater, which also had a high Fe solubility, that the UV-irradiation had not eliminated all organic ligands. On the other hand, model calculations by of Liu and Millero (1999) yielded higher $cFe_{S,in}$ values at pH 8 ($\approx$ 0.15 nmol L^{-1}) similar to our calculated value for the inorganic Fe solubility ($cFe_{S,in}$ = 0.16 nmol L^{-1}). It may be that the measurements made on artificial seawater are in error for reasons we do not yet understand.

Colloidal and soluble ligands

Fe solubility samples were filtered through 0.02 μm Anotop filters and Fe ligand samples were filtered through 0.2 μm cartridge filters. This means that while the Fe solubility measurements are really reflecting the quantity of Fe that can be held in the soluble phase ($cFe_S \leq$ 0.02 μm), the Fe ligand measurements include also bigger phases (0.2 μm $\leq$ FeL $\leq$ 0.02 μm). This could explain why ligand concentrations are eight to ten times higher than expected for the measured Fe solubilities. It appears that there was a colloidal ligand phase (L_C) that adsorbed Fe but did not pass through the 0.02 μm filters and so was not counted towards Fe solubility.

The existence of colloidal ligand species was first demonstrated by Wu et al. (2001), Nishioka et al. (2001), and Boye et al. (2005). Boye et al. (2005) determined that up to 90$\%$ of the ligands occur in the soluble phase (L_S, $<$ 200 kDa). The other 10$\%$ of the dissolved ligand pool exists in the colloidal size fraction (200 kDa $-$ 0.2 μm). Our data show a very different result.

If the soluble Fe fraction is complexed by the soluble ligand fraction in a 1 to 1 ratio, the soluble ligand concentration can be calculated by the following equation:

$$L_S = cFe_S - cFe_{S,in} \tag{4.29}$$

Because $cFe_{S,in}$ depends on temperature, and pH (Liu and Millero, 1999), factors which are relatively stable over the course of the experiment, it should not be changing very much from a value of 0.16 nmol L^{-1}. If so , L_S should be in a linear relationship with L_C. This would suggest that up to 96 $\%$ of the entire dissolved ligand pool are colloidal ligands.

That implies that the decrease of dissolved ligand concentrations after storm events is mostly caused by the decrease of the more reactive colloidal ligand fraction. This would agree with the work of Boye et al. (2005), who postulated that colloidal ligand species are more reactive than the soluble species and are more quickly destroyed and/or diluted during storms.

The ligand concentrations measured here contain both a soluble and a colloidal fraction. Where the trend line in Fig. 4.7 holds true, both ligand fractions must be in equilibrium with each other. For samples which do not fall on the regression line (samples below 80 m (inside and outside the patch) and the entire water column at station 591), soluble ligands must not have reached this particular equilibrium with colloidal ligands. At these spots, the colloidal ligand concentration is lower then observed for the others. This might suggests that below 80 m and in regions with a high biomass (station 591), colloidal ligands are less stable. That could be attributed to the adsorption of colloidal ligands on charged surfaces (Campbell et al., 1997) of settling particulate organic matter (POM), or an increasing release of soluble ligands by the bacterial decomposition of POM.

The data presented here are not sufficient for determination of how this shift in the ligand pool influences biological availability of Fe. Future work on Fe solubility and ligand concentration should distinguish between soluble and colloidal ligands in the ligand pool and supposable differences in the bioavailability of Fe in the soluble and colloidal size fraction.

4.5.4 Ligand and Fe solubility interactions with phosphate

The production and release of organic ligands in natural seawater during the decomposition of organic matter were first noted by Kuma et al. (1996) in the Indian and western North Pacific Ocean and later more precisely described by Kuma and Isoda (2003) and Tani et al. (2003) in the North Pacific. These studies concluded from the linear correlation of Fe solubility with phosphate and nitrate in deeper waters that Fe binding chelators were formed alongside the release of nutrients during the remineralization of sinking organic matter. This could be due to release of ligands from phytoplankton cells during their destruction via zooplankton grazing (Hutchins and Bruland, 1999), cell lysis (Gobler et al., 1997), or to the production of ligands by the bacterial attack with ectoenzymes (Nagata et al., 1998).

Linearity between Fe solubility and nutrient concentrations has also been seen for depths immediately below the seasonal thermocline in the Mauritanian upwelling zone (chapter 3). During the EIFeX experiment in the Southern Ocean however, there is no visible link between organic matter remineralization and Fe ligands or Fe solubility. No strong correlation between Fe solubility (or dissolved ligand concentrations) and phosphate or nitrate concentrations occurs in the data set for either all depths considered together or for just the depths below 100 m considered on their own. This could suggest that production associated with the remineralization of sinking organic matter is not the dominant source of ligands to Southern Ocean surface waters, but that some other process (e.g., Fe limitation) drives the production and intentional release of ligands by bacteria. Alternatively, it might be that the exceptionally high nutrient (and Fe ligand) concentrations of surface and subsurface waters in the Southern Ocean is obscuring the signs of nutrient regeneration and ligand release.

4.5.5 Diel changes of Fe solubility

Although there was not a clear increase in Fe solubility with nutrient concentrations during this mesoscale Fe fertilization experiment, the values did shift somewhat over the course of the day on the 2 days that were investigated in detail (Fig. 4.3). On both days, Fe solubility dropped from slightly higher values in the morning (0.3 to 0.4 nmol L^{-1}) to lower values in the afternoon and evening (0.1 to 0.3 nmol L^{-1}). This was true at depths of 20, 40, and 60 m. On the first of the two days (the one with the less intense global radiation values), the drop is most pronounced in the 20 m samples. On the second, significantly brighter day, the decline in Fe solubility is greatest at the deepest depth. Striking is that despite the rather low values in the afternoon of the first day, Fe solubility values at the beginning of the second day had exceeded their values of the previous morning.

The recovery in Fe solubility values overnight suggests that during the day the destruction of

dissolved ligands exceeds the rate at which they are produced, while at night the opposite is true. The slight decline in Fe solubility during the day might be explained by destruction of organic ligands by sunlight. Although there was a considerable difference in the intensity of the global radiation on day 1 versus day 2, cFe_S reached similar minima in the afternoons. The first photochemical studies of natural organic ligands were performed by Barbeau et al. (2003) and Powell and Wilson-Finelli (2003b). The study of Barbeau et al. (2003) showed that ligands are very different in their sensitivity to UV-irradiation. Some functional groups, like catecholate and hydroxamate binding groups, do not appear to be photochemically reactive when they are bound to Fe and maintain their ability to bind Fe even in the wake of strong irradiation (Barbeau et al., 2003). Catecholate which is not bound to Fe and carboxyl groups (either bound or not bound to Fe(III)) are, on the other hand, sensitive and can be destroyed by UV-irradiation ($\lambda = 200 - 400$ nm). It was also found that during the destruction of organic ligands by sunlight, Fe(III) can be reduced to Fe(II) which is more soluble and generally more bioavailable than Fe(III) (Barbeau et al., 2003) and might also be a significantly source of Fe(II) in seawater.

Our results show a solubility minimum between 0.2 and 0.1 nmol L^{-1} that is essentially the same on the late afternoon of the bright day as it is on the preceding day of muted sunlight. An explanation for this might be that the destruction of the "sensitive" ligands is independent of intensity (Barbeau et al., 2003) over the range of solar intensities experienced in this study.

As a whole, the diel cycle measurements reported here suggest that between 1/3 and 1/2 of the dissolved ligands in the euphotic zone were destroyed during the day. To recover the capacity in cFe_S by the next morning (as was observed), biota would had to produce photochemically reactive organic ligands during the night (Martinez et al., 2000). This might serve a strategy of microorganisms for avoiding Fe limitation. Photochemically reactive ligands, produced by bacteria, scavenge freely available Fe, preventing the formation of

colloidal Fe and increasing the residence time of Fe in seawater.

Some phytoplankton species have the ability to destroy Fe complexes and to transport Fe in the interior space of the cell by enzymatic reactions (Fe(III) reductase, etc.). If 1/3 of the dissolved organic ligands are photochemically reactive, than a non-neglectable amount of organically complexed Fe might be released again as Fe(III) during the day. This would enable phytoplankton and bacteria to assimilate freshly available Fe whether or not they possessed mechanisms to transport FeL into their cells. More work has to be done in this area to quantify the mobilization of Fe by solar radiation.

4.6 Conclusion

Seawater samples for Fe solubility and Fe ligand measurements were collected during a mesoscale Fe fertilization experiment (EIFeX) in the Southern Ocean. Concentrations of dissolved organic ligands during this experiment were more strongly influenced by the resulting phytoplankton bloom than was Fe solubility. The pool of ligands in the studied waters contained both colloidal and soluble ligands. The colloidal and soluble ligand species occurred in a equilibrium with each other in the upper 80 m of the water column especially early in the experiment. This linear relationship between soluble and colloidal ligands was not found below 80 m or at the end of the experiment. The increase in concentrations of soluble ligands and the decrease of colloidal ligands below 80 m and at the end of the fertilization experiment could be explained by a decline in the production and release of ligands by bacteria and by the removal of ligands from the colloidal size fraction through the formation of larger particles over time or by the adsorption of colloidal ligands onto particle surfaces.

The observed change of the ligand pool composition after such Fe fertilization may have a strong impact on the Fe cycle and the residence time of Fe in the fertilized waters. Colloidal,

organically-complexed Fe species may be converted into bigger particles which could then be more rapidly transported than soluble species to the depths below the euphotic zone. This would imply that a greater fraction of the artificially added Fe in mesoscale Fe fertilization experiments is not available in the euphotic zone at the end of experiment.

Measurements of Fe solubility over 2 diel cycles suggested that organic ligands are degraded by UV irradiation during the day. The extent of this decomposition is variable, in part with light intensity, but also with the chemical makeup of the ligands present. In addition, Fe ligand concentrations (and Fe solubilities) recover overnight to values similar to the previous morning, suggesting that biological production of ligands during the night is keeping pace with the photochemical destruction of ligands during the day. Since these processes play key roles in determining the availability and residence time of Fe in surface waters, it would be important to carry out further work on this subject.

The kinetic approach to measuring Fe solubility and Fe ligand concentrations revealed that a relatively large amount of the added Fe is adsorbed onto bottle wall surfaces during the time course of the measurements. The rate of adsorption of Fe onto the walls is slower than the rate of organic complexation of Fe, but the surface capacity of the bottles for Fe is two orders of magnitudes greater than the concentration of dissolved organic ligands in seawater. It is imperative that further work illustrate the extent to which wall adsorption of Fe introduces artifacts into the measurements of Fe solubility and Fe ligand measurements.

Chapter 5

Conclusion

Fe solubility and ligand measurements performed during this PhD work were made to elaborate on the theory of the biogeochemical cycling of Fe in seawater. It could be shown that strong organic ligands increase Fe solubility and therefore the residence time of Fe in seawater. A greater inventory of dissolved and soluble Fe in seawater increases the residence time of Fe in seawater.

- Measurements made during a mesoscale Fe fertilization experiment in the Southern Ocean showed that both a soluble (< 0.02 μm) and colloidal ($0.02 - 0.2$ μm) fractions of dissolved organic ligands are stable. Changes in soluble ligand concentrations were much smaller than changes in colloidal ligand concentrations, implying that observed changes in concentrations of dissolved ligands are driven mostly by changes in the colloidal fraction. The composition of the ligand pool (in terms of the ratio of soluble to colloidal ligands) in the upper mixed layer ($20 - 80$ m) shifted after the peak of biomass was reached in the Fe fertilization experiment. Prior to this, the soluble and colloidal ligand fractions were in some sort of equilibrium, since $[L_d]$ showed a linear correlation with Fe solubility. After this, the same ligand composition as observed below 80 m during the experiment was found in the whole upper mixed layer ($20 -$ 300 m).

  It also appeared that neither organic ligand phase was dominantly produced during the remineralization of organic matter (something that has been seen many times previously in other marine environments). Instead it is likely that their main source was direct release by phytoplankton and bacteria. This conclusion stems from the fact that $[cFe_S]$ did not show a linear correlation with phosphate.

  The decrease of Fe solubility during the day in the upper mixed layer (20 to 60 m) observed during two diel stations may be attributed to the photochemical degradation

of photochemically sensitive ligands during the day. Fe solubility tended to be highest in the morning and lowest in the latter portions of the day, and then high again the following morning. The regeneration of the cFe_S capacity could be attributed to a greater rate of production than destruction of organic ligands during the night, while the decline of solubility during the day could represent the opposite case.

- In contrast to the measurements in the Southern Ocean, measurements made in the Mauritanian upwelling zone did show a significant correlation between measures of organic matter remineralization (pH, oxygen, and phosphate) and cFe_S in subsurface samples ($40 - 80$ m). An increase in Fe solubility with organic matter decomposition could be occurring in several different ways. Organic matter, including intracellular iron binding proteins, could be released from broken phytoplankton cells and solubilized by bacterial enzymes. Alternatively, the linear correlation could be explained by the conversion of particulate binding sites for Fe into the dissolved phase or the complexation of Fe by phosphate released during the bacterial degradation of organic matter. This may suggest that the dominant mode of production of organic ligands differs between the Southern Ocean and the Mauritanian upwelling zone.

- Lab based ultrafiltration experiments on seawater ligand solutions showed that this technique is a powerful tool for separating the particulate and colloidal Fe fraction from the soluble Fe fraction and allows for investigation of the strength of organic ligands for forming organic Fe complexes. The apparatus made it possible to investigate the stability and interconnection of both size fractions. With this work we demonstrated that strong organic chelators, such as DFB, increase Fe solubility by several orders of magnitude over levels found in natural seawaters. It could also be shown that

some of the fundamental equations traditionally used for the transformation of data from samples collected by ultrafiltration need to be modified. A slight modification of the traditional equations brings experimental results into line with those predicted from a computer model.

Mass balance calculations showed that a significant portion of the added ^{55}Fe disappeared from the feed solution before the ultrafiltration was even started. This was found in all untreated seawater samples and in all ligand solutions except for those of the strongest chelator, DFB. A polycarbonate container that was used as storage vessel for the feed solution showed a strong wall sorption effect. Between 20 to 40$\%$ of the added Fe was scavenged by the container wall depending on the ligand solution and could only be removed by a wash with HCl.

Another portion of the added ^{55}Fe disappeared when the ultrafiltration was started. Every cycle of the ultrafiltration apparatus led to a decrease in the colloidal and particulate Fe concentration in the feed solution. A significant portion of the colloidal and particulate fraction during each cycle appears to become adsorbed to the membrane filter. Interestingly, a wash with HCl did not always recover the adsorbed particles and colloids (i.e. it failed with the ligand solutions of 2-keto-D-gluconic acid and phytagel and with untreated seawater samples).

It has to be recognized for future ultrafiltration work that these side effects occur and must be taken into account in any mass balance calculations that are carried out.

Appendix A

Auxiliary information for ultrafiltration studies

Text for solubility calculations for ultrafiltration studies:

$Fe^{3+} + L \leftrightarrow FeL$
$K'_{FeL} = \frac{[FeL]}{[Fe'][L']}$

where [Fe'] is the Fe(III) not complexed with L, and [L'] is the ligand not complexed with the iron in seawater. The solubility of Fe(III) in seawater is then given by the following equation:

$[Fe(III)]_{SW} = [Fe'] + [FeL]$

The concentration of...

$[FeL] = [Fe(III)]_{SW} - [Fe(III)]_{NaCl}$

Thus it can be easily shown that

$[Fe'] = [Fe(III)]_{NaCl}$

then using L' and the final permeate concentration...(problem: as R may not be 1) can estimate K'_{FeL} for each ligand...

$K'_{FeL} = \frac{[Fe(III)]_{SW} - [Fe(III)]_{NaCl}}{[Fe(III)]_{NaCl}[L']}$
$[L]_T = [L'] + [FeL]$
$K'_{FeL} = \frac{[Fe(III)]_{SW} - [Fe(III)]_{NaCl}}{[Fe(III)]_{NaCl}([L]_T - [Fe(III)]_{SW})}$

This is adapted from Liu and Millero (2002): replace NaCl with UVSW?

$K'_{FeL} = \frac{[Fe(III)]_{SW} - [Fe(III)]_{NaCl}}{[Fe(III)]_{NaCl}[L']}$

A.1 Modeling of a two component system in an ultrafiltration study

From model calculations /* calculated derivative fashion − could also use dt1 */

$nVRet = VRet - ts * Vs;$

$nVPerm = VPerm + Vs * ts;$

/* Calculations − maybe change to by moles?*/

$nC1Perm = (C1Perm * VPerm + Pc1 * C1Ret * Vs * ts)/nVPerm;$

$nC2Perm = (C2Perm * VPerm + Pc2 * C2Ret * Vs * ts)/nVPerm;$

$CPerm = nC1Perm + nC2Perm;$

/* Instantaneous permeate concentration */

$iCPerm = Pc1 * C1Ret + Pc2 * C2Ret;$

$nC1Ret = (C1Ret * VRet - Pc1 * C1Ret * Vs * ts)/nVRet;$

$nC2Ret = (C2Ret * VRet - Pc2 * C2Ret * Vs * ts - Vs * ts * kFew)/nVRet;$

$CRet = nC1Ret + nC2Ret;$

$nFewall = Fewall + Vs * ts * kFew;$

/* remove Fe from solution onto filter only from C2*/

A.1.1 Calculations

$CF = \frac{V_0}{V_0 - V_p} = \frac{V_0}{V_r}$

and $V_p = \nu_s * t$, where ν_s is the flow rate

$CF = \frac{V_0}{V_0 - \nu_s t}$
$\frac{\partial CF}{\partial t} = \frac{\nu_s V_0}{(V_0 - \nu_s t)^2}$

More here - basic equation is...

$\frac{\partial C}{\partial t} = \frac{\left(\frac{\partial n}{\partial t} V - n \frac{\partial V}{\partial t}\right)}{V^2}$

so if no volume change then

$\frac{\partial C}{\partial t} = \frac{\left(\frac{\partial n}{\partial t}\right)}{V}$

thus in the present case we have

$n_R = C_{K1} V_R + C_{R2} V_R$
$\frac{\partial n_R}{\partial t} = -P_{c1} C_{K1} \nu_s - k_{FeW} \nu_s$
includes flow rate

$V_R = V_0 - \nu_s t$
$\frac{\partial V_R}{\partial t} = -\nu_s$

Leading to...

$\frac{\partial C_R}{\partial t} = \frac{((-P_{c1} C_{R1} - k_{FeW}) \nu_s V_R - (C_{R1} V_R + C_{R2} V_R) \nu_s)}{V_R^2}$
$\frac{\partial C_R}{\partial t} = \frac{((-P_{c1} C_{R1} - k_{FeW}) \nu_s - (C_{R1} + C_{R2}) \nu_s)}{V_R}$

$$\frac{\partial C_R}{\partial CF} = \frac{\partial C_R}{\partial t}\frac{\partial t}{\partial CF}$$
$$\frac{\partial C_R}{\partial CF} = \frac{\partial C_R}{\partial t}\frac{(V_0-\nu_s t)^2}{\nu_s V_0}$$
$$\frac{\partial C_R}{\partial CF} = \left(\frac{((-P_{c1}C_{R1}-k_{FeW})\nu_s+(C_{R1}+C_{R2})\nu_s)}{V_R}\right)\left(\frac{(V_0-\nu_s t)^2}{\nu_s V_0}\right)$$
$$\frac{\partial C_R}{\partial CF} = \left(\frac{((-P_{c1}C_{R1}-k_{FeW})+(C_{R1}+C_{R2}))}{1}\right)\left(\frac{(V_0-\nu_s t)}{V_0}\right)$$

A.1.2 For Component 1: Retentate

thus in the present case we have

$n_{R1} = C_{R1}V_R$

$\frac{\partial n_{R1}}{\partial t} = -P_{c1}C_{R1}\nu_s$ – includes flow rate

$V_R = V0 - \nu_s t$

$\frac{\partial V_R}{\partial t} = -\nu_s$

Leading to...

$\frac{\partial C_{R1}}{\partial t} = \frac{(-P_{c1}C_{R1}\nu_s V_R + C_{R1}V_R\nu_s)}{V_R^2}$

$\frac{\partial C_{R1}}{\partial t} = \frac{(-P_{c1}C_{R1}\nu_s + C_{R1}\nu_s)}{V_R}$

$\frac{\partial C_{R1}}{\partial t} = \frac{C_{R1}\nu_s(1-P_{c1})}{V_R}$

Furthermore can calculate against CF

$\frac{\partial C_{R1}}{\partial CF} = \frac{\partial C_{R1}}{\partial t}\frac{\partial t}{\partial CF}$

$\frac{\partial C_{R1}}{\partial CF} = \frac{C_{R1}\nu_s(1-P_{c1})}{V_R}\frac{(V_R)^2}{\nu_s V_0} = \frac{C_{R1}V_R(1-P_{c1})}{V_0} = \frac{C_{R1}(1-P_{c1})}{CF}$

$\frac{\partial C_{R1}}{\partial CF} = \frac{C_{R1}(1-P_{c1})}{CF}$ – can be transformed via u-substitution to

$\frac{\partial(lnC_{R1})}{\partial(lnCF)} = 1 - P_{c1}$

A.1.3 For Component 1: Permeate

Case(1): Total permeate concentration

$n_{P1} = C_{P1}V_P$

$\frac{\partial n_{P1}}{\partial t} = P_{c1}C_{R1}\nu_s -$ includes flow rate

$V_R = V_0 - \nu_s t = V_0 - V_P$

$\frac{\partial V_R}{\partial t} = -\nu_s = \frac{\partial V_P}{\partial t}$

Leading to...

$\frac{\partial C_{P1}}{\partial t} = \frac{(P_{c1}C_{R1}\nu_s V_P - C_{P1}V_P\nu_s)}{V_P^2}$

$\frac{\partial C_{P1}}{\partial t} = \frac{(P_{c1}C_{R1}\nu_s - C_{P1}\nu_s)}{V_P}$

Case(2): Instantaneous permeate concentration

$C_{P1i} = P_{c1}C_{R1}$ for any time

Leading to...

$\frac{\partial C_{P1i}}{\partial t} = P_{c1}\frac{\partial C_{R1}}{\partial t}$

Combining from above with

$\frac{\partial C_{R1}}{\partial t} = \frac{C_{R1}\nu_s(1-P_{c1})}{V_R}$

gives

$\frac{\partial C_{P1i}}{\partial t} = P_{c1}\frac{C_{R1}\nu_s(1-P_{c1})}{V_R}$

which can be converted using equation n and n+1 to the following

$$\frac{\partial C_{P1}}{\partial CF} = \frac{P_{c1}C_{R1}\nu_s(V_R)^2(1-P_{c1})}{V_R\nu_s V_0} = \frac{C_{P1i}V_R(1-P_{c1})}{V_0} = \frac{C_{P1i}(1-P_{c1})}{CF}$$

or

$$\frac{\partial(lnC_{P1})}{\partial(lnCF)} = (1 - P_{c1})$$

A.1.4 For Component 2: Retentate - constant rate of loss onto filter

Mass balance and flow considerations.

$n_{R2} = C_{R2}V_R$

$\frac{\partial n_{R2}}{\partial t} = -k_{FeW}\nu_s$ – includes flow rate

$V_R = V_0\nu_s t$

$\frac{\partial V_R}{\partial t} = -\nu_s$

Leading to...

$\frac{\partial C_{R2}}{\partial t} = \frac{(-k_{FeW}\nu_s V_R + C_{R2}V_R\nu_s)}{V_R^2}$

$\frac{\partial C_{R2}}{\partial t} = \frac{(-k_{FeW}\nu_s + C_{R2}\nu_s)}{V_R}$

$\frac{\partial C_{R2}}{\partial t} = \frac{\nu_s(C_{R2} - k_{FeW})}{V_R}$

Solution to this is:

$\frac{\partial C_{R2}}{\partial t} = \frac{\nu_s(C_{R2} - k_{FeW})}{V_R}$

Furthermore:

$\frac{\partial C_{R2}}{\partial CF} = \frac{\partial C_{R2}}{\partial t}\frac{\partial t}{\partial CF}$

$\frac{\partial C_{R2}}{\partial CF} = \frac{\nu_s(C_{R2} - k_{FeW})}{V_R}\frac{(V_R)^2}{\nu_s V_0} = \frac{V_R(C_{R2} - k_{FeW})}{V_0} = \frac{(C_{R2} - k_{FeW})}{CF}$

$\frac{\partial C_{R2}}{\partial CF} = \frac{(C_{R2} - k_{FeW})}{CF}$ –can be transformed via u-substitution to

$\frac{\partial ln(C_{R2} - k_{FeW})}{\partial lnCF} = 1$

For Component 2: Permeate

In the model there is no flow for component 2 across the ultrafiltration membrane.

A.1.5 For Component 2: Retentate - loss proportional to concentration

Mass balance and flow considerations

$n_{R2} = C_{R2}V_R$

$\frac{\partial n_{R2}}{\partial t} = -k_{FeW}C_{R2}\nu_s$ – concentration dependent: k_{FeW} is unitless?

$V_R = V_0\nu_s t$

$\frac{\partial V_R}{\partial t} = -\nu_s$

Leading to...

$\frac{\partial C_{R2}}{\partial t} = \frac{(-k_{FeW}C_{R2}\nu_s V_R + C_{R2}V_R\nu_s\nu_s)}{V_R^2}$

$\frac{\partial C_{R2}}{\partial t} = \frac{(-k_{FeW}C_{R2}\nu_s + C_{R2}\nu_s)}{V_R}$

$\frac{\partial C_{R2}}{\partial t} = \frac{C_{R2}\nu_s(1-k_{FeW})}{V_R}$

Solution to this is:

$C_{R2} = \frac{C_{R2,0}(V_0-\nu_s t)^{(k_{FeW}-1)}}{(V_0)^{(k_{FeW}-1)}}$

Furthermore:

$\frac{\partial C_{R2}}{\partial CF} = \frac{\partial C_{R2}}{\partial t}\frac{\partial t}{\partial CF}$

$\frac{\partial C_{R2}}{\partial CF} = \frac{C_{R2}\nu_s(1-k_{FeW})}{V_R}\frac{(V_R)^2}{\nu_s V_0} = \frac{C_{R2}V_R(1-k_{FeW})}{V_0} = \frac{C_{R2}(1-k_{FeW})}{CF}$

$\frac{\partial C_{R2}}{\partial CF} = \frac{C_{R2}(1-k_{FeW})}{CF}$ – can be transformed via u-substitution to

$\frac{\partial ln(C_{R2})}{\partial lnCF} = 1 - k_{FeW}$

For Component 2: Permeate

In the model there is no flow for component 2 across the ultrafiltration membrane.

A.1.6 For Wall Component: - constant loss rate

Mass balance and flow considerations.

n_{FeW} – Area and ligand coverage per unit area incorporated

$\frac{\partial n_{FeW}}{\partial t} = k_{FeW}\nu_s$

no breakthrough incorporated yet - infinite adsorption...

$\frac{\partial n_{FeW}}{\partial t} = k_{FeW}\nu_s$

$n_{FeW} = k_{FeW}\nu_s t$

Thus a plot of n_{FeW} against t should have a slope of $k_{FeW}\nu_s$. (Note the flow rate is included in this term).

or

$n_{FeW} = k_{FeW}V_P$

$\frac{\partial n_{FeW}}{\partial V_P} = k_{FeW}$

A.1.7 For Wall Component: - loss proportional to concentration

Mass balance and flow considerations.

n_{FeW} – Area and ligand coverage per unit area incorporated

$\frac{\partial n_{FeW}}{\partial t} = k_{FeW} C_{R2} \nu_s$

concentration dependent: k_{FeW} is unitless - no breakthrough incorporated yet - infinite adsorption...

$\frac{\partial n_{FeW}}{\partial t} = k_{FeW} C_{R2} \nu_s$

$\frac{\partial n_{FeW}}{\partial t} = \frac{C_{R2} \nu_s (1 - k_{FeW})}{V_R}$

Plot of different parameters:

$\frac{\partial n_{FeW}}{\partial C_{R2}} = \frac{k_{FeW} C_{R2} \nu_s V_R}{C_{R2} \nu_s (1 - k_{FeW})} = \frac{k_{FeW} V_R}{(1 - k_{FeW})}$

or

$\frac{\partial n_{FeW}}{\partial C_{R2}} = \frac{k_{FeW} C_{R2} V_R}{\nu_s} = k_{FeW} C_{R2}$

Appendix B

Ultrafiltration data

Table B.1: *Shown are the data at the start and the end of the ultrafiltration. The data has been recovered from the linear part of the double log diagram, CF vs. concentration (c_P and c_R), to exclude membrane filter loading effects during the first cycles of ultrafiltration. Notes:* [a] *The colloidal concentration is calculated using equation 2.19 (see text).* [b] $K_{Fe'L}$ *is the conditional stability constant calculated using equation 2.15 (see text).* [c] $K_{Fe'L}$ *determined in experimental studies in seawater or estimated using thermodynamic data for salinity 35 and 20 C.* [d] *This value is 0 by definition, as it is assumed that all organic ligands were destroyed by the UV irradiation. Reference sources:* [1] *Boye et al. (2001),* [2] *Croot and Johansson (2000),* [3] *Croot et al. (2004a),* [4] *Rue and Bruland (1995),* [5] *Hudson et al. (1992),* [6] *Sunda and Huntsman (2003),* [7] *Witter et al. (2000),* [8] *Torres et al. (2005),* [9] *Rijkenberg et al. (2006), and Essington et al. (2005)*

Sample	c_W [nmol L^{-1}] (24 hrs)	c_P [nmol L^{-1}] $CF = 1.3$	c_R [nmol L^{-1}] $CF = 1.3$	c_P [nmol L^{-1}] $CF = 10$	c_R [nmol L^{-1}] $CF = 10$	c'_{Col} [nmol L^{-1}] $CF = 10$[a]	Pc	α'_{FeL}	$logK^b_{Fe'L}$ $CF = 10$	$logK^c_{Fe'L}$
UV-Ant SW	0.15	40.49	0.19	91.84	59.67	0.58				0^d
Ant SW	21.0	5.40	31.49	5.92	66.53	53.57	0.92	33		$11.8 - 12.4^{1-3}$
Co SW	19.5	6.94	34.00	6.96	79.11	52.75	0.96	42		$10.8 - 11.1$ [2]
DFB	0	47.41	50.79	53.27	60.00	5.08	0.97	>340	>9.8	$> 13^4$, 16.5^5
EDTA	15.0	11.92	43.80	11.96	54.21	48.04	1.00	82	9.0	7.8^{5-6}
TAC	11.8	15.74	43.52	16.09	78.59	43.75	0.99	104	9.1	Log $\beta_2 = 12.4^2$
Phytic acid	17.7	5.31	32.28	5.66	66.03	54.16	0.97	34	8.6	12.3^7, $< 0^8$
PP IX[9]	7.80	2.30	39.71	2.62	90.85	37.06	0.89	14	8.2	12.0^4, 12.4^7
2keto-D-Glu	15.0	1.15	50.54	1.42	105.42	58.39	0.88	7	7.8	$Log\beta_2 = 11.1^10$
Phytagel	24.2	9.85	36.48	9.54	57.55	51.78	1.16	62	8.8	

Appendix C

Mauritanian upwelling data

Table C.1: *Table shows the Fe solubility and relevant data of the Mauritanian upwelling zone.*

Station	Latitude	Longitude	Depth	PO_4	O_2	free	Fe_d	cFe_S	*s.d.*
			[m]	[μmol kg^{-1}]	[μmol kg^{-1}]	pH	[nmol L^{-1}]	[nmol L^{-1}]	[nmol L^{-1}]
258	18°01'N	26°01'W	5	0.00	215.1	8.14		0.16	0.00
			40	0.01	215.0	8.17		0.12	0.01
			80	0.09	206.2	8.16		0.21	0.02
			200		85.7			0.36	0.02
261	18°62'N	24°26'W	20	0.03	217.6		0.40	0.21	0.01
			40	0.01	219.7		0.27	0.19	0.02
			60	0.03	227.1		0.47	0.30	0.00
			80	0.07	216.1		0.57	0.31	0.01
272	18°01'N	19°02'W	20	0.08	222.7			0.41	0.03
			40	1.60	43.4			0.66	0.01
			60	1.63	49.9			0.66	0.01
			80	1.71	54.4			0.74	0.01
284	18°50'N	16°59'W	20	0.09	209.3	8.13		0.20	0.00
			40	1.16	92.4	7.90		0.28	0.00
			60	1.50	62.5	7.85		0.52	0.03
			80	1.65	54.4	7.84		0.66	0.00
289	19°00'N	19°00'W	20	0.33	171.6	8.13		0.37	0.05
			40	1.63	33.5	7.90		0.79	0.06
			60	1.71	42.5	7.85		0.62	0.03
			80	1.68	48.0	7.84		0.62	0.04
289	18°49'N	17°03'W	20	0.04	221.1		0.32	0.28	0.02
			40	1.57	125.6		0.30	0.51	0.03
			60		77.1			0.51	0.00
			80		62.6		1.25	0.59	0.01

Appendix D

EIFeX data

Table D.1: *The Table shows the collected data of the EIFeX expedition.*

Station	Latitude	Longitude	Depth [m]	PO_4 [μmol L^{-1}]	NO_3 [μmol L^{-1}]	$Si(OH)_4$ [μmol L^{-1}]	Fe_d [nmol L^{-1}]	cFe_S [nmol L^{-1}]	$s.d.$ [nmol L^{-1}]	L [nmol L^{-1}]	$s.d.$ [nmol L^{-1}]	$LogK_{FeL}$	$s.d.$
427	49°24'S	02°20'W	40	1.69	24.8	18.4	2.20			1.96	0.07	14.07	
			60	1.69	24.8	18.5	0.30	0.39	0.04	2.96	0.06	14.07	
			75	1.67	24.8	18.9	0.23	0.43	0.02	6.02	1.05	11.14	0.17
			85	1.70	24.9	19.1	0.43	0.37	0.00	3.20		15.80	
			95	1.70	24.9	19.0	0.47	0.41	0.01	5.19	0.01	12.31	0.01
			105	1.72	24.9	19.0	0.21	0.41	0.00	6.84	0.30	11.67	0.06
466	49°00'S	02°15'W	35	1.71	24.6	17.3	0.69	0.41	0.01				
			55	1.72	24.8	17.2	0.14	0.33	0.02	3.91	0.04	14.02	0.00
			75	1.74	24.9	17.3	0.14	0.28	0.01				
			95	1.76	24.8	17.4	0.20	0.20	0.01				
508	49°12'S	02°00'W	40	1.72	24.3	16.4	0.57	0.27	0.01				
			50	1.70	24.3	16.3	0.17	0.26	0.00	3.22	0.16	11.68	0.10
			60	1.68	24.3	16.3	0.41	0.28	0.03				
			70	1.69	24.4	16.3	0.21	0.26	0.03				
			75	1.93	24.4	16.1	0.34	0.30	0.01				
			85	1.73	24.4	16.2	0.11	0.23	0.03				
			95	1.73	24.5	16.5	0.23	0.22	0.03				
			105	1.79	24.6	17.2	0.17	0.25	0.02				
513	49°37'S	02°09'W	25	1.55	23.6	13.8		0.18	0.06				
			35	1.55	23.7	13.8	0.36	0.28	0.03	2.87	0.25	11.67	0.05
			45	1.59	24.0	13.9	0.21	0.36	0.02	5.80	1.00	11.70	0.03
			55	1.66	24.4	14.2	0.59	0.31	0.02	3.95	0.68	11.89	0.01
			60	1.65	24.3	14.3	0.26	0.38	0.02	5.86	0.42	10.89	0.07
			80	1.68	24.4	14.6	0.19	0.29	0.05	2.55	0.35	11.23	0.06
			100	1.69	24.5	15.1	0.22	0.35	0.02	2.30	0.12	12.50	0.02
			120	1.77	25.1	17.7	0.31	0.34	0.04	2.80	0.27	11.87	0.03
514	49°16'S	02°20'W	25	1.70	24.1	9.2	0.21	0.30	0.05				
			35	1.70	24.1	9.3		0.36	0.01				
			45	1.71	24.1	9.3		0.39	0.03				
			55	1.70	24.1	9.2	0.15	0.28	0.03				
			60	1.69	24.1	9.2	0.38	0.31	0.00				

Table D.2: *Sequel to Table D.1*

Station	Latitude	Longitude	Depth [m]	PO_4 [μmol L^{-1}]	NO_3 [μmol L^{-1}]	$Si(OH)_4$ [μmol L^{-1}]	Fe_d [nmol L^{-1}]	cFe_S [nmol L^{-1}]	$s.d.$ [nmol L^{-1}]	L [nmol L^{-1}]	$s.d.$ [nmol L^{-1}]	$LogK_{FeL}$	$s.d.$
514	49°16'S	02°20'W	80	1.73	24.3	10.8	0.26	0.30	0.03				
			100	1.78	24.8	12.9	0.21	0.27	0.03				
			120	1.88	25.6	16.3	0.20	0.11	0.01				
543	49°29'S	02°27'W	25	1.66	24.1	12.3	0.38	0.28	0.03				
			35	1.64	24.1	12.4	0.26	0.22	0.03	1.69	0.19	12.05	0.06
			45	1.62	24.0	12.4	0.28	0.34	0.04				
			55	1.63	24.1	12.4	0.27	0.27	0.00				
			60	1.64	24.1	12.4	0.22	0.31	0.02				
			80	1.65	24.2	12.6	0.23	0.28	0.03				
			100	1.79	24.8	15.0	0.16	0.36	0.01				
			120	2.09	27.5	22.5	0.17	0.34	0.02				
553	49°28'S	02°25'W	50				0.65			1.48	0.10		
			150				0.50			2.44	0.03	12.62	0.02
570	49°26'S	02°03'W	40				0.34			2.34	0.08	13.04	0.01
			80				0.11			1.83	0.04	11.54	0.31
			150				0.08			3.06	0.51	11.69	0.03
			300				0.10			1.39	0.02	12.75	0.01
580	49°08'S	02°15'W	50				0.35			1.76	0.11	12.58	0.04
			150				0.23			2.05	0.12	12.34	0.01
			300				0.28			2.19	0.03	12.00	0.03
591	49°25'S	02°26'W	20	1.61	23.4	8.1	0.25	0.37	0.03	2.92	0.23	11.70	0.01
			40	1.58	23.5	7.8	0.52	0.37	0.01	2.05	0.12	12.26	0.00
			60	1.57	23.4	7.9	0.45	0.53	0.05	2.10	0.10	12.53	0.01
			100	1.58	23.5	8.5	0.19	0.38	0.00				
			150	2.03	27.7	23.7	1.31	0.38	0.00	3.09	0.11	12.46	0.28
			200	2.17	30.8	30.7	0.18	0.33	0.01				
			250	2.30	33.2	37.9	0.38	0.31	0.06				
			300	2.45	35.5	50.2	0.22	0.38	0.01	2.09	0.07	12.15	0.03

List of Figures

Bibliography

Allard, T., Menguy, N., Salomon, J., Calligaro, T., Weber, T., Calas, G., and Benedetti, M. 2004. Revealing forms of iron in river-borne material from major tropical rivers of the Amazon Basin (Brazil). Geochimica et Cosmochimica Acta, 68(14):3079–3094.

Assmy, P., Henjes, J., Klaas, C., and Smetacek, V. 2007. Mechanisms determining species dominance in a phytoplankton bloom induced by the iron fertilization experiment EisenEx in the Southern Ocean. Deep Sea Research Part I: Oceanographic Research Letters, 54(3):340–362.

Baker, A. and Croot, P. L. 2009. Atmospheric and marine controls on aerosol iron solubility in seawater . Marine Chemistry, DOI: 10.1016/j.marchem.2008.09.003.

Baker, A., French, M., and Linge, K. 2006a. Trends in aerosol nutrient solubility along a westeast transect of the Saharan dust plume. Geophysical Research Letters, 33:1–4.

Baker, A., Jickells, T., Witt, M., and Linge, K. 2006b. Trends in the solubility of iron, aluminium, manganese and phosphorus in aerosol collected over the Atlantic Ocean. Marine Chemistry, 98:43–58.

Baker, A. R. and Jickells, T. 2006. Mineral particle size as a control on aerosol iron solubility. Geophysical Research Letters, 33:1–4.

Barbeau, K. 2006. Photochemistry of Organic Iron(3+) Complexing Ligands in Oceanic Systems. Photochemistry and Photobiology, 82:1505–1516.

Barbeau, K., Rue, E. L., Bruland, K. W., and Butler, A. 2001. Photochemical cycling of iron in the surface ocean mediated by microbial Fe(3+) binding ligands. Nature, 413(6854):409–413.

Barbeau, K., Rue, E. L., Trick, C., Bruland, K. W., and Butler, A. 2003. Photochemical reactivity of siderophores produced by marine heterotrophic bacteria and cyanobacteria based on characteristic Fe(3+) binding groups. Limnology and Oceanography, 48(3):1069–1078.

Batinic-Haberle, I., Spasojevic, I., and Crumbliss, A. 1994. Hydrolysis of Ferrioxamine B in Aqueous Micellar Solution. Inorganic Chemistry, 33:3151–3158.

Bergquist, B. and Boyle, E. 2006. Dissolved iron in the tropical and subtropical Atlantic Ocean. Global Biogeochemical Cycles, 20:1–14.

Bergquist, B. A., Wu, J., and Boyle, E. A. 2007. Variability in oceanic dissolved iron is dominated by the colloidal fraction. Geochimica et Cosmochimica Acta, 71(12):2960.

Blain, S., Queguiner, B., Armand, L., Belviso, S., Bombled, B., Bopp, L., Bowie, A., Brunet, C., Brussaard, C., Carlotti, F., Christaki, U., Corbiere, A., Durand, I., Ebersbach, F., Fuda, J.-L., Garcia, N., Gerringa, L., Griffiths, B., Cuigue, C., Guillerm, C., Jaquet, S., Jeandel, C., Laan, P., Lefevre, D., Lo Monaco, C., Malits, A., Mosseri, J., Obernosterer, I., Park, Y.-H., Picheral, M., Pondaven, P., Remenyi, T., Sandroni, V., Sarthou, G., Savoye, N., Scouarnec, L., Souhaut, M., Thuiller, D., Timmermans, K., Trull, T., Uitz, J., van Beek, P., Veldhuis, M., Vincent, D., Viollier, E., Vong, L., and Wagener, T. 2007. Effect of natural iron fertilization on carbon sequestration in the Southern Ocean. Nature, 446(7139):1070–1074.

Boyd, P., Watson, A., Law, C., Abraham, E., Trull, T., Murdoch, R., Bakker, D., Bowie, A., Buesseler, K., Chang, H., Charette, M., Croot, P., Downing, K., Frew, R., Gall, M., Hadfield, M., Hall, J., Harvey, M., Jameson, G., LaRoche, J., Liddicoat, M., Ling, R., Maldonado, M., McKay, R., Nodder, S., Pickmere, S., Pridmore, R., Rintoul, S., Safi, K., Sutton, P., Strzepek, R., Tanneberger, K., Turner, S., Waite, A., and Zeldis, J. 2000. A mesoscale phytoplankton bloom in the polar Southern Ocean stimulated by iron fertilization. Nature, 407(6805):695–702.

Boyd, P. W., Jickells, T., Law, C. S., Blain, S., Boyle, E. A., Buesseler, K. O., Coale, K. H., Cullen, J. J., de Baar, H. J. W., Follows, M., Harvey, M., Lancelot, C., Levasseur, M., Owens, N. P. J., Pollard, R., Rivkin, R. B., Sarmiento, J., Schoemann, V., Smetacek, V., Takeda, S., Tsuda, A.,

Turner, S., and Watson, A. J. 2007. Mesoscale Iron Enrichment Experiments 1993-2005: Synthesis and Future Directions. Science, 315(5812):612–617.

Boye, M., Nishioka, J., Croot, P. L., Laan, P., Timmermans, K. R., and de Baar, H. J. W. 2005. Major deviations of iron complexation during 22 days of a mesoscale iron enrichment in the open Southern Ocean. Marine Chemistry, 96(3-4):257–271.

Boye, M., van den Berg, C., de Jong, J. T. M., Leach, H., Croot, P. L., and de Baar, H. J. W. 2001. Organic complexation of iron in the Southern Ocean. Deep-Sea Research Part A: Oceanographic Research Letters, 48:1477–1497.

Boyle, E., Edmond, J., and Sholkovitz, E. 1977. The mechanism of iron removal in estuaries. Geochimica et Cosmochimica Acta, 41(9):1313.

Boyle, E. A., Bergquist, B. A., Kayser, R. A., and Mahowald, N. 2005. Iron, manganese, and lead at Hawaii Ocean Time-series station ALOHA: Temporal variability and an intermediate water hydrothermal plume. Geochimica et Cosmochimica Acta, 69(4):933–952.

Bruland, K. W., Rue, E. L., Smith, G. J., and DiTullio, G. R. 2005. Iron, macronutrients and diatom blooms in the Peru upwelling regime: brown and blue waters of Peru. Marine Chemistry, 93(2-4):81–103.

Buck, K., Lohan, M., Berger, C., and Bruland, K. W. 2007. Dissolved iron speciation in two distinct river plumes and an estuary: Implications for riverine iron supply. Limnology and Oceanography, 52(2):843–855.

Byrne, R. and Kester, D. 1976. A potentiometric study of ferric ion complexes in synthetic media and seawater. Marine Chemistry, 4(3):275–287.

Byrne, R., Luo, Y., and Young, R. 2000. Iron hydrolysis and solubility revisited: observations and comments on iron hydrolysis characterizations. Marine Chemistry, 70(1-3):23–35.

Byrne, R., Yao, W., Luo, Y., and Wang, B. 2005. The dependence of Fe(3+) hydrolysis on ionic strength in NaCl solutions. Marine Chemistry, 97:34–48.

Campbell, P. G. C., Twiss, M. R., and Wilkinson, K. J. 1997. Accumulation of natural organic matter on the surfaces of living cells: implications for the interaction of toxic solutes with aquatic biota. Canadian Journal of Fisheries and Aquatic Sciences, 54:2543–2554.

Cassar, N., Bender, M., Barnett, B., Fan, S., Moxim, W., Levy II, H., and Tilbrook, B. 2007. The Southern Ocean Biological Response to Aelian Iron Input. Science, 317:1067–1070.

Chase, Z., Hales, B., Cowles, T., Schwartz, R., and van Geen, A. 2005. Distribution and variability of iron input to Oregon coastal waters during the upwelling season. Journal of Geophysical Ressearch, 110:1–14.

Chen, M. and Wang, W.-X. 2001. Bioavailability of natural colloid-bound iron to marine plankton: Influences of colloidal size and aging. Limnology and Oceanography, 46(8):1956–1967.

Coale, K., Johnson, K., Chavez, F., Buesseler, K., Barber, R., Brzezinski, M., Cochlan, W., Millero, F., Falkowski, P., Bauer, J., Wanninkhof, R., Kudela, R., Altabet, M., Hales, B., Takahashi, T., Landry, M., Bidigare, R., Wang, X., Chase, Z., Strutton, P., Friederich, G., Gorbunov, M., Lance, V., Hilting, A., Hiscock, M., Demarest, M., Hiscock, W., Sullivan, K., Tanner, S., Gordon, R., Hunter, C., Elrod, V., Fitzwater, S., Jones, J., Tozzi, S., Koblizek, M., Roberts, A., Herndon, J., Brewster, J., Ladizinsky, N., Smith, G., Cooper, D., Timothy, D., Brown, S., Selph, K., Sheridan, C., Twining, B., and Johnson, Z. 2004. Southern Ocean Iron Enrichment Experiment: Carbon Cycling in High- and Low-Si Waters. Science, 304(5669):408–414.

Croot, P., Andersson, M., Öztürk, M., and Turner, D. 2004a. The Distribution and Speciation of Iron along 6° East, in the Southern Ocean. Deep-Sea Research II: Topical Studies in Oceanography, 51:2857–2879.

Croot, P., Frew, R., Sander, S., Hunter, K., Ellwood, M., Pickmere, S., Abraham, E., Law, C. S., Smith, M., and Boyd, P. 2007. Physical mixing effects on iron biogeochemical cycling: FeCycle experiment. Journal of Geophysical Research, 112:1–18.

Croot, P. and Johansson, M. 2000. Determination of Iron Speciation by Cathodic Stripping Voltammetry in Seawater Using the Competing Ligand 2-(2-Thiazolylazo)-p-cresol (TAC). Electroanalysis, 12(8):565–576.

Croot, P., Streu, P., and Baker, A. R. 2004b. Short residence time for iron in surface seawater impacted by atmospheric dry deposition from Saharan dust events. Geophysical Research Letters, 31:doi.1029/2004GL020153.

Croot, P. L., Bluhm, K., Schlosser, C., Streu, P., Breitbarth, E., Frew, R., and Van Ardelan, M. 2008. Regeneration of Fe(II) during EIFeX and SOFeX. Geophysical Reseach Letters, 35:1–5.

Croot, P. L. and Laan, P. 2002. Continuous shipboard determination of Fe(II) in Polar waters using flow injection analysis with chemiluminescence detection. Analytica Chimica Acta, 466:261–273.

Cullen, J., Bergquist, B., and Moffett, J. 2006. Thermodynamic characterization of the partitioning of iron between soluble and colloidal species in the Atlantic Ocean. Marine Chemistry, 98:295–303.

De Baar, H., Boyd, P., Coale, K., Landry, M., Tsuda, A., Assmy, P., Bakker, D., Bozec, Y., Barber, R., Brzezinski, M., Buesseler, K., Boye, M., Croot, P., Gervais, F., Gorbunov, M., Harrison, P., Hiscock, W., Laan, P., Lancelot, C., Law, C., Levasseur, M., Marchetti, A., Millero, F., Nishioka, J., Nojiri, Y., van Oijen, T., Riebesell, U., Rijkenberg, M., Saito, H., Takeda, S., Timmermans, K., Veldhuis, M., Waite, A., and Wong, C. S. 2005. Synthesis of iron fertilization experiments: From the Iron Age in the Age of Enlightenment. Journal of Geophysical Research, 110:1–24.

De Baar, H., Buma, A., Nolting, R., Cade, G., Jacques, G., and Trguer, P. 1990. On iron limitation of the Southern Ocean: experimental observations in the Weddell and Scotia Seas. Marine Ecology Progress Series, 65(2):105–122.

de Jong, J. T. M., Boye, M., Schoemann, V., Nolting, R., and de Baar, H. 2000. Shipboard techniques based on flow injection analysis for measuring dissolved Fe, Mn and Al in seawater. Journal of Environmental Monitoring, 2:496–502.

Dickson, A. G. and Goyet, C. 1994. Handbook of methods for the analysis of the various parameters of the carbon dioxide system in seawater (Version 2). U.S. DOE.

Eldridge, M., Trick, C., Alm, M., DiTullio, G., Rue, E. L., Bruland, K. W., Hutchins, D., and Wilhelm, S. 2004. Phytoplankton community response to a manipulation of bioavailable iron in HNLC waters of the subtropical Pacific Ocean. Aquatic Microbial Ecology, 35:79–91.

Elrod, V., Berelson, W., Coale, K., and Johnson, K. 2004. The flux of iron from continental shelf sediments: A missing source for global budgets. Geophysical Research Letters, 31:1–4.

Erickson III, D., Hernandez, J., Ginoux, P., Gregg, W., McClain, C., and Christian, J. 2003. Atmospheric iron delivery and surface ocean biological activity in the Southern Ocean and Patagonian region. Geophysical Research Letters, 30(12):1–11.

Essington, M. E., Nelson, J. B., and Holden, W. L. 2005. Gibbsite and goethite solubility: The influence of 2-ketogluconate and citrate. Soil Science Society of America Journal, 69:996–1008.

Fischer, A., Kroon, J., Verburg, T., Teunissen, T., and Wolterbeek, H. 2007. On the relevance of iron adsorption to container materials in small-volume experiments on iron marine chemistry: ^{55}Fe-aided assessment of capacity, affinity and kinetics. Marine Chemistry, 107(4):533–546.

Fitzwater, S. E., Johnson, K. S., Elrod, V. A., Ryan, J. P., Coletti, L. J., Tanner, S. J., Gordon, R. M., and Chavez, F. P. 2003. Iron, nutrient and phytoplankton biomass relationships in upwelled waters of the California coastal system. Continental Shelf Research, 23(16):1523–1544.

Fung, I., Meyn, S., Tegen, I., Doney, S., John, J., and Bishop, J. 2000. Iron supply and demand in the upper ocean. Global Biogeochemical Cycles, 14(1):281–295.

Fuse, H., Takimura, O., Kamimura, K., and Yamaoka, Y. 1993. Marine Algae Excrete Large Molecular Weight Compounds Keeping Fe Dissolved. Bioscience, Biotechnology and Biochemistry, 57(3):509–510.

Gaiero, D., Probst, J. L., Depetris, P. J., Bidart, S. M., and Leleyter, L. 2003. Iron and other transition metals in Patagonian riverborne and windborne materials: Geochemical control and transport to the Southern South Atlantic Ocean. Geochimica et Cosmochimica Acta, 67:3603–3623.

Gerringa, L., Herman, P., and Poortvliet, T. 1995. Comparison of the linear Van den Berg/Ruzic transformation and a non-linear fit of the Langmuir isotherm applied to Cu speciation data in the estuarine environment. Marine Chemistry, 48(2):131–142.

Gerringa, L. J. A., De Baar, H. J. W., and Timmermans, K. R. 2000. A comparison of iron limitation

of phytoplankton in natural oceanic waters and laboratory media conditioned with EDTA. Marine Chemistry, 53:255–267.

Gervais, F., Riebesell, U., and Gorbunov, M. 2002. Changes in primary productivity and chlorophyll a in response to iron fertilization in the Southern Polar Frontal Zone. Limnology and Oceanography, 47(5):1324–1335.

Gobler, C. J., Hutchins, D. A., Fisher, N. S., Cosper, E. M., and Sanudo-Wilhelmy, S. A. 1997. Release and bioavailability of C, N, P, Se, and Fe following viral lysis of a marine chrysophyte. Limnology and Oceanography, 42(7):1492–1504.

Grasshoff, K., Erhardt, M., and Kremling, K. 1999. Methods of seawater analysis. Wiley-VCH, 3 Edition.

Guieu, C., Huang, W. W., Martin, J. M., and Yong, Y. Y. 1996. Outflow of trace metals into the Laptev Sea by the Lena River. Marine Chemistry, 53(3-4):255–267.

Guo, L., Hunt, B., and Santschi, P. 2001. Ultrafiltration Behavior Of Major Ions (Na, Ca, Mg, F, Cl, And SO_4) In Natural Waters. Water Research, 35(6):1500–1508.

Halstead, M. J. R., Cunninghame, R. G., and Hunter, K. A. 2000. Wet deposition of trace metals to a remote site in Fiordland, New Zealand. Atmospheric Environment, 34(4):665–676.

Hasselloev, M., Buesseler, K. O., Pike, S., and Dai, M. 2007. Application of cross-flow ultrafiltration for the determination of colloidal abudances in suboxic ferrous-rich ground waters. Science of The Total Environment, 372(2-3).

Haygood, M., Holt, P., and Butler, A. 1993. Aerobactin production by a planktonic marine Vibrio sp. Limnology and Oceanography, 38(5):1091–1097.

Hoffmann, L., Peeken, I., Lochte, K., Assmy, P., and Veldhuis, M. 2006. Different reactions of Southern Ocean phytoplankton size classes to iron fertilization. Limnology and Oceanography, 51(3):1217–1229.

Hovind, H. R. 1975. Thiazolylazo Dyes and Their Applications in Analytical Chemistry. The Analyst, 100:769–796.

Hudson, R. J. M., Covault, D. T., and Morel, F. M. M. 1992. Investigations of iron coordination and redox reactions in seawater using ^{59}Fe radiometry and ion-pair solvent extraction of amphiphilic iron complexes. Marine Chemistry, 38(3-4):209–235.

Hutchins, D. A. and Bruland, K. W. 1994. Grazer-mediated regeneration and assimilation of Fe, Zn and Mn from planktonic prey. Marine Ecology Progress Series, 110:259–269.

Hutchins, D. A. and Bruland, K. W. 1999. Grazer-mediated regeneration and assimilation of Fe, Zn and Mn from planktonic prey. Marine Ecology Progress Series, 110:259–269.

Hutchins, D. A., Franck, V. M., Brzezinski, M. A., and Bruland, K. W. 1999a. Inducing phytoplankton iron limitation in iron-replete coastal waters with a strong chelating ligand. Limnology and Oceanography, 44(4):1009–1018.

Hutchins, D. A., Witter, A. E., Butler, A., and Luther, G. W. 1999b. Competition among marine phytoplankton for different chelated iron species. Nature, 400(6747):858–861.

Jickells, T. D., An, Z. S., Andersen, K. K., Baker, A. R., Bergametti, G., Brooks, N., Cao, J. J., Boyd, P. W., Duce, R. A., Hunter, K. A., Kawahata, H., Kubilay, N., laRoche, J., Liss, P. S., Mahowald, N., Prospero, J. M., Ridgwell, A. J., Tegen, I., and Torres, R. 2005. Global Iron Connections Between Desert Dust, Ocean Biogeochemistry, and Climate. Science, 308(5718):67–71.

Johnson, K. S., Chavez, F., and Friederich, G. 1999. Continental-shelf sediments as a primary source of iron for coastal phytoplankton. Nature, 398:697–700.

Johnson, K. S., Coale, K., Elrod, V., and Tindale, N. 1994. Iron photochemistry in seawater from the equatorial Pacific. Marine Chemistry, 46:319–334.

Kari, F. G., Hilger, S., and Canonica, S. 1995. Determination of the Reaction Quantum Yield of the Photochemical Degradation of Fe(3+)-EDTA: Implications for the Environmental Fate of EDTA in Surface Waters. Environmental Science Technology, 29:1008–1017.

Khoe, G. and Robins, R. 1988. The Complexation of Iron(III) with Sulphate, Phosphate, or Arsenate Ion in Sodium Nitrate Medium at 25°C. Journal of the Chemical Society, Dalton Transition, pages 2015–2021.

King, D., Lounsbury, H., and Millero, F. 1995. Rates and Mechanism of Fe(II) Oxidation and Nanomolar Total Iron Concentrations. Environmental Science Technology, 29:818–824.

Kondo, Y., Takeda, S., Nishioka, J., Obata, H., Furuya, K., Johnson, W. K., and Wong, C. S. 2008. Organic iron (III) complexing ligands during an iron enrichment experiment in the western subarctic North Pacific. Geophysical Research Letters, 35:1–5.

Kuma, K. and Isoda, Y. 2003. Control on dissolved iron concentrations in deep waters in the western North Pacific: Fe(3+) hydroxide solubility. Journal of Geophysical Research, 108(C9):1–10.

Kuma, K., Katsumoto, A., Kawakami, H., Takatori, F., and Matsunaga, K. 1998a. Spatial variability of Fe(3+) hydroxide solubility in the water column of the northern North Pacific Ocean. Deep Sea Research Part A: Oceanographic Research Letters, 45:91–113.

Kuma, K., Katsumoto, A., Nishioka, J., and Matsunaga, K. 1998b. Size-fractionated iron concentrations and Fe(3+) hydroxide solubilities in various coastal waters. Estuarine, Coastal and Shelf Science, 47:275–283.

Kuma, K., Katsumoto, A., Shiga, N., Sawabe, T., and Matsunaga, K. 2000. Variation of size-fractionated Fe concentrations and Fe(3+) hydroxide solubilities during a spring phytoplankton bloom in Funka Bay (Japan). Marine Chemistry, 71(1-2):111.

Kuma, K. and Matsunaga, K. 1995. Availability of colloidal ferric oxides to coastal marine phytoplankton. Marine Biology, 122(1):1–11.

Kuma, K., Nakabayashi, S., Suzuji, K., Kudo, I., and Matsunaga, K. 1992a. Photo-reduction of Fe(3+) by dissolved organic substances and existence of Fe(2+) in seawater during spring blooms. Marine Chemistry, 37:15–27.

Kuma, K., Nakabayashi, S., Suzuki, K., and Matsunaga, K. 1992b. Dissolution rate and solubility of colloidal hydrous ferric oxide in seawater. Marine Chemistry, 38:133–143.

Kuma, K., Nishioka, J., and Matsunaga, K. 1996. Controls on Fe(3+) hydroxide solubility in seawater: The influence of pH and natural organic chelators. Limnology and Oceanography, 41(3):396–407.

Lam, P., Bishop, J., Henning, C., Marcus, M., Waychunas, G., and Fung, I. 2006. Wintertime phytoplankton bloom in the subarctic Pacific supported by continental margin iron. Global Biogeochemical Cycles, 20:1–12.

Lewis, E. and Wallace, D. 1998. Program Developed for CO_2 System Calculations, ORNL/CDIAC-105,. Technical report, Carbon Dioxide Information Analysis Center, Oak Ridge National Laboratory, U.S. Department of Energy, Oak Ridge, Tennessee.

Liu, H. and Millero, F. J. 1999. The solubility of iron hydroxide in sodium chloride solutions. Geochimica et Cosmochimica Acta, 63(19/20):3487–3497.

Liu, X. and Millero, F. 2002. The solubility of iron in seawater. Marine Chemistry, 77:43–54.

Logan, B. E. and Qing, J. 1990. Molecular-Size Distributions Of Dissolved Organic-Matter. Journal of Environmental Engineering, 116:1046–1062.

Macrellis, H., Trick, C., Rue, E., Smith, G., and Bruland, K. 2001. Collection and detection of natural iron-binding ligands from seawater. Marine Chemistry, 76(3):175.

Mali, G., Sala, M., Arcon, I., Kaucic, V., and J., K. 2006. Insight into the Short-Range Structure of Amorphous Iron Inositol Hexaphosphate as Provided by sup31supP NMR and Fe X-ray Absorption Spectroscopy. Journal of Physical Chemistry, 110:23060–23067.

Martin, J. H., Coale, K. H., Johnson, K. S., Fitzwater, S. E., Gordon, R. M., Tanner, S. J., Hunter, C. N., Elrod, V. A., Nowicki, J. L., Coley, T. L., Barber, R. T., Lindley, S., Watson, A. J., Vanscoy, K., Law, C. S., Liddicoat, M. I., Ling, R., Stanton, T., Stockel, J., Collins, C., Anderson, A., Bidigare, R., Ondrusek, M., Latasa, M., Millero, F. J., Lee, K., Yao, W., Zhang, J. Z., Friederich, G., Sakamoto, C., Chavez, F., Buck, K., Kolber, Z., Greene, R., Falkowski, P., Chisholm, S. W., Hoge, F., Swift, R., Yungel, J., Turner, S., Nightingale, P., Hatton, A., Liss, P., and Tindale, N. W. 1994. Testing The Iron Hypothesis In Ecosystems Of The Equatorial Pacific-Ocean. Nature, 371(6493):123–129.

Martin, J. H. and Fitzwater, S. E. 1988. Iron-Deficiency Limits Phytoplankton Growth In The Northeast Pacific Subarctic. Nature, 331(6154):341–343.

Martinez, J., Carter-Franklin, J., Mann, E., Martin, K., Haygood, M., and Butler, A. 2003. Structure and membrane affinity of a suite of amphiphilic siderophores produced by a marine bacterium. Proceedings of the National Academy of Sciences, 100(7):3754–3759.

Martinez, J., Zhang, G., Holt, P., Jung, H.-T., Carrano, C., Haygood, M., and Butler, A. 2000. Self-Assembling Amphiphilic Siderophores from Marine Bacteria. Science, 287:1245–1247.

Mayer, L. M. 1999. Extent of coverage of mineral surfaces by organic matter in marine sediments. Geochimica et Cosmochimica Acta, 63(2):207–215.

McCormack, P., Worsfold, P., and Gledhill, M. 2003. Separation and Detection of Siderophores Produced by Marine Bacterioplankton Using High-Performance Liquid Chromatography with Electrospray Ionization Mass Spectrometry. Analytical Chemistry, 75:2647–2652.

Milas, M., Shi, X., and Rinaudo, M. 1990. On the Physicochemical Properties of Gellan Gum. Biopolymers, 30:451–464.

Millero, F. 1986. The pH of esturine waters. Limnology and Oceanography, 31:839–847.

Millero, F. and Sotolongo, S. 1989. The oxidation of Fe(2+) with H_2O_2 in seawater. Geochimica et Cosmochimica Acta, 53:1867–1873.

Millero, F., Sotolongo, S., and Izaguirre, M. 1986. The oxidation kinetics of Fe(2+) in seawater. Geochimica et Cosmochimica Acta, 51:793–801.

Millero, F. J. 1998. The solubility of Fe(3+) in seawater. Earth and Planetary Science Letters, 154:323–329.

Miyoshi, E., Takaya, T., Williams, P. A., and Nishinari, K. 1996. Effects of sodium chloride and calcium chloride on the interaction between gellan gum and konjac glucomannan. Journal Of Agricultural And Food Chemistry, 44(9):2486–2495. 0021-8561.

Nagata, T., Fukuda, R., Koike, I., Kogure, K., and Kirchmann, D. L. 1998. Degradation by bacteria of membrane and soluble protein in seawater. Aquatic Microbial Ecology, 14:29–27.

Nakabayashi, S., Kuma, K., Sasaoka, K. Saitoh, S., Mochizuki, M., Shiga, N., and Kusakabe, M. 2002. Variation in Fe(3+) solubility and iron concentration in the northwestern North Pacific Ocean. Limnology and Oceanography, 47(3):885–892.

Nakajima, T., Ikehara, T., and Nishi, T. 1996. Observation of gellan gum by scanning tunneling microscopy. Carbohydrate Polymers, 30:77.

Nelson, J. and Essington, M. 2005. The Association Constants of H(+) and Ca(2+) with 2-Keto-D-Gluconate in Aqueous Solutions. Journal of Solution Chemistry, 34(7):789–800.

Nishinari, K. 1999. Physical Chemistry and Industrial Application of Gellan Gum, volume 114 of Progress in Colloid and Polymer Science. Springer, Berlin und Heidelberg.

Nishioka, J., Takeda, S., de Baar, H. J. W., Croot, P. L., Boye, M., Laan, P., and Timmermans, K. R. 2005. Changes in the concentration of iron in different size fractions during an iron enrichment experiment in the open Southern Ocean. Marine Chemistry, 95(1-2):51.

Nishioka, J., Takeda, S., Wong, C. S., and Johnson, W. K. 2001. Size-fractionated iron concentrations in the northeast Pacific Ocean: distribution of soluble and small colloidal iron. Marine Chemistry, 74(2-3):157–179.

Nowack, B. and Sigg, L. 1996. Adsorption of EDTA and Metal-EDTA Complexes onto Goethite. Journal of Colloidal and Interface Science, 177:106–121.

Obata, H., Karatani, H., and Nakayama, E. 1993. Automated Determination of Iron in Seawater by Chelating Resin Concentration and Chemiluminescence Detection. Analytical Chemistry, 65:1524–1528.

Oeztuerk, M., Croot, P. L., Bertilsson, S., Abrahamsson, K., Karlson, B., David, R., Fransson, A., and Sakshaug, E. 2004. Iron enrichment and photoreduction of iron under PAR and UV in the presence of hydrocarboxylic acid: Implications for phytoplankton growth in the Southern Ocean. Deep Sea Research Part II: Topical Studies in Oceanography, 51:2841–2856.

Orsi, A., Whitworth III, T., and Nowlin Jr, W. 1995. On the meridional extent and fronts of the

Antarctic Circumpolar Current. Deep Sea Research Part I: Oceanographic Research Papers, 42(5):641–673.

Planquette, H., Statham, P., Fones, G., Charette, M., Moore, C., Salter, I., Nedelec, F., Taylor, S., French, M., Baker, A. R., Mahowald, N., and Jickells, T. D. 2007. Dissolved iron in the vicinity of the Crozet Islands, Southern Ocean. Deep Sea Research Part II: Topical Studies in Oceanography, 54(18-20):1999–2019.

Pollard, R. T., Salter, I., Sanders, R. J., Lucas, M. I., Moore, C. M., Mills, R. A., Statham, P. J., Allen, J. T., Baker, A. R., Bakker, D. C. E., Charette, M. A., Fielding, S., Fones, G. R., French, M., Hickman, A. E., Holland, R. J., Hughes, J. A., Jickells, T. D., Lampitt, R. S., Morris, P. J., Nedelec, F. H., Nielsdottie, M., Planquette, H., Popova, E. E., Poulton, A. J., Read, J. F., Seeyave, S., Smith, T., Stinchcombe, M., Taylor, S., Thomalla, S., Venables, H. J., Williamson, R., and Zubkov, M. V. 2009. Southern Ocean deep-water carbon export enhanced by natural iron fertilization. Nature, 457(7229):577–580.

Powell, R. and Donat, J. 2001. Organic complexation and speciation of iron in the South and Equatorial Atlantic. Deep Sea Research Part II: Topical Studies in Oceanography, 48:2877–2893.

Powell, R. and Wilson-Finelli, A. 2003a. Importance of organic Fe complexing ligands in the Mississippi River plume. Estuarine, Coastal and Shelf Science, 58:757–763.

Powell, R. and Wilson-Finelli, A. 2003b. Photochemical degradation of organic iron complexing ligands in seawater. Aquatic Sciences, 65:367–374.

Purawatt, S., Siripinyanond, A., and Shiowatana, J. 2007. Flow field-flow fractionation inductively coupled optical emission spectrometric investigation of the size-based distribution of iron complexed to phytic and tannic acids in a food suspension: implications for iron availability. Analytical and Bioanalytical Chemistry, 389:733–742.

Quigley, M. S., Santschi, P. H., Hung, C.-C., Guo, L., and Honeyman, B. D. 2002. Importance of acid polysaccharides for ^{234}Th complexation to marine organic matter. Limnology and Oceanography, 47:367–377.

Raiswell, R., Benning, L. G., Davidson, L., and Tranter, M. 2008a. Nanoparticulate bioavailable iron minerals in icebergs and glaciers. Mineralogical Magazine, 72(1):345–348.

Raiswell, R., Benning, L. G., Tranter, M., and Tulaczyk, S. 2008b. Bioavailable iron in the Southern Ocean: the significance of the iceberg conveyor belt. Geochemical Transactions, 9(1):1–9.

Reitmeyer, R., Powell, R. T., Landing, W. M., and Measures, C. I. 1996. Colloidal aluminum and iron in seawater: An intercomparison between various cross-flow ultrafiltration systems. Marine Chemistry, 55(1-2):75.

Rijkenberg, M., Gerringa, L., Carolus, V., Velzeboer, I., and de Baar, H. 2006. Enhancement and inhibition of iron photoreduction by individual ligands in open ocean seawater. Geochimica et Cosmochimica Acta, 70(11):2790–2805.

Robertson, D. E. 1968. The adsorption of trace elements in sea water on various container surfaces. Analytica Chimica Acta, 42:533.

Rue, E. and Bruland, K. 1995. Complexation Of Iron(3+) By Natural Organic-Ligands In The Central North Pacific As Determined By A New Competitive Ligand Equilibration Adsorptive Cathodic Stripping Voltammetric Method. Marine Chemistry, 50(1-4):117–138.

Rue, E. and Bruland, K. 1997. The role of organic complexation on ambient iron chemistry in the equatorial Pacific Ocean and the response of a mesoscale iron addition experiment. Limnology and Oceanography, 42(5):901–910.

Saito, M. A. and Schneider, D. L. 2006. Examination of precipitation chemistry and improvements in precision using the $Mg(OH)_2$ preconcentration inductively coupled plasma mass spectrometry (ICP-MS) method for high-throughput analysis of open-ocean Fe and Mn in seawater. Analytica Chimica Acta, 565:222–233.

Santana-Casiano, J., Gonzalez-Davila, M., and Millero, F. 2006. The role of Fe(2+) species on the oxidation of Fe(2+) in natural waters in the presence of O_2 and H_2O_2. Marine Chemistry, 99:70–82.

Sato, M., Takeda, S., and Furuya, K. 2007. Iron regeneration and organic iron(III)-binding ligand production during in situ zooplankton grazing experiment. Marine Chemistry, 106(3-4):471.

Schlosser, C. and Croot, P. L. 2008. Application of cross-flow filtration for determining the solubility of iron species in open ocean seawater. Limnology and Oceanography: Methods, 6:630–642.

Schwarzenbach, H. and Schwarzenbach, K. 1963. Hydroxamatkomplexe I. Die Stabilitat der Eisen(III)-Komplexe einfacher Hydroxamsauren und des Ferrioxamins B. Helvetica Chimica Acta, 46:1390–1401.

Smetacek, V. and participants, c. 2005. The expedition ANT XXI/3 of R/V Polarstern. Berichte zur Polarforschung, Alfred-Wegener-Institut für Polar- und Meeresforschung, 500:1–134.

Soffer, Y., Adin, A., and Gilron, J. 2004. Threshold flux in fouling of UF membranes by colloidal iron. Desalination, 161:207–221.

Soffer, Y., Gilron, J., and Adin, A. 2002. Streaming potential and SEM-EDX study of UF membranes fouled by colloidal iron. Desalination, 146:115–121.

Stramma, L., Huettle, S., and Schafstall, J. 2005. Water masses and currents in the upper tropical Atlantic off Northwest Afrika. Journal of Geophysical Research, 110:1–18.

Sunda, W. and Huntsman, S. 2003. Effect of pH, light, and temperature on Fe-EDTA chelation and Fe hydrolysis in seawater. Marine Chemistry, 84:35–47.

Sundquist, E. 1993. The global carbon dioxide budget. Science, 259:934–941.

Takeda, S. and Tsuda, A. 2005. An in situ iron-enrichment experiment in the western subarctic Pacific (SEEDS): Introduction and summary. Progress in Oceanography, 64:95–109.

Tani, H., Nishioka, J., Kuma, K., Takata, H., Yamashita, Y., Tanoue, E., and Midorikawa, T. 2003. Iron(3+) hydroxide solubility and humic-type fluorescent organic matter in the deep water column of the Okhotsk Sea and the northwestern North Pacific Ocean. Deep Sea Research Part I: Oceanographic Research papers, 50:1063–1078.

Timmermans, K. R., Gerringa, L. J. A., de Baar, H. J. W., van der Wagt, B., Veldhuis, M. J. W., de Jong, J. T. M., Croot, P. L., and Boye, M. 2001. Growth rates of large and small southern ocean diatoms in relation to availability of iron in natural seawater. Limnology and Oceanography, 46(2):260–266.

Torres, J. et al. 2005. Solution behaviour of myo-inositol hexakisphosphate in the presence of multivalent cations. Prediction of a neutral pentamagnesium species under cytosolic/nuclear conditions. Journal of Inorganic Biochemistry, 99:828.

Town, R. and van Leeuwen, H. 2005. Measuring Marine Iron(3+) Compexes by CLV/AdSV. Environmental Chemistry, 2:80–84.

Turner, A., Paphazy, M. J., Haygarth, P. M., and Mckelvie, I. 2002. Inositol phosphates in the environment. Philosophical Transactions Of The Royal Society Of London Series B-Biological Sciences, 357:449–469.

Turner, D. R. and Hunter, K. A. 2001a. The Biogeochemistry of Iron in Seawater. Atmospheric Iron Inputs in the Oceans. John Wiley, N.J.

Turner, D. R. and Hunter, K. A. 2001b. The Biogeochemistry of Iron in Seawater. Distribution, Sources and Sinks of Iron in Seawater. John Wiley, N.J.

van den Berg, C. 1995. Evidence for organic complexation of iron in seawater. Marine Chemistry, 50(1-4):139–157.

van den Berg, C. 2006. Chemical Speciation of Iron in Seawater by Cathodic Stripping Voltammetry with Dihydroxynaphthalene. Analytical Chemistry, 78:156–163.

Wagener, T., Guieu, C., Losno, R., Bonnet, S., and Mahowald, N. 2008. Revisiting atmospheric dust export to the Southern Hemisphere ocean: Biogeochemical implications. Global Biogeochemical Cycles, 22:1–13.

Waite, T., Schäfer, A., Fane, A., and Heuer, A. 1999. Colloidal Fouling of Ultrafiltration Membranes: Impact of Aggregate Structure and Size. Journal of Colloidal and Interface Science, 212:264–274.

Wang, W. and Dei, R. 2003. Bioavailability of iron complexed with organic colloids to the cyanobacteria Synechococcus and Trichodesmium. Aquatic Microbial Ecology, 33:247–259.

Wells, M. and Goldberg, E. 1994. The distribution of colloids in the Northern Atlantic and Southern Ocean. Limnology and Oceanography, 39(2):286–302.

Wells, M. L. 1999. Manipulating iron availability in nearshore waters. Limnology and Oceanography, 44(4):1002–1008.

Wells, M. L. 2003. The level of iron enrichment required to initiate diatom blooms in HNLC waters. Marine Chemistry, 82(1-2):101–114.

Wells, M. L. and Goldberg, E. D. 1993. Colloid aggregation in seawater. Marine Chemistry, 41(4):353.

Wells, M. L., Mayer, L. M., Donard, O. F. X., Sierra, M. M. D., and Ackelson, S. G. 1991. The Photolysis Of Colloidal Iron In The Oceans. Nature, 353(6341):248–250.

Witter, A. E., Hutchins, D. A., Butler, A., and Luther III, G. 2000. Determination of conditional stability constants and kinetic constants for strong model Fe-binding ligands in seawater. Marine Biology, 69:1–17.

Witter, A. E. and Luther, G. W. 1998. Variation in Fe-organic complexation with depth in the Northwestern Atlantic Ocean as determined using a kinetic approach. Marine Chemistry, 62(3-4):241.

Wu, J. 2007. Determination of picomolar iron in seawater by double $Mg(OH)_2$ precipitation isotope dilution high-resolution ICPMS. Marine Chemistry, 103(3-4):370.

Wu, J., Boyle, E., Sunda, W., and Wen, L. 2001. Soluble and Colloidal Iron in the Oligotrophic North Atlantic and North Pacific. Science, 293:847–849.

Wu, J. and Luther, G. 1995. Complexation of Fe(3+) by natural organic ligands in the Northwest Atlantic Ocean by a competitive ligand equilibration method and a kinetic approach. Marine Chemistry, 50(1-4):159–177.

Danksagung

Zu aller erst möchte ich mich bei allen bedanken, die mich tatkräftig unterstützt und zum Gelingen dieser Dissertation beigetragen haben.

Ein herzliches Dankeschön geht an Herrn Prof. Dr. Doug Wallace welcher mir die Möglichkeit gegeben hat diese Dissertation am IFM-GEOMAR anfertiegen zu können und mir bei anliegenden Fragen immer hilfreich zur Seite stand.

Ein Dankeschön auch an Herrn Dr. Peter L. Croot, auf dessen Idee sich meine Arbeit begründet und der diese Arbeit möglich gemacht hat. Ich bedanke mich für die tatkräftige Unterstützung bei technischen wie auch theoretischen Fragestellungen und für die tolle Arbeitsatmosphäre.

Ein weiteres Dankeschön an alle Mitarbeiter aus der Chemischen und Biologischen Ozeanographie die immer ein offenes Ohr für mich hatten und bei wissenschaftlichen Fragenstellungen immer versucht haben zu helfen. Namentlich möchte ich hier nennen: Prof. Dr. Arne Körtzinger, Priv.-Doz. Dr. Hermann Bange und Dr. Birgit Quack.

Ein herzliches Dankeschön auch an Peter Streu für die durchgeführten Labormessungen und der mir mit Tips und Tricks immer hilfreich im Labor, auf See und im "Holsteinstadion" zur Seite stand. Und natürlich den anderen Technikern, ohne dessen gemessenen Daten viele Sachen nicht so heraus gekommen wären (hier sind Frank und Susann zu nennen).

Einen Dank auch an unsere Ute Weidinger die bei Administrativen Fragen immer versucht hat zu helfen und für jeden Spass zu haben war.

Weiterhin ein Dankeschönden an die Mitarbeitern aus dem TLZ, die bei speziellen Wünschen immer schnell versucht haben zu helfen.

Ein großes Dankeschön an meine Freundin Christina die mich auch in den letzten paar Wochen, vor Abgabe dieser Arbeit, ertragen hat und sehr beim gelingen dieser Arbeit beigetragen hat.

Und "last but not least" möchte ich meinen lieben Eltern, Manfred und Ute, sowie meiner Oma Selma für ihr grenzenloses Vertrauen und ihre Unterstützung danken, ohne die mein Studium und diese Doktorarbeit, nicht möglich gewesen wäre. Vielen Dank für Alles!